DEUTSCHES ELEKTRONEN-SYNCHROTRON DESY

DESY 88-188
December 1988

Radiative Corrections in the Standard Model and Their Rôle for Precision Tests of the Electroweak Theory

W.F.L. Hollik
II. Inst. f. Theoretische Physik, Univ. Hamburg

ISSN 0418-9833

NOTKESTRASSE 85 · 2 HAMBURG 52

To be sure that your preprints are promptly included in the
HIGH ENERGY PHYSICS INDEX ,
send them to the following address (if possible by air mail) :

DESY
Bibliothek
Notkestrasse 85
2 Hamburg 52
Germany

DESY 88-188
December 1988

ISSN 0418-9833

Radiative Corrections in the Standard Model and Their Rôle for Precision Tests of the Electroweak Theory

WOLFGANG F.L. HOLLIK
II. Institut für Theoretische Physik
Universität Hamburg, FRG *

Abstract

We present a detailed description of the on-shell electroweak radiative corrections calculation together with a list of formulae for 4-fermion processes complete at the one-loop level and with the accuracy required for precision experiments at the e^+e^- colliders LEP and SLC. Applications are discussed to the mass interdependence of the weak vector bosons, the weak mixing angle, and to the precisely measurable on-resonance observables Z mass, width, forward-backward and polarization asymmetries for leptonic and hadronic final states. Comparisons with the results of other calculations have been performed as far as possible with satisfactory agreement in the predictions for the measurable quantities.

*address after April 1, 1989: CERN, TH-Division, CH-1211 Genève 23

Contents

Chapter 1

Introduction

With the e^+e^- colliders LEP and SLC going into operation in the nearby future the investigation of the weak interaction enters a new era of precision experiments. For a long period weak interaction effects have been known from nuclear physics and low energy particle physics phenomenology, starting already in 1896 with the observation of nuclear β decay by Bequerel. The historical path was marked out by a lot of surprising discoveries which have substantially contributed in shaping our understanding of the basic constituents of matter and their fundamental interactions:
- the existence of neutrinos - the violation of apparently fundamental symmetries like parity and CP invariance - the appearance of internal quantum numbers like lepton numbers, hypercharge, and isospin, leading to the family structure of the fundamental fermions - the observation of neutral currents - and the culmination in the spectacular discovery of the heavy vector bosons $W^{\pm}$, Z having been predicted by the Glashow-Salam-Weinberg model as the successful conclusion in a long development of theoretical concepts [1].

This GSW model originally conceived for leptons, then extended to the hadronic sector incorporating the concept of Cabbibo resp. Kobayashi-Maskawa mixing [2], has become the "electroweak standard model": the presently most comprehensive formulation of a theory of the unified electroweak interaction, theoretically consistent and in agreement with all experimentally known phenomena of electroweak origin [3]. The trace of this development is quite different from that encountered in formulating Quantum Electrodynamics (QED) as the theory of pure electromagnetic forces: the quantized form of Maxwell's theory has been well established for nearly 60 years and has kept its principal structure since the pioneering work of Dirac, Heisenberg, and Pauli; later developments [4] simplified the practical perturbative handling tremendously.

The relatively long period for which QED has been available made it possible to subject it to experimental tests like measurements of the anomalous g factor of the electron and the muon [5] proving the correctness of the theoretical concept to an accuracy which is as yet unique in the wide area of probing the fundamental laws of physics. Those precision tests were milestones in revealing the basic character of QED as a quantized field theory since the theoretical predictions follow from a systematic application of the field theoretical version of quantum mechanical perturbation theory. Although the higher order perturbative terms are usually quite complicated in their concrete manifestations they are finally the consequence of a simply structured Lagrangian. This Lagrangian can be considered the classical Lagrangian of a corresponding unquantized theory which, however, would never give rise to the small measurable effects following from the quantized version. Hence, the

experimental verification of the quantum effects confirms that quantum field theory is the adequate theoretical framework for the description of the fundamental interactions.

Testing a theory at its quantum level becomes possible if the following conditions are satisfied:

(i) existence of a theory that makes precise predictions beyond the lowest order,

(ii) availability of experiments which are sensitive to such small effects.

Both conditions have been fulfilled in case of QED.

The spectacular prediction of the weak vector bosons from the unification of electromagnetic and weak interactions and their experimental verification have a parallel in the physics of electromagnetism:

Maxwell's unification of the electric and the magnetic forces led to the prediction of electromagnetic waves propagating with the velocity of light. Thus, the experimental proof of their existence and properties by Hertz's experiments has been the confirmation of the field theory of the electromagnetic interaction at the classical level, whereas the further efforts in course of the 20th century have confirmed the same field theory also at the quantum level.

Quite analogously, the electroweak unification has predicted the existence of massive vector bosons with masses of the order of the Fermi scale $(G_F\sqrt{2})^{-\frac{1}{2}} \approx 250$ GeV, which was known experimentally from earlier days' data on particle decays. The appearance of a second parameter necessary for specifying the precise mass values, the electroweak mixing angle $\sin^2\theta_W$, comes in since the unification is not really complete but still involves two independent coupling constants. This small "defect" (from an aesthetic point of view) requires one more experimental information obtained e.g. from neutrino scattering. The experimental verification of that prediction in $p\bar{p}$ collisions [6] may be considered a confirmation of the standard model at the classical level.

In complete analogy to QED, the standard model as a quantized gauge field theory allowing a perturbative treatment beyond the lowest order exhibits higher order effects which are measurable in suitable experiments. But in contrast to QED, the experimental facilities so far have not yet reached that high level of precision necessary for detecting the quantum effects (there are, however, already strong indications for the presence of higher order contributions [3]). In the sense of our analogy to electromagnetism, we are presently in the phase after Hertz's experiments but before measuring Lamb shift and anomalous magnetic moments. This situation will considerably change with the experiments at LEP and SLC which for the first time will become sensitive to the quantum structure of the unified electroweak interaction.

The electroweak standard model is a non-abelian gauge theory based on the gauge group $SU(2)\times U(1)$ where the ideas of Yang-Mills theories, isospin invariance, spontaneous symmetry breaking, and Higgs mechanism merge in one common concept. The possibility to perform perturbative calculations for measurable quantities order by order in terms of a few input parameters is substantially based on the renormalizability of this class of theories which was proved by 't Hooft in 1971 [7]. The input parameters themselves cannot be predicted but have to be taken from appropriate experiments.

The virtue of renormalizability has motivated the calculation of the higher order quantum effects, the "radiative corrections ", to processes accessible by the experimental facilities. Such processes have been the weak decays of particles, and scattering processes mediated by

the electroweak interaction: neutrino-lepton and neutrino-nucleon scattering, as well as e^+e^- annihilation. These are processes where the fundamental fermions interact with each other via the exchange of gauge bosons. For the purely leptonic reactions this is obvious; if hadrons are involved the basic electroweak processes are considered to be the corresponding subreactions at the level of quarks as their constituents. According to the structure of the fermion - gauge boson interaction these kinds of fundamental reactions are all of the type of 4-fermion processes. Since also at LEP the fundamental processes which can be investigated with high precision are those of fermion pair production $e^+e^- \to f\bar{f}$ we are primarily concerned with the question of radiative corrections to 4-fermion processes.

Electroweak processes between fermions can essentially be described with help of three input parameters (besides fermion masses and mixing angles), e.g. the gauge coupling constants g_2, g_1 according to SU(2) and U(1), and the Higgs field vacuum expectation value v. Since there is no a-priori preference given to a specific parameter set these can be replaced by any other three quantities with the only requirement of being independent and obeying the theoretical relations to the previous ones. Since the input parameters have to be taken finally from experiment it is more practical to deal with a set where each parameter has a direct connection to a specific experiment and is a well measured quantity, for example [8]:

- the fine structure constant $\alpha = 1/137.03604(11)$, obtained from Thomson scattering; [1]
- the Fermi constant $G_\mu = 1.166344(11) \times 10^{-5}$ GeV^{-2}, obtained from the μ lifetime; [2]
- the mixing angle $\sin^2\theta_W = 0.231 \pm 0.006$, obtained from neutrino-quark scattering [16].

The muon decay process $\mu \to e\nu_\mu\bar{\nu}_e$ is the most accurateley investigated weak decay process. From the muon lifetime the effective Fermi model coupling constant G_μ is derived which is free of radiative corrections, except of purely electromagnetic ones [9]. The electromagnetic fine structure constant α is in addition also free of electromagnetic corrections [10].

The standard model in its lowest order application yields the following relations between this experimental input and the masses of the $W^\pm$ and Z bosons:

$$M_W^2 = \frac{\pi\alpha}{\sqrt{2}G_\mu \sin^2\theta_W}, \tag{1.1}$$

$$\frac{M_W^2}{M_Z^2} = 1 - \sin^2\theta_W . \tag{1.2}$$

These relations can be used to obtain the masses from the input data given above. With the possibility of measuring directly the vector boson masses in e^+e^- colliders with high precision ($\Delta M_Z = 20 - 50$ MeV at LEP I [11], $\Delta M_W = 100$ MeV at LEP 200 [12]) the question for the "best" input would lead to a different answer: Take the most precisely measured quantities

$$\alpha, \quad G_\mu, \quad M_Z \tag{1.3}$$

as input parameters for fixing the theory, and predict the other quantities M_W and $\sin^2\theta_W$ from the relations given above for testing the theory. Indeed, with M_Z we enter a precision

[1] we refer to Thomson scattering since it is the low energy limit of Compton scattering and measures the classical electron charge; for determinations of α with high precision other methods like applications of the Josephson or the quantum Hall effect are more practical

[2] since we deal always with its value as derived from τ_μ we prefer the notation G_μ instead of G_F

level of 0.05%. The W mass, however, is not yet within reach for the next future with a comparable accuracy, and so we are left with $\sin^2\theta_W$ as the quantity for precision tests in the phase of LEP I.

But how to improve on the experimental accuracy of $\sin^2\theta_W$?

From neutrino-electron scattering one expects an uncertainty of ± 0.005 [106]. The present error in $\sin^2\theta_W$ from neutrino-hadron data is not expected to become sizably smaller in future neutrino nucleon scattering experiments. The key to a substantial improvement is instead found in measuring charge and polarization asymmetries in the processes $e^+e^- \to f\bar{f}$ at the peak of the Z resonance. These quantities depend in lowest order only on the ratios of the vector and axial vector coupling constants of the fermions to the Z boson

$$x_{e,f} = \frac{v_{e,f}}{a_{e,f}} = 1 - 4 \mid Q_{e,f} \mid \sin^2\theta_W \tag{1.4}$$

and hence only on $\sin^2\theta_W$ (Q_f denotes the electric fermion charges). As an example of particular importance we mention the left-right asymmetry

$$A_{LR} = \frac{\sigma_L - \sigma_R}{\sigma_L + \sigma_R} = \frac{2\,x_e}{1 + x_e^2} \tag{1.5}$$

where $\sigma_{L,R}$ are the total cross sections for left- and right-handed incoming electrons. By a measurement of A_{LR} a determination of $\sin^2\theta_W$ will become feasible with an accuracy of ± 0.0004 (assuming 10^6 Z events) [13,14] matching the precision of the input data. Without longitudinal beam polarization, one would obtain $\Delta \sin^2\theta_W = 0.001$ from the forward-backward asymmetry A_{FB} in $e^+e^- \to \mu^+\mu^-$ for the same number of Z's [13,15].

From the experimental input parameters α, G_μ, $\sin^2\theta_W$ as specified above we obtain with help of the relations (1.1), (1.2) the following values for the boson masses:

$$M_W = 77.6 \pm 1.0\,\mathrm{GeV}, \quad M_Z = 88.5 \pm 0.8\,\mathrm{GeV}\,.$$

When compared to the measured masses [8]

$$(M_W)_{exp} = 80.9 \pm 1.3\,\mathrm{GeV}, \quad (M_Z)_{exp} = 91.9 \pm 1.7\,\mathrm{GeV}$$

they show that the lowest order expressions are not precise enough as to reproduce the experimental results within two standard deviations. This is already a signal for the presence of radiative corrections . In view of the much more precise measurements of M_Z and $\sin^2\theta_W$ in forthcoming e^+e^- collisions the inclusion of higher order effects in the relations (1.1-2) for the $M_W \leftrightarrow M_Z \leftrightarrow \sin^2\theta_W$ interdependence becomes mandatory.

But also the relations between $\sin^2\theta_W$ and the asymmetries at the Z resonance are modified after including radiative corrections; they deviate from the simple lowest order expressions like (1.5), for example. Since the higher order contributions turn out to be significantly larger than the expected experimental accuracy in LEP experiments their proper treatment is a necessity for the asymmetries as well. Their experimental verification, in connection with measurements of the boson masses, will be a milestone in establishing the electroweak standard model as a quantized field theory.

Due to their virtual presence in the higher order loop diagrams also those particles of the standard model outfit enter the predictions for processes between the established fermions

which until now have escaped the direct experimental grip: the Higgs boson as the remnant of the spontaneous symmetry breaking, and the top quark as the missing member of the third fermion generation. The present status forces us to introduce their masses as additional independent input parameters which are only very little theoretically and experimentally constrained. Precision experiments being sensitive to the M_H, m_t dependent radiative correction effects may also be understood as probing the presently empirically unknown part of the standard model.

This sensitivity to empirically unknown particles applies in the same way also to all kinds of new objects which are connected with ideas beyond the minimal standard model ("new physics") as far as these objects couple to gauge bosons and/or to the known fermions. Concrete realizations are encountered for example in the concepts of more fermion generations, more Higgs fields, supersymmetry, as well as in the rich variety of phenomenology inspired by superstrings. The radiative corrections hence are going to open a window also to these "new physics effects". This is of particular importance for particles which are too heavy to be produced directly. This has to be considered the second important aspect for the role of radiative corrections in the interplay between theoretical effort and high precision experiments.

From present days experiments there are no indications for structures beyond the minimal model. For this reason we may expect that new physics effects, if present, will manifest themselves in terms of only small deviations from the standard model predictions, of the order of the minimal radiative corrections. In order to isolate possible signals due to extra structures the reliable calculation of the standard model radiative corrections is necessary for establishing a solid background. These standard model radiative corrections are the topic of the present article. For discussions of new physics effects we refer to the current literature, in particular to the reviews by Lynn, Peskin, Stuart [17] and Hollik [18] together with the work quoted therein. They are outside the intention of this article, although the strategy outlined here allows a rather direct continuation to new physics as well.

For concrete higher order calculations the specification of the parameters in terms of which renormalization and presentation of results is performed is necessary. The calculation of radiative corrections to the vector boson masses when derived from G_μ and $\sin^2\theta_W$ (defined by means of neutrino scattering) was done by Veltman [19]. Marciano [20,22] and Sirlin [21,22] applied the electroweak "on-shell scheme" in order to obtain the quantum effects in the correlation between M_Z, M_W, $\sin^2\theta_W$, resulting in the famous formula

$$M_W^2 = \frac{\pi\alpha}{\sqrt{2}G_\mu}\cdot\frac{1}{\sin^2\theta_W(1-\Delta r)} \tag{1.6}$$

replacing (1.1), where Δr summarizes the higher order terms. The relation (1.2) is unchanged; it is rather understood as the definition of the weak mixing angle in terms of the boson masses and hence is valid in all orders of perturbation theory. Moreover, in this way the dependence of $\sin^2\theta_W$ on a specific process has been removed.

The electroweak on-shell scheme is the most natural extension of the familiar on-shell renormalization scheme of QED. It utilizes such quantities for the free parameters of the model which are measurable in physical processes with all particles on their mass shell. These quantities are the masses themselves specifying the particle content of the model (M_W, M_Z, M_H, m_f) together with α as a coupling constant. In a strict sense, G_μ would no longer be an on-shell parameter in the standard model since the W boson involved in

muon decay is off-shell. It can, however, uniquely be expressed in terms of the on-shell quantities by means of (1.6). The advantage of the on-shell scheme is the unambigous physical meaning of the free parameters, their independence of perturbation theory, and the transparency of the renormalization relating the "bare" parameters of the classical Lagrangian to the physically measurable parameters of the quantized renormalized Lagrangian. Since the input for the standard model is more involved than in case of QED or QCD this transparency is appreciated also for comparing the results of various independent calculations and checking their consistency.

Since quite a number of calculations had been performed in the past applying different strategies and renormalization schemes the Trieste Workshop on Radiative Corrections in 1983 [23] was held in order to clarify the somewhat confusing situation at that time. A consensus was found among the participants, and a proposal was made for calculating and organizing higher order effects in the standard model [23] which in further course was also more explicitly documented in the Radiative Correction Study Group report [24], presented by Dydak [25] at the LEP 200 Workshop at Aachen [12] in 1986, and can be summarized as follows: perform calculations in the on-shell scheme and impose the relation (1.6)

$$G_\mu = G_\mu(\alpha, M_W, M_Z, M_H, m_e, m_\mu, \ldots)$$

as a constraint from which M_W can be fixed after the other parameters have been specified. This allows to get rid of the experimental uncertainty induced by M_W.

The on-shell scheme has become popular in a lot of practical applications (see for example [23], [24], and the collection of references given there). In our context we want to mention explicitly only those activities which are tightly related to the topic of this paper: the calculation of the radiative corrections to $e^+e^- \to \mu^+\mu^-$, first performed by Passarino and Veltman [26] for the range outside the Z resonance; with restriction to the electromagnetic subclass by Greco, Pancheri, Srivastava [27], Berends, Kleiss, Jadach [28], and Böhm, Hollik [29]; the complete one-loop calculation for the PETRA/PEP energy range by Böhm, Hollik [30] and the corresponding calculation of the weak subclass by Brown, Decker, Paschos [31]; the inclusion of the resonance range by Wetzel [32], Lynn, Stuart [33], and Hollik [34]. The last two references contain also the radiative corrections to the left-right asymmetry (1.5) and are as yet the only calculations for this important quantity complete in the virtual corrections at the one-loop level. In a similar way Bhabha scattering has also been accomplished [105].

Meanwhile essential progress has also been made in the calculation and implementation of QED corrections in higher than one-loop order [35-38]; in connection with the precise calculation of the Z boson width [39,40] they are essential in forming the Z resonance line shape from which M_Z will be measured. The position of the peak maximum and its relation to M_Z turns out to be insensitive to the values of the other parameters [41,42] which is crucial for M_Z being an independently measurable input quantity. Moreover, the resummation of the large contributions from light and heavy fermions to all orders in the leading terms was performed in [43] and this article. The corresponding effects in $\sin^2\theta_W$ can match the experimental precision, and a comparison between the results of [43] and ours is needed at the high level of accuracy as required nowadays. With the assistance by Burgers [42] we found satisfactory agreement between the two independent calculations.

The intention of this article is threefold:

(i) to give a comprehensive description of the on-shell scheme for practical use and to outline its application to the calculation of radiative corrections, in particular to the $M_W - M_Z - \sin^2\theta_W$ correlation and the fundamental e^+e^- processes $e^+e^- \to f\bar{f}$;

(ii) to collect numerical results for the various accurately measurable quantities where the input parameters are taken from a range of current interest, allowing also a comparison with other work;

(iii) to present a complete collection of all radiative correction formulae in one place needed for discussing the topics of (i) with the required accuracy, except of the hard bremsstrahlung part and the higher order QED terms. The hard photon corrections depend in general on the specific experimental set up and are more conveniently treated by Monte Carlo simulations [28,44]. [3]

The spirit of this article is mainly a practical one. For this reason we restrict ourselves to the minimum part of general formalism necessary for understanding and handling the listed expressions; for details concerned with the more formal part we refer to [45] which has been the starting point for the further development. In some places we deviate from ref. [45]; this will be mentioned explicitly in the corresponding text passages. For other elaborate discussions of the on-shell renormalization see refs. [46-48].

The article is subdivided in six major parts:

First we specify the classical Lagrangian, the basic notations and conventions, and give the ingredients needed for the lowest order description of 4-fermion processes.

The next section outlines the on-shell renormalization as required for our further applications. It contains also the general expressions for the renormalized 2- and 3-point functions which become concrete when combined with the explicit terms of the appendix.

This general part is followed by the application to the muon life time with a discussion of the input parameters and the $M_W - M_Z - \sin^2\theta_W$ correlation.

The treatment of the Z width and e^+e^- processes is performed in the subsequent two sections. The general formulae for the $e^+e^- \to f\bar{f}$ differential cross section include longitudinal as well as transverse initial state polarizations. Numerical results for total and partial Z decay widths, Z line shape, total cross section, and various on-resonance asymmetries are listed and discussed.

Finally, in the appendix we put together the explicit expressions needed for making this paper self-contained and a useful collection of radiative corrections formulae as well. A very condensed listing of the formulae in the on-shell scheme has recently been published in [49]; it is, however, not yet as complete as the present one in the 3- and 4-point functions.

[3] analytical calculations for specific quantitities without applying phase space cuts are contained in [50-53]

Chapter 2

Classical Lagrangian and basic notations

In this section we specify our notation and give the tree level Lagrangian as it will be used as starting point for higher order calculations. Moreover, we want to provide a set of formulae following from the tree level Lagrangian which allows us to perform calculations of measurable quantities in lowest order. This will become of importance when we are going to discuss the magnitude of radiative corrections with respect to the "Born approximation".

According to the general principles of constructing a gauge invariant field theory with a spontaneous symmetry breaking mechanism the gauge, Higgs, and fermion parts of the electroweak classical Lagrangian

$$\mathcal{L}_{cl} = \mathcal{L}_G + \mathcal{L}_H + \mathcal{L}_F \tag{2.1}$$

are specified in the following way:

2.1 Gauge fields

The isotriplet of vector fields W^a_μ, $a = 1,2,3$, and the isosinglet vector field B_μ transforming under gauge transformations according to the adjoint representation of the gauge group SU(2)×U(1) lead to the field strenght tensors

$$W^a_{\mu\nu} = \partial_\mu W^a_\nu - \partial_\nu W^a_\mu + g_2\, \epsilon_{abc}\, W^b_\mu W^c_\nu,$$

$$B_{\mu\nu} = \partial_\mu B_\nu - \partial_\nu B_\mu. \tag{2.2}$$

g_2 denotes the non-abelian SU(2) gauge coupling constant, whereas g_1 is the abelian U(1) coupling. From the field tensors (2.2) the pure gauge field Lagrangian

$$\mathcal{L}_G = -\frac{1}{4} W^a_{\mu\nu} W^{\mu\nu,a} - \frac{1}{4} B_{\mu\nu} B^{\mu\nu} \tag{2.3}$$

is formed.

2.2 Higgs field and Higgs - gauge field interaction

The electric charge operator Q is built from the generators $\vec{I}$ of the weak isospin and the weak hypercharge Y obeying the Gell-Mann Nishijima relation

$$Q = I_3 + \frac{Y}{2}. \tag{2.4}$$

For spontaneous breaking of the SU(2)×U(1) symmetry leaving the electromagnetic gauge subgroup $U(1)_{em}$ unbroken a single complex scalar doublet field with hypercharge $Y = 1$

$$\Phi(x) = \begin{pmatrix} \phi^+(x) \\ \phi^0(x) \end{pmatrix} \tag{2.5}$$

is coupled to the gauge fields

$$\mathcal{L}_H = (D_\mu \Phi)^+ (D^\mu \Phi) - V(\Phi). \tag{2.6}$$

with the covariant derivative

$$D_\mu = \partial_\mu - i\, g_2\, I_a W_\mu^a + i\, \frac{g_1}{2}\, B_\mu \tag{2.7}$$

The Higgs field self interaction

$$V(\Phi) = -\mu^2\, \Phi^+ \Phi + \frac{\lambda}{4} (\Phi^+ \Phi)^2 \tag{2.8}$$

is constructed in a way that it gives rise to spontaneous symmetry breaking. With help of the non-vanishing vacuum expectation value v, related to the coefficients of the potential V by

$$v = \frac{2\mu}{\sqrt{\lambda}}\,, \tag{2.9}$$

the field (2.5) can be written in the following way:

$$\Phi(x) = \begin{pmatrix} \phi^+(x) \\ (v + H(x) + i\chi(x))/\sqrt{2} \end{pmatrix} \tag{2.10}$$

where the components ϕ^+, H, χ now have zero vacuum expectation values.

The real component $H(x)$ describes physical neutral scalar particles with mass

$$M_H = \mu\sqrt{2}. \tag{2.11}$$

The Higgs field components have triple and quartic self couplings following from V, and couplings to the gauge fields via the kinetic term of (2.6). In addition, Yukawa couplings to fermions are introduced in order to make the charged fermions massive.

2.3 Fermion fields, fermion-gauge and fermion-Higgs interaction

The left-handed fermion fields of each lepton and quark family (color index is suppressed)

$$\psi_j^L = \begin{pmatrix} \psi_{j+}^L \\ \psi_{j-}^L \end{pmatrix}$$

with doublet index j are grouped into SU(2) doublets with component index $\sigma = \pm$, and the right-handed fields into singlets

$$\psi_j^R = \psi_{j\sigma}^R .$$

Each left and right-handed multiplet is an eigenstate of the weak hypercharge Y such that the relation (2.4) is fulfilled. The covariant derivative

$$D_\mu = \partial_\mu - i\, g_2\, I_a W_\mu^a + i\, g_1 \frac{Y}{2} B_\mu \tag{2.12}$$

induces the fermion-gauge field interaction. The interaction with the Higgs field is specified in terms of Yukawa couplings:

$$\mathcal{L}_F = \sum_{j\sigma} \left\{ \psi_j^L i\gamma^\mu D_\mu \psi_j^L + \psi_{j\sigma}^R i\gamma^\mu D_\mu \psi_{j\sigma}^R \right\} \tag{2.13}$$

$$+ \mathcal{L}_{Yukawa} .$$

The Yukawa term is conveniently expressed in the doublet field components (2.5). We write it down for one family of leptons and quarks only, neglecting quark mixing:

$$\begin{aligned} \mathcal{L}_{Yukawa} &= -g_l (\overline{\nu}_L \phi^+ l_R + \overline{l}_R \phi^- \nu_L + \overline{l}_L \phi^0 l_R + \overline{l}_R \phi^{0*} l_L) \\ &= -g_d (\overline{u}_L \phi^+ d_R + \overline{d}_R \phi^- u_L + \overline{d}_L \phi^0 d_R + \overline{d}_R \phi^{0*} d_L) \\ &\quad - g_u (\overline{u}_R \phi^+ d_L + \overline{d}_L \phi^- u_R + \overline{u}_R \phi^0 u_L + \overline{u}_L \phi^{0*} u_R) . \end{aligned} \tag{2.14}$$

with Yukawa coupling constants $g_{l,d,u}$ which are related to the masses of the charged fermions by eq. (2.23). ϕ^- denotes the adjoint of ϕ^+.

2.4 Physical parameters

The gauge invariant Higgs-gauge field interaction in the kinetic part of (2.6) leads to mass terms for the vector bosons in the non diagonal form

$$\frac{1}{2}\left(\frac{g_2}{2}v\right)^2 (W_1^2 + W_2^2) + \frac{v^2}{4}\left(W_\mu^3, B_\mu\right) \begin{pmatrix} g_2^2 & g_1 g_2 \\ g_1 g_2 & g_2^2 \end{pmatrix} \begin{pmatrix} W_\mu^3 \\ B_\mu \end{pmatrix} . \tag{2.15}$$

The physical content becomes transparent by performing the transformation from the fields W_μ^a, B_μ (in terms of which the symmetry is manifest) to the "physical" fields

$$W_\mu^\pm = \frac{1}{\sqrt{2}} (W_\mu^1 \pm W_\mu^2) \tag{2.16}$$

and

$$\begin{aligned} Z_\mu &= +\cos\theta_W\, W_\mu^3 + \sin\theta_W\, B_\mu \\ A_\mu &= -\sin\theta_W\, W_\mu^3 + \cos\theta_W\, B_\mu \end{aligned} \tag{2.17}$$

In these fields the mass term (2.15) is diagonal and has the form

$$M_W^2\, W_\mu^+ W^{-\mu} + \frac{1}{2}(A_\mu, Z_\mu) \begin{pmatrix} 0 & 0 \\ 0 & M_Z^2 \end{pmatrix} \begin{pmatrix} A^\mu \\ Z^\mu \end{pmatrix} \tag{2.18}$$

with

$$\begin{aligned} M_W &= \frac{1}{2} g_2 v \\ M_Z &= \frac{1}{2}\sqrt{g_1^2 + g_2^2}\, v \end{aligned} \tag{2.19}$$

if the mixing angle in (2.17) is chosen as

$$\cos\theta_W = \frac{M_W}{M_Z} = \frac{g_2}{\sqrt{g_1^2 + g_2^2}}. \tag{2.20}$$

Identifying A_μ with the photon field which couples via the electric charge $e = \sqrt{4\pi\alpha}$ to the electron, e can be expressed in terms of the gauge couplings in the following way

$$e = \frac{g_1 g_2}{\sqrt{g_1^2 + g_2^2}} \tag{2.21}$$

or

$$g_2 = \frac{e}{\sin\theta_W}, \quad g_1 = \frac{e}{\cos\theta_W}. \tag{2.22}$$

Finally, from the Yukawa coupling terms in (2.14) the fermion masses are obtained:

$$m_{j\sigma} = g_{j\sigma}\, \frac{v}{\sqrt{2}}\,. \tag{2.23}$$

The relations (2.9, 11, 19, 21, 23) allow to replace the original set of parameters

$$g_2, \quad g_1, \quad \lambda, \quad \mu^2, \quad g_{j\sigma} \tag{2.24}$$

by the equivalent set of more physical parameters

$$e, \quad M_W, \quad M_Z, \quad M_H, \quad m_{j\sigma} \tag{2.25}$$

where each of them can be measured directly in a suitable experiment.

For the important class of charged and neutral current processes between fermions the coupling constants for the vector and axial vector currents as they follow from (2.13) can be expressed in terms of e, M_W, M_Z : {notation: $f = (j\sigma)$, $f' = (j\sigma')$}

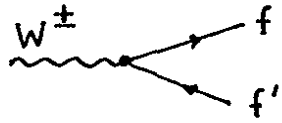

$$= i e \gamma_\mu (1 - \gamma_5) \frac{1}{2\sqrt{2} \sin\theta_W} \tag{2.26}$$

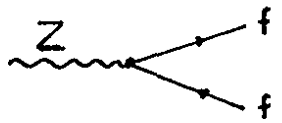

$$= i \epsilon \gamma_\mu (v_f - a_f \gamma_5)$$

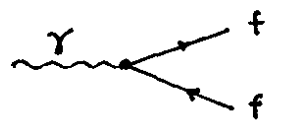

$$= -i e Q_f \gamma_\mu$$

with the neutral current coupling constants

$$\begin{aligned} v_f &= \frac{I_3^f - 2Q_f \sin^2\theta_W}{2 \sin\theta_W \cos\theta_W} \\ a_f &= \frac{I_3^f}{2 \sin\theta_W \cos\theta_W}. \end{aligned} \tag{2.27}$$

Q_f and I_3^f denote charge and third isospin component of f. Together with the photon propagator (Feynman gauge)

$$- \frac{i g^{\mu\nu}}{k^2} \tag{2.28}$$

and the W and Z propagators in the unitary gauge

$$i \frac{-g^{\mu\nu} + k^\mu k^\nu / M_V^2}{k^2 - M_V^2} \tag{2.29}$$

we have a set of rules allowing the calculation of cross sections and lifetimes for neutral and charged current processes at the tree level. Application to the μ decay

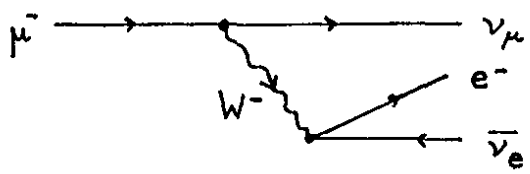

yields the result for the μ lifetime (neglecting powers of m_μ^2/M_W^2):

$$\tau_\mu^{-1} = \frac{\alpha^2}{384\pi} m_\mu^5 \left(1 - \frac{8m_e^2}{m_\mu^2}\right) \frac{1}{M_W^2 \sin^2\theta_W}. \tag{2.30}$$

Identification with the result of the Fermi model with pointlike interaction

$$\tau_\mu^{-1} = \frac{G_\mu^2}{192\pi^3} m_\mu^5 \left(1 - \frac{8m_e^2}{m_\mu^2}\right) \tag{2.31}$$

leads to the relation

$$M_W^2 \sin^2\theta_W = \frac{\pi\alpha}{\sqrt{2}G_\mu}. \tag{2.32}$$

Together with

$$\sin^2\theta_W = 1 - \frac{M_W^2}{M_Z^2} \tag{2.33}$$

this gives a correlation between the mass value M_W and M_Z since α and G_μ are known with practically negligible experimental errors. Moreover, after M_Z has been specified, M_W is also fixed

$$M_W^2 = \frac{M_Z^2}{2}\left(1 + \sqrt{1 - \frac{4A}{M_Z^2}}\right) \tag{2.34}$$

and the neutral and charged current coupling constants (2.26), (2.27) are determined by means of

$$\sin^2\theta_W = \frac{1}{2}\left(1 - \sqrt{1 - \frac{4A}{M_Z^2}}\right) \tag{2.35}$$

where

$$A = \frac{\pi\alpha}{\sqrt{2}G_\mu} = (37.281GeV)^2\,. \tag{2.36}$$

The relations (2.32) and (2.33) are in general modified by the inclusion of radiative corrections depending on the details of a chosen renormalization scheme. In the on-shell scheme (2.33) remains valid also in higher order, and (2.32) is modified according to

$$M_W^2 \sin^2\theta_W = \frac{\pi\alpha}{\sqrt{2}G_\mu}\frac{1}{1-\Delta r} \tag{2.37}$$

where the radiative correction Δr depends on all the parameters (2.25) of the model, in particular on the mass of the Higgs boson M_H and the top quark m_t which do not enter the tree level result (2.32).

Chapter 3

Renormalization

In this section we want to give an overview over the strategy and to put together all the results which we will need for the discussion of 4-fermion processes including radiative corrections.

3.1 Quantization

Since the S matrix element for any physical process is a gauge invariant quantity it is possible to work in the unitary gauge with no unphysical particles in internal lines. For a systematic treatment of the quantization of $\mathcal{L}_{cl}$ and for higher order calculations, however, one better relies to a renormalizable gauge. This can be done by adding to $\mathcal{L}_{cl}$ the gauge fixing Lagrangian

$$\mathcal{L}_{fix} = -\frac{1}{2}\left(F_\gamma^2 + F_Z^2 + 2F_+F_-\right) \tag{3.1}$$

with linear gauge fixings of the 't Hooft type:

$$\begin{aligned} F_\pm &= \frac{1}{\sqrt{\xi^W}}\left(\partial^\mu W_\mu^\pm \mp iM_W\xi^W\phi^\pm\right) \\ F_Z &= \frac{1}{\sqrt{\xi^Z}}\left(\partial^\mu Z_\mu - M_Z\xi^Z\chi\right) \\ F_\gamma &= \frac{1}{\sqrt{\xi^\gamma}}\partial^\mu A_\mu \,. \end{aligned} \tag{3.2}$$

In this class of 't Hooft gauges the vector boson propagators have the form

$$\frac{i}{k^2 - M_V^2}\left(-g^{\mu\nu} + \frac{(1-\xi^V)k^\mu k^\nu}{k^2 - \xi^V M_V^2}\right). \tag{3.3}$$

For completion of the renormalizable Lagrangian the Faddeev-Popov ghost term $\mathcal{L}_{gh}$ has to be added [54] in order to balance the undesired effects in the unphysical components introduced by $\mathcal{L}_{fix}$:

$$\mathcal{L} = \mathcal{L}_{cl} + \mathcal{L}_{fix} + \mathcal{L}_{gh} \tag{3.4}$$

where

$$\mathcal{L}_{gh} = \bar{u}^\alpha(x)\,\frac{\delta F^\alpha}{\delta\theta^\beta(x)}\,u^\beta(x) \tag{3.5}$$

with ghost fields u^γ, u^Z, $u^\pm$, and $\frac{\delta F^\alpha}{\delta\theta^\beta}$ being the change of the gauge fixing operators (3.2) under infinitesimal gauge transformations characterized by $\theta^\alpha(x) = \{\theta^a(x), \theta^Y(x)\}$.

In the 't Hooft-Feynman gauge ($\xi = 1$) the vector boson propagators (3.3) become particularly simple: the transverse and longitudinal components, as well as the propagators for the unphysical Higgs fields $\phi^\pm$, χ and the ghost fields $u^\pm$, u^Z develop poles which coincide with the masses of the corresponding physical particles $W^\pm$ and Z.

This feature is lost if higher order corrections to the 2-point functions are included. Although the individual poles for the unphysical propagators do no longer coincide with the physical ones the validity of the Slavnov-Taylor identities [55] guarantees that those relevant combinations of (unphysical) 2-point functions which enter the S-matrix elements for processes between physical particles arrange the poles of the S-matrix in their correct places.

On the other hand, it is possible to choose the gauge in a form

$$\xi^\alpha = 1 + \delta\xi^\alpha$$

which deviates from the 't Hooft-Feynman gauge by contributions of the one-loop order. The gauge parameters $\delta\xi^\alpha$ may then be adjusted in a way that the pole structure in the unphysical sector remains the same as for $\xi^\alpha = 1$ in lowest order. By investigating the relevant Slavnov-Taylor identities with Higgs and ghost self energies it follows that the renormalization in the unphysical sector (at the one-loop level) can be treated as decoupled from the renormalization in the physical sector (the 2- and 3-point functions for the physical degrees of freedom). Since it is our aim to arrive at a complete one-loop presentation of physical amplitudes for scattering processes between fermions where Higgs contributions can be neglected at the tree level and where longitudinal propagators give only terms of order m_f^2/M_Z^2, it is sufficient that we restrict ourselves to the physical sector. [1] For this reason we disregard in the following discussion all higher order contributions to the longitudinal vector boson propagators (those proportional to $k^\mu k^\nu$) and to the unphysical Higgs and ghost propagators. A complete list of these unphysical propagators can be found in [45].

3.2 The strategy

The tree level Lagrangian (2.1) of the minimal SU(2)×U(1) model involves a certain number of free parameters which are not fixed by the theory. The definition of these parameters and their relation to measurable quantities is the content of a renormalization scheme. The parameters (or appropriate combinations) can be determined from specific experiments with help of the theoretical results for cross sections and lifetimes. After this procedure of defining the physical input other observables can be calculated allowing verification or falsification of the theory by comparison with the corresponding experimental results.

In higher order perturbation theory not only the predictions for observables testing the model are modified but also the relations between the formal input parameters and their defining experiment are different from the tree level relations in general. Moreover, the procedure is obscured by the appearence of divergencies in the higher order contributions which have to be subtracted in a way consistent with the physical interpretation and with

[1] also valid for boson production processes $e^+e^- \to \gamma\gamma, \gamma Z, ZZ, WW$

the Slavnov-Taylor identities. This operation leads to a redefinition of the parameters in the Lagrangian by an infinite amount. Therefore we abandon the use of the parameters in the original "bare" Lagrangian, the "bare" parameters, and express everything in terms of finite "renormalized" parameters (which can be measured) and counter terms which absorb the divergent parts of the loop contributions. Although this would be sufficient to obtain finite S-matrix elements the off-shell Green functions are not finite by themselves even after this renormalization. This reflects the feature that amplitudes of "bare" fields between the vacuum and one-particle states are not the wave functions normalized to unity, due to the presence of self interactions. In order to obtain finite propagators and vertices also the bare fields in $\mathcal{L}$ have to be redefined in terms of renormalized fields. In this way the "bare" Lagrangian is split into a "renormalized" Lagrangian and a counter term Lagrangian which renders the results for all Green functions in a given order finite. Formally this is done by multiplicative renormalization for each field

$$\phi \rightarrow \sqrt{Z_2}\,\phi$$

and for each parameter in $\mathcal{L}$

$$g \rightarrow Z_1\, g$$

with renormalization constants

$$Z_i = 1 + \delta Z_i.$$

The simplest way to obtain a set of finite Green functions consists in the "minimal subtraction scheme" [56] where (in dimensional regularization) the singular part of each divergent diagram is subtracted and the parameters are defined at a certain renormalization mass scale μ. This scheme has become popular in QCD where due to the absence of free fundamental particle states there is no preference for a specific mass scale in the renormalization procedure.

This situation is different in QED and in the electroweak theory. There the classical Thomson scattering and the particle masses set natural scales where the parameters can be defined. In QED the favoured renormalization scheme is the on-shell scheme where $e = \sqrt{4\pi\alpha}$ and the electron, muon, ... masses are used as input parameters. The finite parts of the counter terms are fixed by the renormalization conditions that the fermion propagators have poles at their physical masses, and e becomes the $ee\gamma$ coupling constant in the Thomson limit of Compton scattering. The extraordinary meaning of the Thomson limit for the definition of the renormalized coupling constant is elucidated by the theorem [10] that the exact Compton cross section at low energies becomes equal to the classical Thomson cross section. In particular this means that e resp. α is free of infrared corrections, and that its numerical value is independent of the order of perturbation theory, only determined by the accuracy of the experiment.

The direct and most natural extension of this QED on-shell scheme leads to the on-shell scheme of the electroweak SU(2)×U(1) theory. It was proposed first by Ross and Taylor [57] and became popular in a lot of practical applications [23,24]. Since e and the particle masses are singularly distinguished parameters the physical content becomes best transparent in terms of the set

$$e,\ M_W,\ M_Z,\ M_H,\ m_f \tag{3.6}$$

as input parameters, together with the physical fields

$$W^{\pm}_{\mu},\ Z_{\mu},\ A_{\mu}$$

from (2.16-17).

Since there is no room for the mixing angle θ_W as an independent quantity we take over the simplest definition in terms of the physical W and Z masses

$$\sin^2\theta_W = 1 - \frac{M_W^2}{M_Z^2} \tag{3.7}$$

which was proposed first by Sirlin [21]. This definition is independent of a specific process and is valid to all orders of perturbation theory.

The advantages of the on-shell renormalization scheme are obvious:

- The input parameters have a clear and unambigous physical meaning and can be measured directly in suitable experiments.
- All parameters (except M_H and m_t) are experimentally known.
- The Thomson cross section from which α is obtained is exact to all orders of perturbation theory.
- The one-loop corrections to $e^+e^- \to f\bar{f}$ can be naturally separated into "QED corrections" (which means bremsstrahlung type corrections) and "non-QED" or "weak corrections". This feature is of importance for the implementation of higher order contributions into Monte Carlo programs. Moreover, the bulk of QED corrections comes from the infrared soft photons which couple with the Thomson α to the charged fermion currents.

A conceptual problem seems to arise with the light quark mass parameters as input since neither their precise values nor their physical meaning are unambigously known. Fortunately, in our weak radiative corrections they appear only in the vector boson self energies where their contribution can be replaced by the experimentally known cross section for $e^+e^- \to hadrons$ via a dispersion relation (see the discussion in 4.3). All other finite mass terms are of order m_f^2/M_Z^2 and vanish in the light quark limit.

Quark masses also appear in the virtual and real photonic corrections to processes like $e^+e^- \to q\bar{q}$ and $e^-q \to e^-q$. The singular terms which do not vanish for $m_q \to 0$ in e^+e^- annihilation into quark pairs $e^+e^- \to q\bar{q}(\gamma)$ are cancelled by the inclusion of collinear hard final state bremsstrahlung [58] which corresponds to the proper treatment for realistic experiments. In deep inelastic electron-proton scattering all singular mass terms can be absorbed by a re-definition of the distribution functions for the quarks inside the proton [59].

Therefore, our lack of knowledge about the quark masses is no obstacle for practical applications.

3.3 Multiplicative renormalization

After this qualitative discussion we want to specify the on-shell renormalization scheme quantitatively. Following the general principles to obtain the renormalized Lagrangian plus counter terms we attach multiplicative renormalization constants to each free parameter and each symmetry multiplet of fields in $\mathcal{L}$, eq. (3.4):

$$\begin{aligned}
W_\mu^a &\to \left(Z_2^W\right)^{1/2} W_\mu^a \\
B_\mu &\to \left(Z_2^B\right)^{1/2} B_\mu \\
\psi_j^L &\to \left(Z_L^j\right)^{1/2} \psi_j^L \\
\psi_{j\sigma}^R &\to \left(Z_R^{j\sigma}\right)^{1/2} \psi_{j\sigma}^R \\
\Phi &\to \left(Z^\Phi\right)^{1/2} \Phi \\
g_2 &\to Z_1^W \left(Z_2^W\right)^{-3/2} g_2 \\
g_1 &\to Z_1^B \left(Z_2^B\right)^{-3/2} g_1 \\
v &\to \left(Z^\Phi\right)^{1/2} (v - \delta v) \\
g_{j\sigma} &\to \left(Z^\Phi\right)^{-1/2} Z_1^{j\sigma}\, g_{j\sigma}
\end{aligned} \tag{3.8}$$

The renormalization transformations for μ^2, λ, and the ghost fields are not listed explicitely here since we do not need them for the fermionic processes at the one-loop level. For completeness we again refer to [45].

A couple of remarks are in order:

Field renormalization ensures that we arrive at finite Green functions. For physical S matrix elements the results obtained in this way are equivalent to those derived without field renormalization, as done in [21,22] . The field renormalization in (3.8) is performed in a way that it respects the gauge symmetry by introducing the minimal number of field renormalization constants. Therefore also the counter term Lagrangian and the renormalized Green functions reflect the gauge symmetry. The price for this, however, is that not all residues of the propagators can be normalized to one. As a consequence, any calculation with the renormalized Lagrangian will have to include finite multiplicative wave function renormalization factors for some of the external lines in S matrix elements.

It is of course possible to perform the renormalization in such a way that these finite corrections do not appear [46,48,60]. But then the Lagrangian will contain many constants which have to be calculated in terms of the few fundamental parameters.

The renormalization of the Higgs vacuum expectation value v absorbs the linear term in the Higgs potential, which comes in by the appearance of tadpole diagrams in one-loop order, in such a way that the relation

$$v = \frac{2\mu}{\sqrt{\lambda}}$$

remains valid for the renormalized parameters. As a practical consequence of this tadpole renormalization all tadpole graphs can be omitted in the renormalized vector boson 2-point functions. They are, however, necessary to make the mass counter terms gauge independent.

Table 3.1: Strategy for one-loop calculations

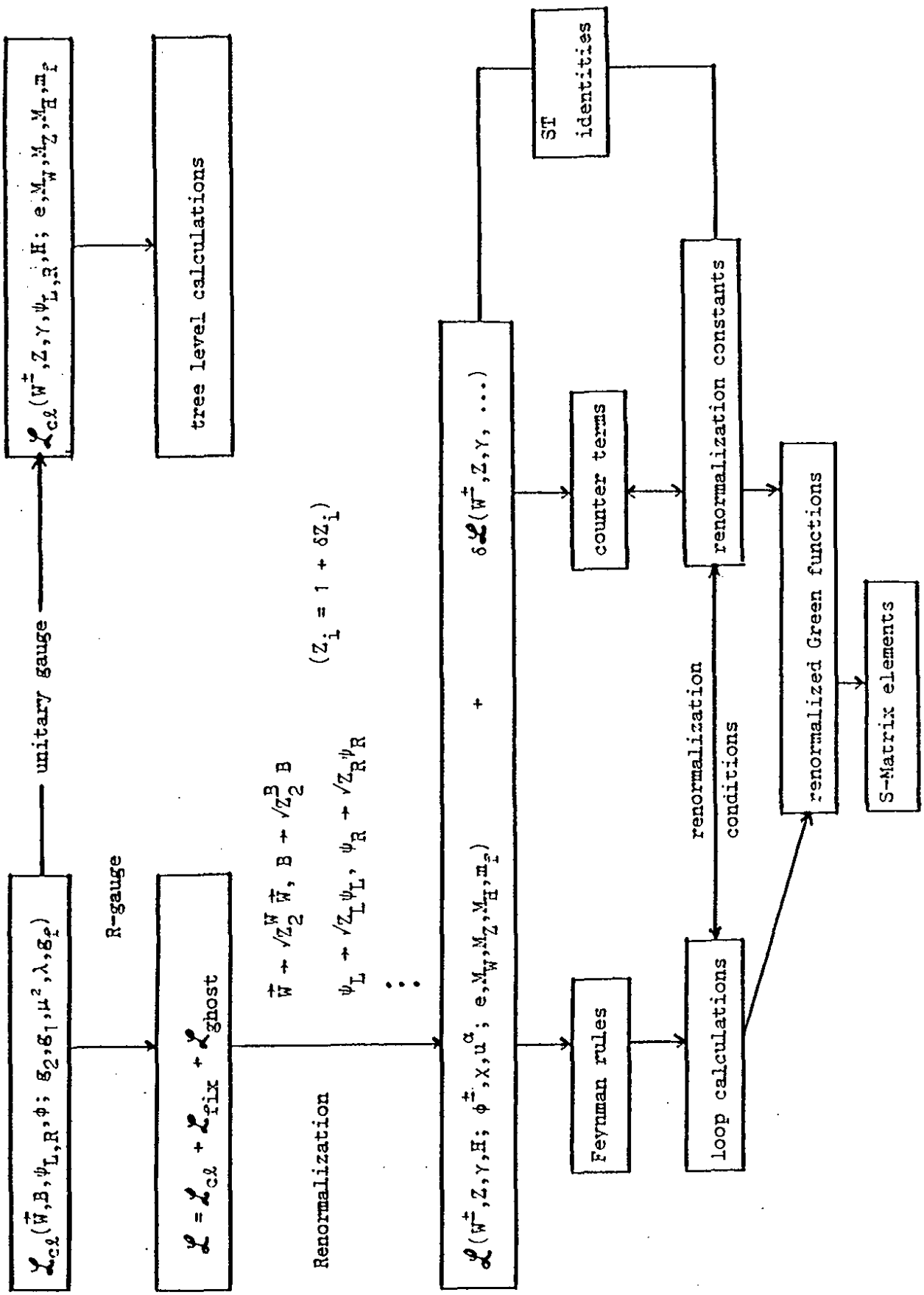

The systematic way for obtaining results for physical amplitudes in one-loop order is scheduled in table 3.1. The expansion

$$Z_i = 1 + \delta Z_i$$

of the renormalization constants introduced via (3.8) yields the renormalized Lagrangian $\mathcal{L}$ which can now be re-parametrized in terms of the physical parameters (3.6) and the physical fields A_μ, Z_μ, $W_\mu^\pm$, H (also the unphysical Higgs field components $\phi^\pm$, χ, and the ghost fields u are present in the R_ξ gauge), and the counter term Lagrangian $\delta\mathcal{L}$. From $\delta\mathcal{L}$ the counter term Feynman rules are derived. After rewriting them in terms of (3.6) the counter term graphs have to be added to the loop integrals which follow from $\mathcal{L}$. The renormalization constants in (3.8) are fixed afterwards by imposing the appropriate renormalization conditions which define the physical meaning of the used parameters. The results are finite Green functions in terms of (3.6) from which the S matrix elements for all processes of interest can be obtained. The validity of Slavnov-Taylor (ST) identities allows to control the consistency of the procedure and to check the correctness of the calculations.

When all the renormalization constants have been fixed in this way the counter terms for any matrix element of a physical process in one-loop order are already determined by the structure of $\delta\mathcal{L}$.

The side path outlined in the upper right corner of table 3.1 leads to the tree level results which have been put together in section 2.4 for the fermion - gauge boson interaction.

3.4 Renormalization conditions

The renormalization conditions for the physical degrees of freedom can be separated into two classes: the on-shell subtraction of the self energies which makes the particle content of the theory evident, and the generalization of the QED charge renormalization. Since we have introduced more renormalization constants than physical parameters we are free to fix the supernumerary ones by the requirement of residue = 1 for a corresponding number of propagators. In order to be as close as possible to the common QED renormalization these residue conditions are imposed on the photon and the charged lepton propagators.

The on-shell subtraction conditions can be written in a graphical way where the shaded blobs denote the *renormalized* one-particle irreducible amputated 2-point functions (self energies) which consist of the diagrams in Figures 3.1-5 together with the corresponding counter terms from Appendix A:

(3.9)

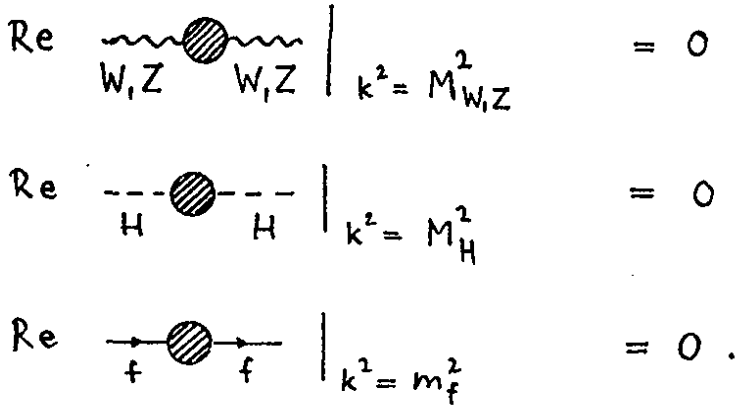

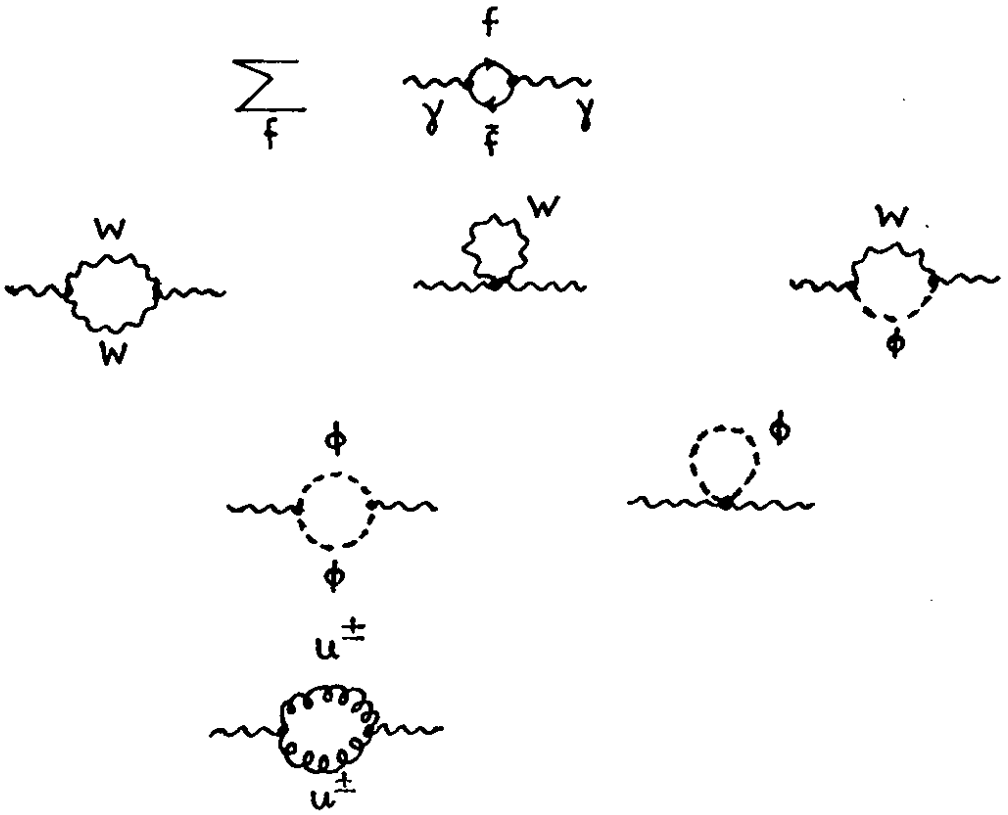

Figure 3.1: Photon self energy

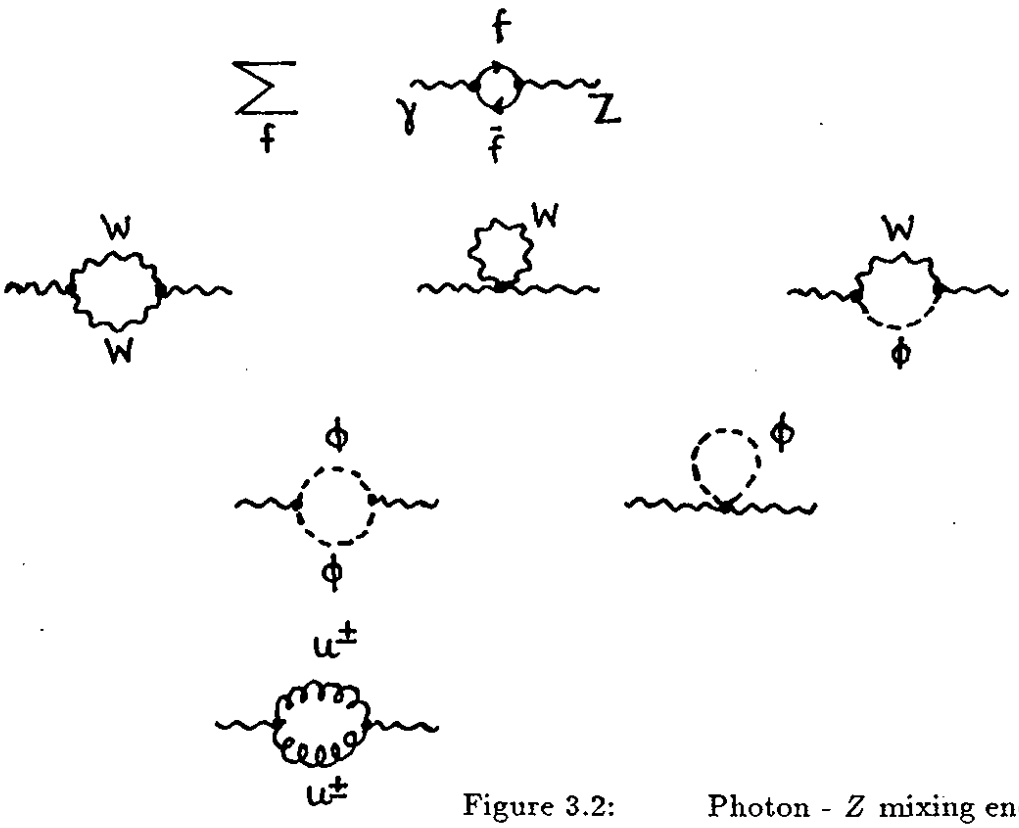

Figure 3.2: Photon - Z mixing energy

Figure 3.3: Z boson self energy

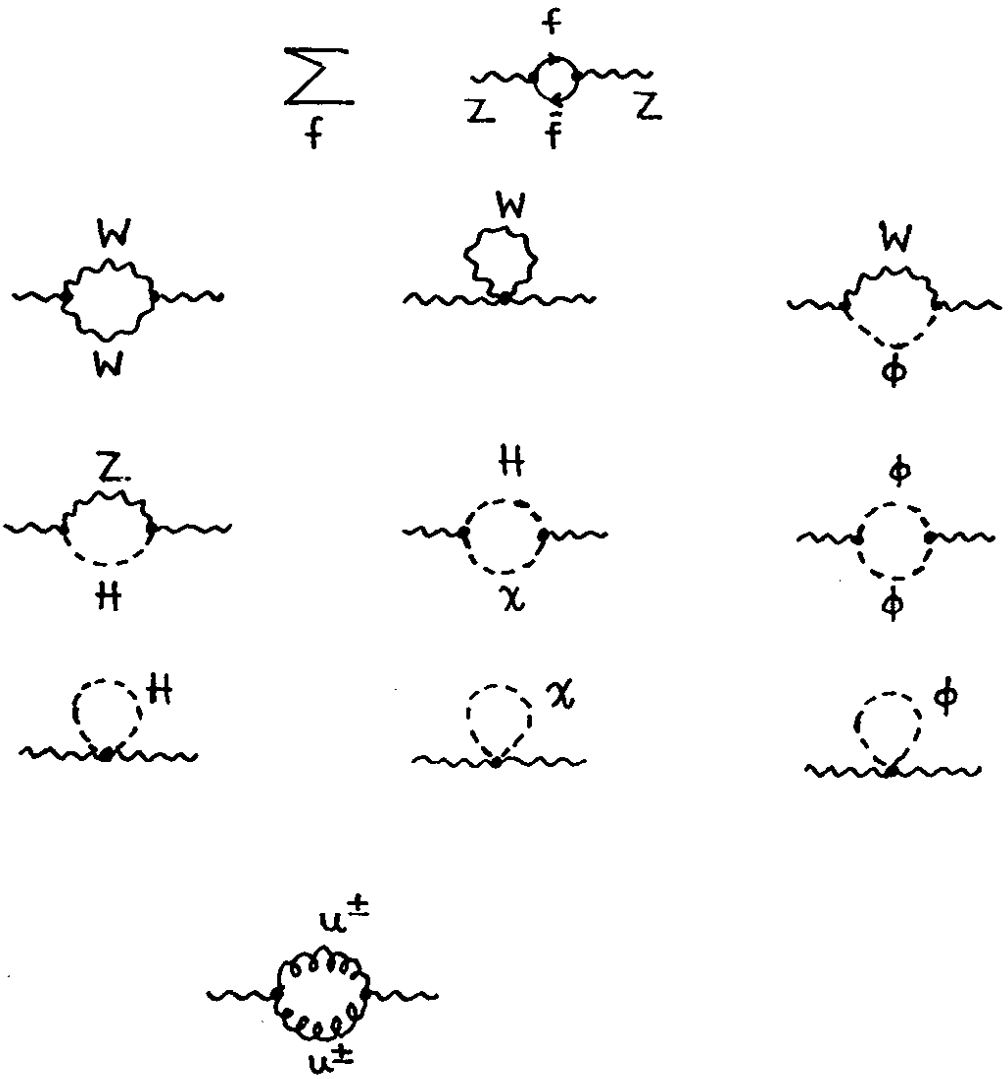

Figure 3.4: W boson self energy

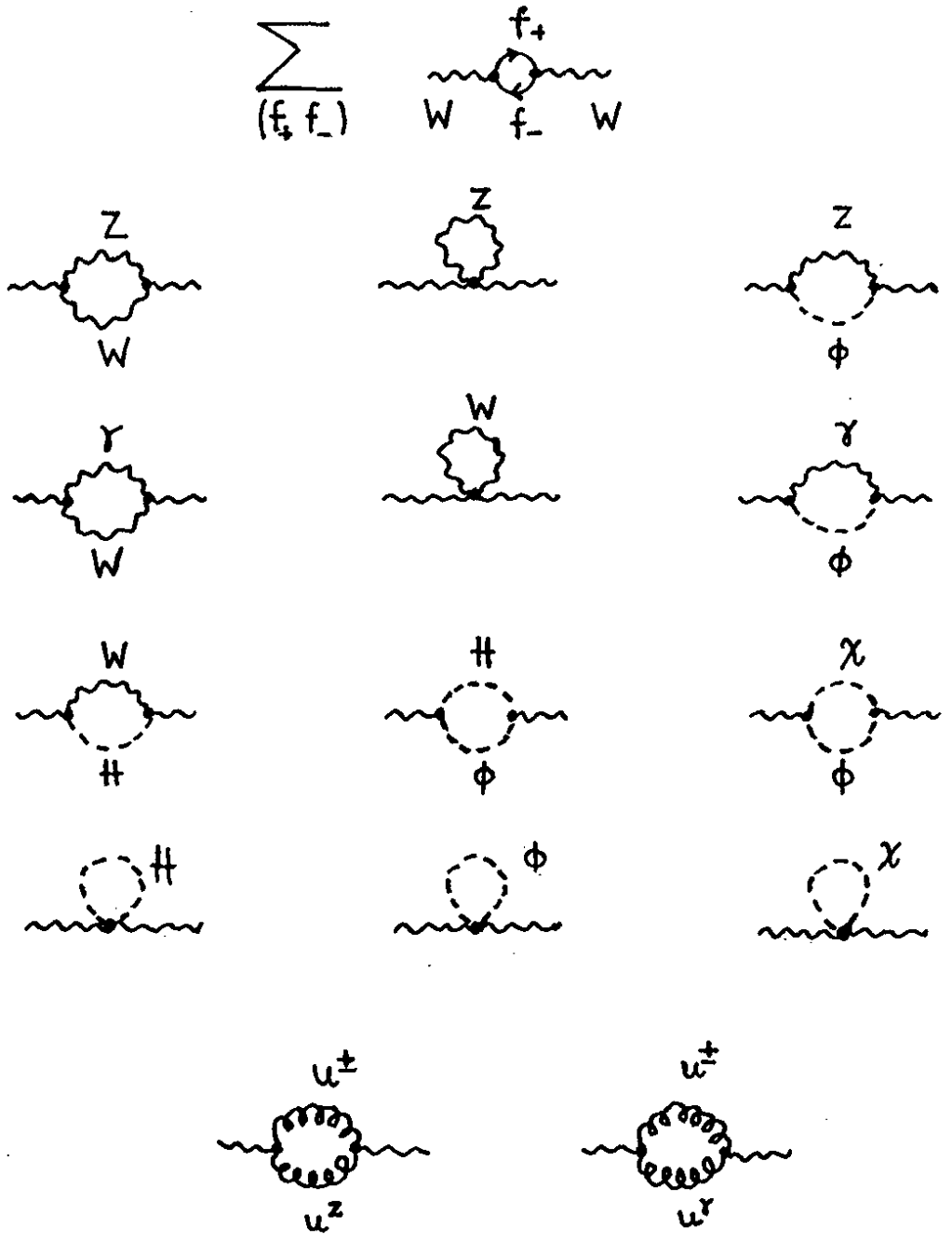

With the renormalized irreducible γee vertex (Figure 3.6 plus counter terms)

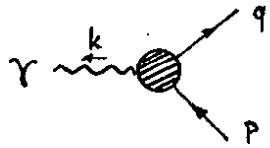

the second class of renormalization conditions can be depicted as follows:

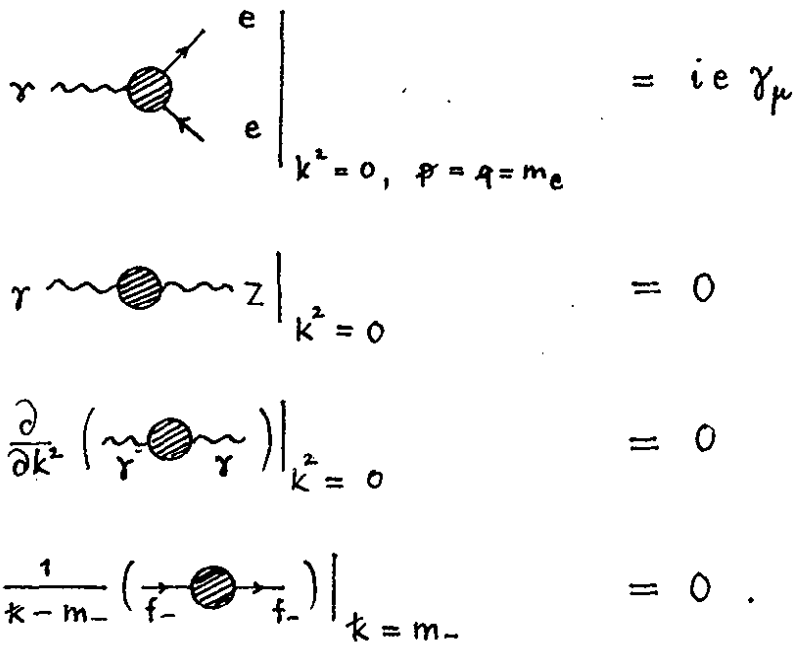

(3.10)

The last condition is formulated for charged leptons and quarks with $I_3 = -1/2$. It means a condition for the left and right handed fermion field renormalization constants Z_L, Z_R^-. In the case of leptons Z_L also determines the neutrino field renormalization. For the $I_3 = +1/2$ quarks an additional Z_R^+ for the right handed fields is at our disposal. This constant can be adjusted in a way that the renormalized left and right handed parts of the up-type propagators have equal residues at $k^2 = m_+^2$ (but $\neq 1$).

In order to write (3.9-10) in analytical form we have to specify first the normalization of the irreducible self energies:

The self energies Σ^j ($j = \gamma,\ Z,\ W,\ \gamma Z$) are related to the transverse components of the vector boson propagators $D^j_{\mu\nu}$ by ($V = \gamma,\ Z,\ W$)

$$\begin{aligned} D^V_{\mu\nu}(k) &= -ig_{\mu\nu}\left(\frac{1}{k^2 - M_V^2} - \frac{1}{k^2 - M_V^2}\,\Sigma^V(k^2)\,\frac{1}{k^2 - M_V^2}\right) \\ D^{\gamma Z}_{\mu\nu}(k) &= +ig_{\mu\nu}\,\frac{1}{k^2 - M_Z^2}\,\Sigma^{\gamma Z}(k^2)\,\frac{1}{k^2}. \end{aligned} \tag{3.11}$$

The fermion self energy Σ^f is related to the fermion propagator in the following way:

$$S_F^f(k) = \frac{i}{\not k - m_f} - \frac{i}{\not k - m_f}\,\Sigma^f(k)\,\frac{1}{\not k - m_f}. \tag{3.12}$$

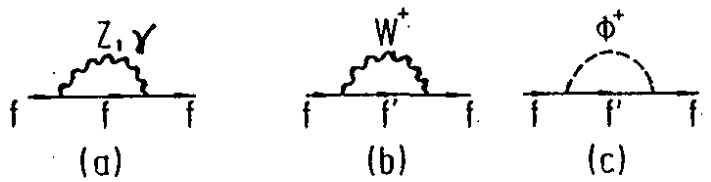

Figure 3.5: Fermion self energy

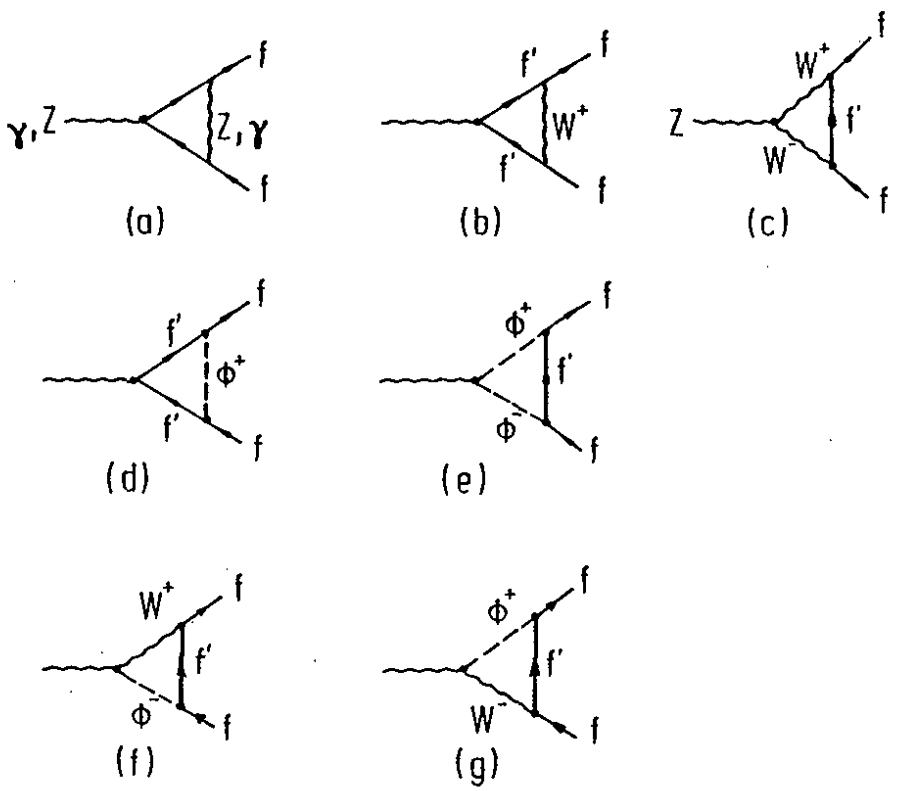

Figure 3.6: Vertex corrections

Σ^f can be decomposed according to

$$\begin{aligned}\Sigma^f(k) &= \not{k}\,\Sigma_V^f(k^2) + \not{k}\,\gamma_5\,\Sigma_A^f(k^2) + m_f\,\Sigma_S^f(k^2) \\ &= \not{k}\,\frac{1-\gamma_5}{2}\,\Sigma_L^f(k^2) + \not{k}\,\frac{1+\gamma_5}{2}\,\Sigma_R^f(k^2) + m_f\,\Sigma_S^f(k^2)\end{aligned} \tag{3.13}$$

with invariant functions $\Sigma^f_{V,A,S}$ resp. $\Sigma^f_{L,R,S}$.

All renormalized quantities are denoted by the same symbols as the corresponding unrenormalized ones in connection with a superscript $\hat{}$.

Then the conditions (3.9) read [2]:

$$\mathrm{Re}\,\hat{\Sigma}^W(M_W^2) = \mathrm{Re}\,\hat{\Sigma}^Z(M_Z^2) = \mathrm{Re}\,\hat{\Sigma}^f(m_f^2) = 0\,. \tag{3.14}$$

The equations corresponding to (3.10) are:

$$\begin{aligned}\hat{\Gamma}^{\gamma ee}_\mu(k^2=0, \not{p}=\not{q}=m_e) &= ie\gamma_\mu \\ \hat{\Sigma}^{\gamma Z}(0) &= 0 \\ \frac{\partial\hat{\Sigma}^\gamma}{\partial k^2}(0) &= 0 \\ \lim_{\not{k}\to m_-}\frac{1}{\not{k}-m_-}\,\hat{\Sigma}^f(k)\,u_-(k) &= 0\end{aligned} \tag{3.15}$$

if u_- is the wave function for the $I_3 = -1/2$ particle.

The renormalized quantities are composed by the unrenormalized ones and the counter terms as specified in Appendix A. The system of equations (3.14) and (3.15) can be inverted to give the renormalization constants needed for the gauge propagators and the gauge field - fermion vertices.

3.5 Renormalization constants

The solution of the system (3.14,15) yields all those renormalization constants which we need for the vector boson propagators, the fermion - gauge boson vertex corrections, and the fermion wave function renormalization. We write them down in terms of the unrenormalized expressions which can be found in analytical form in the appendix.

The mass counter terms for the W and Z self energies follow immediately from the unrenormalized on-shell values by means of (3.14):

$$\begin{aligned}\delta M_W^2 &= \mathrm{Re}\,\Sigma^W(M_W^2) \\ \delta M_Z^2 &= \mathrm{Re}\,\Sigma^Z(M_Z^2)\,.\end{aligned} \tag{3.16}$$

[2] In the following we skip the Higgs subtraction since we do not need it for our applications

Their dependence on the $Z_i^{\gamma,Z}$ $(i = 1,2)$, which is specified in the appendix, together with the set of equations (3.15) yields (see also the discussion in 3.6.2):

$$\begin{aligned}
\delta Z_2^\gamma &= -\Pi^\gamma(0) \equiv -\frac{\partial \Sigma^\gamma}{\partial k^2}(0) \qquad (3.17)\\
\delta Z_1^\gamma &= -\Pi^\gamma(0) - \frac{s_W}{c_W}\frac{\Sigma^{\gamma Z}(0)}{M_Z^2}\\
\delta Z_2^Z &= -\Pi^\gamma(0) - 2\frac{c_W^2 - s_W^2}{s_W c_W}\frac{\Sigma^{\gamma Z}(0)}{M_Z^2} + \frac{c_W^2 - s_W^2}{s_W^2}\left(\frac{\delta M_Z^2}{M_Z^2} - \frac{\delta M_W^2}{M_W^2}\right)\\
\delta Z_1^Z &= -\Pi^\gamma(0) - \frac{3c_W^2 - 2s_W^2}{s_W c_W}\frac{\Sigma^{\gamma Z}(0)}{M_Z^2} + \frac{c_W^2 - s_W^2}{s_W^2}\left(\frac{\delta M_Z^2}{M_Z^2} - \frac{\delta M_W^2}{M_W^2}\right)\\
\delta Z_2^W &= -\Pi^\gamma(0) - 2\frac{c_W}{s_W}\frac{\Sigma^{\gamma Z}(0)}{M_Z^2} + \frac{c_W^2}{s_W^2}\left(\frac{\delta M_Z^2}{M_Z^2} - \frac{\delta M_W^2}{M_W^2}\right)
\end{aligned}$$

The last constant δZ_2^W is not independent but is a linear combination of δZ_2^γ and δZ_2^Z (see Appendix A). It is given here for completeness since we will need it in further course. As an abbreviation we have introduced the notations

$$s_W = \sin\theta_W, \quad c_W = \cos\theta_W. \qquad (3.18)$$

For the fermion fields we obtain for the doublet renormalization constants δZ_L and the singlet renormalization constants δZ_R^- in the $I_3 = -1/2$ states from (3.15):

$$\begin{aligned}
\delta Z_L &= -\Sigma_L(m_-^2) - m_-^2\left[\Sigma_L'(m_-^2) + \Sigma_R'(m_-^2) + 2\Sigma_S'(m_-^2)\right] \qquad (3.19)\\
\delta Z_R^- &= -\Sigma_R(m_-^2) - m_-^2\left[\Sigma_L'(m_-^2) + \Sigma_R'(m_-^2) + 2\Sigma_S'(m_-^2)\right]
\end{aligned}$$

The $\Sigma_{L,..}$ are the invariant functions of (3.13), and $\Sigma_{L,..}'$ denotes the derivative

$$\Sigma_{L,..}'(k^2) = \frac{\partial \Sigma_{L,..}}{\partial k^2}.$$

Rearranging the constants in (3.19) by

$$\delta Z_V^- = \frac{1}{2}(\delta Z_L + \delta Z_R^-), \quad \delta Z_A^- = \frac{1}{2}(\delta Z_L - \delta Z_R^-)$$

(3.19) can also be written as

$$\begin{aligned}
\delta Z_V^- &= -\Sigma_V(m_-^2) - m_-^2\left[\Sigma_V'(m_-^2) + 2\Sigma_S'(m_-^2)\right]\\
\delta Z_A^- &= +\Sigma_A(m_-^2). \qquad (3.20)
\end{aligned}$$

In the case of leptons δZ_L in (3.19) renormalizes immediately also the neutrino propagator with the consequence that its residue is different from 1 by the finite amount

$$\Sigma_L^\nu(0) + \delta Z_L. \qquad (3.21)$$

Therefore, in external ν lines a finite wave function renormalization factor

$$1 + \frac{1}{2}(\Sigma_L^\nu(0) + \delta Z_L) \qquad (3.22)$$

has to be inserted.

For the right handed u-type quarks an additional condition has to be imposed in order to fix δZ_R^+. We will treat the $I_3 = +1/2$ quarks in a way that the residues for their left and right handed propagators become equal. This looks somewhat arbitrary. In S matrix elements, however, in the sum

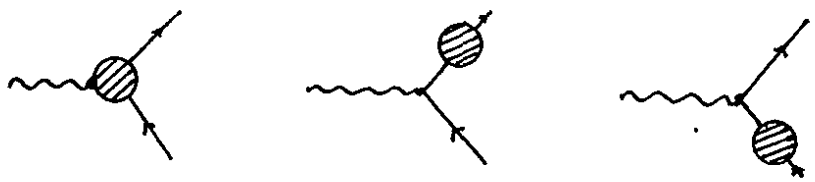

this unsymmetric treatment is compensated by the corresponding renormalized 3-point vertices.

3.6 Renormalized self energies and vertex corrections

After the determination of the renormalization constants in (3.16)-(3.19) we are now able to write down the final form for the renormalized self energies and vertices as we will use them in the subsequent applications to fermionic processes.

3.6.1 Vector boson self energies

The renormalized diagonal and non-diagonal self energies are:

$$\begin{aligned}
\hat{\Sigma}^\gamma(k^2) &= \Sigma^\gamma(k^2) - \Pi^\gamma(0)\cdot k^2 \qquad (3.23)\\
\hat{\Sigma}^{\gamma Z}(k^2) &= \Sigma^{\gamma Z}(k^2) - \Sigma^{\gamma Z}(0) - k^2 \frac{c_W s_W}{c_W^2 - s_W^2}\left(\delta Z_2^Z - \delta Z_2^\gamma\right)\\
&= \Sigma^{\gamma Z}(k^2) - \Sigma^{\gamma Z}(0) + k^2\left\{2\frac{\Sigma^{\gamma Z}(0)}{M_Z^2} - \frac{c_W}{s_W}\left(\frac{\delta M_Z^2}{M_Z^2} - \frac{\delta M_W^2}{M_W^2}\right)\right\},\\
\hat{\Sigma}^Z(k^2) &= \Sigma^Z(k^2) - \delta M_Z^2 + \delta Z_2^Z(k^2 - M_Z^2),\\
\hat{\Sigma}^W(k^2) &= \Sigma^W(k^2) - \delta M_W^2 + \delta Z_2^W(k^2 - M_W^2)
\end{aligned}$$

with δZ_2^Z and δZ_2^W from (3.17).

If "new physics" would be present in form of new particles which couple to the gauge bosons but not directly to the external fermions in a 4-fermion process like $e^+e^- \to \mu^+\mu^-$ the formulae (3.23) are general enough that those effects can be built in. For a discussion of new physics effects we refer to [17,18] and the work quoted therein.

3.6.2 Vertex corrections

The electromagnetic vertex for on-shell fermions

For general fermions f (but $f \neq t$), with momenta p and q the unrenormalized contribution to the electromagnetic vertex Γ_μ is given by the sum of the diagrams in Figure 3.6, denoted by Λ_μ:

$$\Gamma_\mu^{\gamma f f}(k^2) = -ie\,Q_f\,\gamma_\mu - ie\,\Lambda_\mu^{\gamma f} \tag{3.24}$$

with $(k^2 = (p-q)^2)$

$$\begin{aligned}\Lambda_\mu^{\gamma f} &= \gamma_\mu\,\Lambda_V^{\gamma f}(k^2) - \gamma_\mu\gamma_5\,\Lambda_A^{\gamma f}(k^2) + (p+q)_\mu\,\frac{F_M^{\gamma f}(k^2)}{m_f} \\ &= \gamma_\mu\left[\Lambda_V^{\gamma f}(0) + F_V^{\gamma f}(k^2)\right] - \gamma_\mu\gamma_5\left[\Lambda_A^{\gamma f}(0) + F_A^{\gamma f}(k^2)\right] + (p+q)_\mu\,\frac{F_M^{\gamma f}(k^2)}{m_f}\end{aligned} \tag{3.25}$$

In (3.25) the finite form factors $F_{V,A}$ have been split off which fulfill the relations

$$F_{V,A}(0) = 0\,. \tag{3.26}$$

The condition of charge renormalization can be formulated as a condition for the vector part $\Lambda_V^{\gamma e}(0)$ of the electron vertex correction: [3]

$$-\Lambda_V^{\gamma e}(0) + \delta Z_V^e + \delta Z_1^\gamma - \delta Z_2^\gamma + \frac{4s_W^2 - 1}{4s_W c_W}\,\frac{\Sigma^{\gamma Z}(0)}{M_Z^2} = 0\,. \tag{3.27}$$

which fixes the charge renormalization constant δZ_1^γ in the counter term.

The validity of the $U(1)_Y$ Ward identity, which is formally identical to the QED Ward identity [61], yields the following relation between the field and coupling renormalization constants for the U(1) part:

$$\delta Z_1^B = \delta Z_2^B\,.$$

Using the appendix formula (A.1) together with the structure of the mixing counter term in (A.2) and the condition $\hat{\Sigma}^{\gamma Z}(0) = 0$ the following identity for the photon field and charge renormalization constants is obtained:

$$\delta Z_1^\gamma - \delta Z_2^\gamma = -\frac{s_W}{c_W}\,\frac{\Sigma^{\gamma Z}(0)}{M_Z^2}\,. \tag{3.28}$$

This identity shows that the charge renormalization constant δZ_1^γ, although fixed in terms of an electron specific process, is general and fermion independent. In combination with (3.27) we obtain:

$$-\Lambda_V^{\gamma e}(0) + \delta Z_V^e = \frac{1}{4s_W c_W}\,\frac{\Sigma^{\gamma Z}(0)}{M_Z^2}\,. \tag{3.29}$$

The r.h.s. is a universal quantity which does not depend on the specific fermion type of the vertex. It has its origin in the non-abelian boson loops in the $\gamma - Z$ mixing, Figure 3.2. The

[3] The form (3.27) follows from Appendix A, eqs. (A.2) and (A.7), together with the mixing condition $\hat{\Sigma}^{\gamma Z}(0) = 0$

virtual photon and Z exchanges in the vertex corrections, Figure 3.6, are cancelled by the corresponding contributions in the on-shell electron self energy, Figure 3.5. Individually they depend on the fermion type.

The generalization of the QED Ward identity to the non-abelian case leads to further identities [45] like the following one:

$$-k^\mu \left(\Lambda_\mu^{\gamma e}(k^2) + \Lambda_\mu^{\gamma\nu}(k^2)\right) = \Sigma^e(p) - \Sigma^e(q)\,. \tag{3.30}$$

Evaluation of (3.30) for the vector part and writing the electromagnetic neutrino vertex as

$$\Lambda_\mu^{\gamma\nu} = \gamma_\mu(1-\gamma_5)\,\Lambda^{\gamma\nu}(k^2) \tag{3.31}$$

yields with help of (3.27):

$$\Lambda^{\gamma\nu}(0) - \frac{1}{4s_W c_W}\frac{\Sigma^{\gamma Z}(0)}{M_Z^2} = 0\,. \tag{3.32}$$

Evaluating the axial vector part of (3.30) we find:

$$\Lambda_A^{\gamma e}(0) - \delta Z_A^e + \frac{1}{4s_W c_W}\frac{\Sigma^{\gamma Z}(0)}{M_Z^2} = 0\,. \tag{3.33}$$

A look into Appendix A.3 shows us that the l.h.s are the renormalized neutrino and axial electron form factors. The relations (3.32,33) state that the renormalized electromagnetic axial current of the electron and the electromagnetic neutrino current vanish for $k^2 = 0$, i.e for real photons.

The renormalized vector and axial vector form factors for the electron and the neutrino electromagnetic current consist therefore of the contributions from the diagrams in Figure 3.6 (Higgs contributions can be neglected) which have been subtracted at the real photon momentum squared $k^2 = 0$.

The diagram with the non-abelian 3-boson coupling in Figure 3.6 is universal, i.e. independent of the specific fermions. All fermion dependences in $\Lambda_{V,A}^{\gamma f}(0)$ are compensated by the $\delta Z_{V,A}$ for the corresponding fermions. As a consequence, all electromagnetic vertex corrections, together with the finite Z factors for external u-type quarks, can be written in terms of renormalized vector and axial vector form factors [4]

$$\hat{\Gamma}_\mu^{\gamma f f} = -ie\,Q_f\,\gamma_\mu - ie\,\gamma_\mu\left(F_V^{\gamma f}(k^2) - \gamma_5\,F_A^{\gamma f}(k^2)\right) \tag{3.34}$$

which vanish for real photons:

$$F_{V,A}^{\gamma f}(0) = 0\,. \tag{3.35}$$

The analytical expressions for the form factors are listed in Appendix C. Note that their light fermion approximation ($f \neq b, t$) deviate from the form given in [45]: the finite external wave function renormalization for the $I_3 = +1/2$ fermions which always go together with the corresponding vertex corrections are included in the formulae of this appendix.

Heavy fermions were not accounted for in [45].

[4] the magnetic form factors do not play a role for light fermions in high k^2 processes and we will skip them here

The weak neutral current vertex

Since we have exhausted meanwhile our store of renormalization constants the form of all other vertex corrections is already fixed.

The condition for the renormalized $\gamma - Z$ mixing

$$\hat{\Sigma}^{\gamma Z}(0) = 0 \tag{3.36}$$

in connection with the form of the mixing counter term (A.2) in Appendix A determines the weak neutral current renormalization constant δZ_1^Z:

$$\begin{aligned} \delta Z_1^Z - \delta Z_2^Z &= \delta Z_1^\gamma - \delta Z_2^\gamma - \frac{c_W^2 - s_W^2}{c_W s_W} \frac{\Sigma^{\gamma Z}(0)}{M_Z^2} \\ &= -\frac{c_W}{s_W} \frac{\Sigma^{\gamma Z}(0)}{M_Z^2} . \end{aligned} \tag{3.37}$$

Quite in analogy to the electromagnetic vertex renormalization this process independent term renormalizes the non-abelian vertex contributions in the diagrams of Figure 3.6, whereas the fermion type dependent contributions are renormalized by the external fermion legs. As a consequence, also the renormalized neutral current vertices have the same structure as the electromagnetic ones; their form factors vanish at $k^2 = 0$ if external wave function renormalization is included:

$$\hat{\Gamma}_\mu^{Zff} = ie\gamma_\mu(v_f - a_f\gamma_5) + ie\gamma_\mu\left(F_V^{Zf}(k^2) - \gamma_5 F_A^{Zf}(k^2)\right) \tag{3.38}$$

with

$$F_V^{Zf}(0) = F_A^{Zf}(0) = 0 . \tag{3.39}$$

The form factors can also be found in Appendix C (the remark for the electromagnetic vertex on p. 32 applies also here).

In summary, the result of our renormalization procedure can be converted into a simple recipe for obtaining the renormalized γ and Z vector and axial vector vertices including external finite wave function renormalization (for light fermions $f \neq b, t$)) :

Calculate the sum of all contributing one-loop vertex diagrams and subtract its value at the momentum transfer $k^2 = 0$.

The vertex corrections typically amount to the order of 1%. In applications where only a few percent accuracy is required it is therefore justified to restrict oneself to the 2-point functions if a simplified discussion is wanted.

Concluding this section, it should be noted that the renormalized vertex corrections can be obtained by a straight-forward evaluation of the renormalization conditions in section 3.5 without relying explicitly on Ward identities. The utilization of Ward identities, however, is helpful for a deeper understanding and for cross checking the results.

Chapter 4

Input parameters

The electroweak part of 4-fermion processes can be described with help of essentially three parameters (besides the Higgs and fermion masses). These parameters have been chosen to be α and M_W, M_Z because the renormalization conditions get a simple form and the physical transparency is most obvious. The Z mass will be measured with an accuracy of ± 50 MeV, probably ± 20 MeV [11,14] at the e^+e^- colliders LEP and SLC. On the other hand, the W mass M_W will not be known as precisely as to make the induced uncertainty in the radiative corrections negligible ($\Delta M_W = \pm 100$ MeV with LEP 200 [12]).

There is, however, a further well measured quantity: the muon lifetime τ_μ resp. the effective Fermi coupling constant G_μ which can be used to calculate M_W when M_Z has been specified. This requires the consideration of the radiative corrections to the muon decay process in the standard model. For concrete calculations we choose the 't Hooft-Feynman gauge.

4.1 Radiative corrections to the muon lifetime

The lowest order matrix element for $\mu^- \to \nu_\mu \bar{\nu}_e e^-$ in the Standard Model is represented by the W exchange diagram

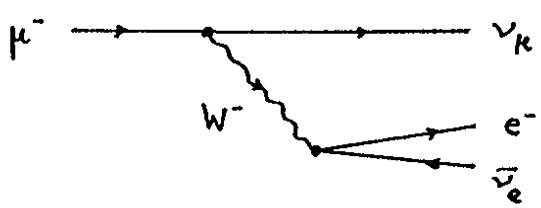

and reads (neglecting terms $\sim m_\mu^2/M_W^2$):

$$\mathcal{M}_B = -\frac{ie^2}{8s_W^2 M_W^2}\,\bar{u}'_\nu \gamma_\rho (1-\gamma_5) u_\mu \cdot \bar{u}'_e \gamma^\rho (1-\gamma_5) v'_\nu \,. \tag{4.1}$$

(4.1) leads to the Born formula for the μ lifetime

$$\frac{1}{\tau_\mu^0} = \frac{\alpha^2}{384\pi}\,\frac{m_\mu^5}{M_W^4 s_W^4}\left(1 - \frac{8m_e^2}{m_\mu^2}\right) \tag{4.2}$$

which, if identified with the Fermi model result

$$\frac{1}{\tau_\mu^F} = \frac{G_\mu^2 m_\mu^5}{192\pi^3}\left(1 - \frac{8m_e^2}{m_\mu^2}\right) \tag{4.3}$$

yields the tree level relation

$$M_W^2\, s_W^2 = \frac{\pi\alpha}{\sqrt{2}G_\mu}\,. \tag{4.4}$$

The virtual QED correction in the Fermi model

(4.5)

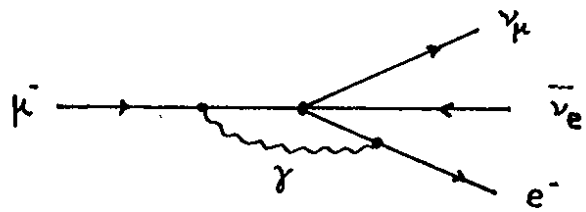

together with the real bremsstrahlung corrections integrated over the full phase space

(4.6)

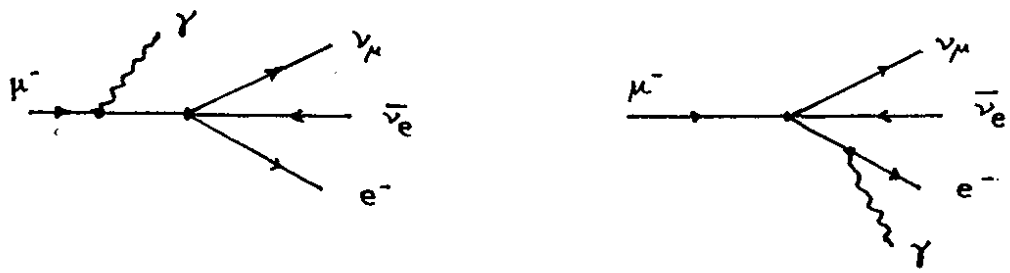

yield (4.3) times a QED correction factor [9]

$$C_{QED}^{Fermi} = 1 + \frac{\alpha}{2\pi}\left(\frac{25}{4} - \pi^2\right)\,. \tag{4.7}$$

In the standard model the virtual photon correction corresponding to (4.5) is a box diagram:

$$\mathcal{M}_{Box}^{\gamma W} = \tag{4.8}$$

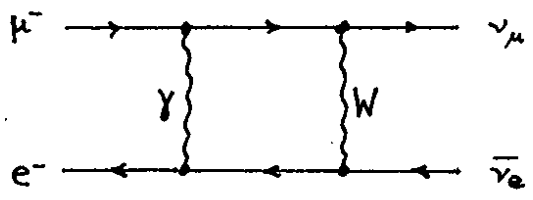

With the photon mass λ as an infrared regularization this box graph for momentum transfer $\ll M_W^2$ can be written in such a way that the virtual QED correction (4.5) of the effective Fermi model is split off:

$$\mathcal{M}^{\gamma W}_{Box} = \mathcal{M}_B \cdot \frac{\alpha}{4\pi}\left(\log\frac{M_W}{m_e} + \log\frac{M_W}{m_\mu} - 2\log\frac{m_e}{\lambda} - 2\log\frac{m_\mu}{\lambda} + \frac{9}{2}\right) + \qquad (4.9)$$

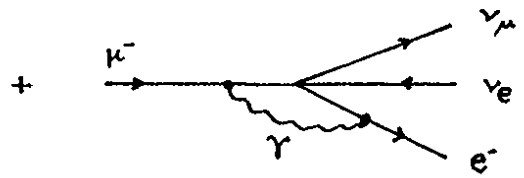

The split off point-like term combines with the real bremsstrahlung diagrams to give the QED correction factor (4.7) to the decay width formula τ_μ^{-1}.

The left-over term in (4.9), together with the weak vertex corrections

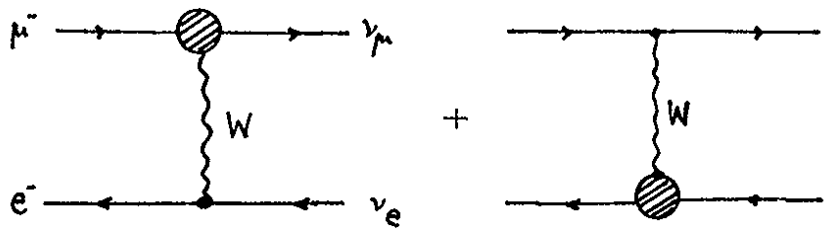

$$\begin{aligned} &= \mathcal{M}_B \cdot \left(\Lambda^{We\nu} + \Lambda^{W\mu\nu} + 2\delta Z_1^W - 2\delta Z_2^W + \delta Z_L^{(\mu,\nu)} + \delta Z_L^{(e,\nu)}\right) \\ &= \mathcal{M}_B \cdot \left(\Lambda^{We\nu} + \Lambda^{W\mu\nu}\right) \end{aligned} \qquad (4.10)$$

where

$$\begin{aligned} \Lambda^{W\ell\nu} &= \frac{\alpha}{4\pi}\left\{\frac{3(3c_W^2-1)}{2s_W^2} - 2\log\frac{M_W}{m_\ell} + 2\log\frac{m_\ell^2}{\lambda^2}\right. \\ &\quad \left. + \left(1 - \frac{7}{2s_W^2} + \frac{3}{s_W^4}\right)\log c_W^2\right\}, \quad \ell = e,\mu \ , \end{aligned} \qquad (4.11)$$

with the UV finite ν wave function renormalization factors according to (3.22)

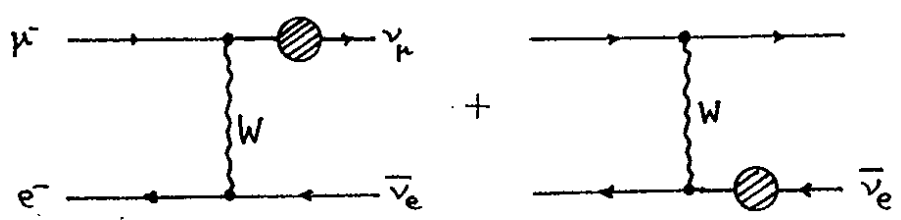

$$\begin{aligned} &= \mathcal{M}_B \cdot \frac{1}{2}\left(\Sigma_L^{\nu_e}(0) + \delta Z_L^{(e,\nu)} + \Sigma_L^{\nu_\mu}(0) + \delta Z_L^{(\mu,\nu)}\right) \\ &= \mathcal{M}_B \cdot \frac{\alpha}{4\pi}\cdot\frac{1}{2}\left(9 - \log\frac{m_e^2}{M_Z^2} - 2\log\frac{m_e^2}{\lambda^2} - \log\frac{m_\mu^2}{M_Z^2} - 2\log\frac{m_\mu^2}{\lambda^2}\right) \ , \end{aligned} \qquad (4.12)$$

and with the massive box diagrams

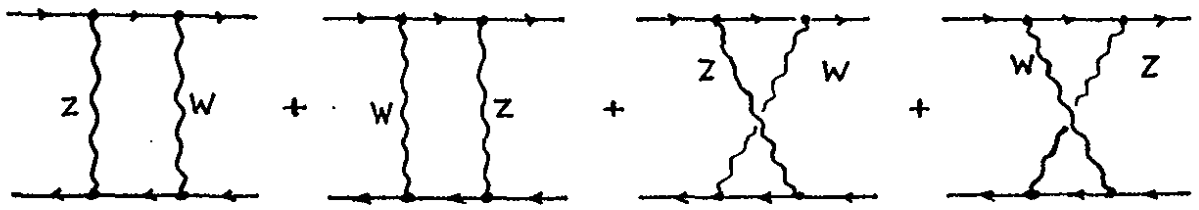

$$= -\mathcal{M}_B \cdot \frac{\alpha}{4\pi}\left(1 - \frac{5}{s_W^2} + \frac{5}{2s_W^4}\right)\log(c_W^2) \tag{4.13}$$

yields a UV and IR finite virtual correction term

$$\delta_V = \frac{\alpha}{4\pi s_W^2}\left(6 + \frac{7 - 4s_W^2}{2s_W^2}\log c_W^2\right) \tag{4.14}$$

to the Born matrix element:

$$\mathcal{M}_V = \mathcal{M}_B \cdot (1 + \delta_V)\,. \tag{4.15}$$

Summing up the irreducible W self energy to all orders

according to the solution of Dyson's equation in the one-loop approximation, leads to the following replacement in the W propagator:

$$\frac{1}{k^2 - M_W^2} \rightarrow \frac{1}{k^2 - M_W^2 + \hat{\Sigma}^W(k^2)} \approx -\frac{1}{M_W^2} \cdot \frac{1}{1 - \frac{\hat{\Sigma}^W(0)}{M_W^2}}\,. \tag{4.16}$$

With (4.17) and (4.18) the matrix element for μ decay with weak corrections can be written as

$$\mathcal{M}_W = \mathcal{M}_B \cdot \frac{1 + \delta_V}{1 - \frac{\hat{\Sigma}^W(0)}{M_W^2}} \approx \mathcal{M}_B \cdot \frac{1}{1 - \Delta r} \tag{4.17}$$

where

$$\Delta r = \frac{\hat{\Sigma}^W(0)}{M_W^2} + \frac{\alpha}{4\pi s_W^2}\left(6 + \frac{7 - 4s_W^2}{2s_W^2}\log c_W^2\right)\,. \tag{4.18}$$

This yields the following modification of the tree level formula (2.32):

$$M_W^2 \, s_W^2 = \frac{\pi\alpha}{\sqrt{2}G_\mu} \cdot \frac{1}{1-\Delta r} = \frac{(37.281\, GeV)^2}{1-\Delta r} \tag{4.19}$$

which was derived first by Sirlin [21].

The geometrical summation (4.17) corresponds to the summation of the leading logarithms according to the renormalization group [20]. Therefore, the leading logarithmic terms

$$\sim \alpha^n \log^n \frac{M_Z^2}{m_f^2}$$

coming from the light fermion loops are contained to all orders in the form (4.19).

Through $\hat{\Sigma}^W$ which gets loop contributions from all particles of the model (see Figure 3.4) Δr is a quantity depending on the full parameter set (3.6). Together with the definition (3.7) of $\sin^2\theta_W$ in terms of the boson masses the following relation equivalent to (4.19)

$$M_W^2 \left(1 - \frac{M_W^2}{M_Z^2}\right) = \frac{\pi\alpha}{\sqrt{2}G_\mu} \cdot \frac{1}{1-\Delta r(\alpha, M_W, M_Z, M_H, m_t)} \tag{4.20}$$

plays a central role in the discussion of the electroweak parameters. Its importance is twofold:

- It is interesting by itself since it allows a comparison of the $M_W - M_Z - \sin^2\theta_W$ correlation with the experimental data.
- It provides a value for M_W (after specifying the other masses) as well as for $\sin^2\theta_W$, which can be used as numerical input parameters for the calculations of other measurable quantities of interest. This will largely be utilized in the applications of the following sections.

Before entering into a quantitative analysis of (4.20) we have to discuss the treatment of the input concerned with the fermionic contributions to the weak radiative corrections.

4.2 Contributions from fermion loops

The closed fermion loop contributions to the transverse components of the vector boson self energies constitute a gauge invariant subset of the one-loop radiative corrections and, in general, also the dominating part. [1] In this section we want to give a list of approximations to the relatively involved exact expressions in (3.23) and Appendix B which are valid in the light fermion limit $|\, k^2 \,| \gg m_f^2$, $f \neq t$, and discuss their asymptotic behaviour with respect to a heavy top quark. These simplified approximate formulae will allow a better understanding of the role of the fermion contributions.

[1] The fermion loop contributions have been treated seperately also in two recent papers [62] in order to illustrate the size of the left-over terms of the full radiative corrections

4.2.1 Photon self energy

The fermionic part of the renormalized γ self energy in (3.23)

$$\hat{\Sigma}^{\gamma}_{ferm}(k^2) \equiv k^2\,\hat{\Pi}^{\gamma}_{ferm}(k^2) + i\,\mathrm{Im}\,\hat{\Sigma}^{\gamma}_{ferm} \tag{4.21}$$

at large values $k^2 \gg m_f^2$ can be written as follows (real part only):

$$\begin{aligned}\hat{\Pi}^{\gamma}_{ferm}(k^2) &= \frac{\alpha}{4\pi}\frac{4}{3}\sum_{f\neq t} Q_f^2\left(\frac{5}{3} - \log\frac{k^2}{m_f^2} + O(\frac{m_f^2}{k^2})\right) \\ &\quad + \hat{\Pi}^{\gamma}_{top}(k^2)\end{aligned} \tag{4.22}$$

where the sum extends over all flavor and color indices (except t).

For large m_t the top term

$$\hat{\Pi}^{\gamma}_{top} = N_C \cdot \frac{\alpha}{3\pi} Q_t^2 \left\{ F(k^2, m_t, m_t)\left(1 + \frac{2m_t^2}{k^2}\right) - \frac{1}{3}\right\} \tag{4.23}$$

with $N_C = 3$ and F from Appendix B tends to zero:

$$\hat{\Pi}^{\gamma}_{top} \approx \frac{\alpha}{3\pi} N_C \frac{k^2}{6m_t^2}\,.$$

Hence, heavy fermions decouple from the photon.

4.2.2 Z and W self energies

The fermionic part of the renormalized Z self energy in (3.23) can be separated in the following way:

$$\begin{aligned}\hat{\Sigma}^{Z}_{ferm}(k^2) &= \Sigma^{Z}_{ferm}(k^2) - \mathrm{Re}\,\Sigma^{Z}_{ferm}(M_Z^2) \\ &\quad + (k^2 - M_Z^2)\Big\{-\hat{\Pi}^{\gamma}_{ferm}(0) \\ &\quad + \frac{c_W^2 - s_W^2}{s_W^2}\,\mathrm{Re}\left(\frac{\Sigma^{Z}_{ferm}(M_Z^2)}{M_Z^2} - \frac{\Sigma^{W}_{ferm}(M_W^2)}{M_W^2}\right)\Big\}\end{aligned} \tag{4.24}$$

yielding the real part for $\mid k^2 \mid \gg m_f^2$:

$$\begin{aligned}\hat{\Pi}^{Z}_{ferm}(k^2) &\equiv \frac{\mathrm{Re}\,\hat{\Sigma}^{Z}_{ferm}(k^2)}{k^2 - M_Z^2} \\ &= \frac{\alpha}{4\pi}\sum_{f\neq t}\Big\{\frac{4}{3}Q_f^2\left(\frac{5}{3} - \log\frac{M_Z^2}{m_f^2}\right) + \frac{c_W^2 - s_W^2}{6s_W^4}\log c_W^2 \\ &\quad - \frac{4}{3}\left(v_f^2 + a_f^2\right)\frac{k^2}{k^2 - M_Z^2}\log\frac{\mid k^2 \mid}{M_Z^2}\Big\} \\ &\quad + \hat{\Pi}^{Z}_{top}(k^2)\,.\end{aligned} \tag{4.25}$$

Asymptotically, for large m_t we have as the leading top term:

$$\hat{\Pi}^Z_{top} \approx \frac{\alpha}{4\pi} \frac{3(c_W^2 - s_W^2)}{4 s_W^4} \cdot \frac{m_t^2}{M_W^2} \,. \tag{4.26}$$

In a similar way we can write for the fermionic contribution to the renormalized W self energy in (3.23):

$$\begin{aligned} \hat{\Sigma}^W_{ferm}(k^2) \;=\; & \Sigma^W_{ferm}(k^2) \;-\; \mathrm{Re}\,\Sigma^W_{ferm}(M_W^2) \\ & + (k^2 - M_W^2)\Big\{ -\Pi^\gamma_{ferm}(0) \\ & + \frac{c_W^2}{s_W^2}\,\mathrm{Re}\left(\frac{\Sigma^Z_{ferm}(M_Z^2)}{M_Z^2} - \frac{\Sigma^W_{ferm}(M_W^2)}{M_W^2} \right) \Big\} \,. \end{aligned} \tag{4.27}$$

The quantity of main interest for our purposes is

$$\frac{\hat{\Sigma}^W_{ferm}(0)}{M_W^2}$$

which enters the radiative correction Δr in (4.18):

$$\begin{aligned} \frac{\hat{\Sigma}^W_{ferm}(0)}{M_W^2} \;\equiv\; & (\Delta r)_{ferm} \\ =\; & \frac{\alpha}{4\pi} \sum_{f \neq t} \left\{ \frac{4}{3} Q_f^2 \left(\log \frac{M_Z^2}{m_f^2} - \frac{5}{3} \right) - \frac{c_W^2 - s_W^2}{6 s_W^4} \log c_W^2 \right\} \\ & + (\Delta r)_{top} \,. \end{aligned} \tag{4.28}$$

In the asymptotic region for large m_t the leading top term is given by

$$(\Delta r)_{top} \approx -\frac{\alpha}{4\pi} \frac{3 c_W^2}{4 s_W^4} \cdot \frac{m_t^2}{M_W^2} \,. \tag{4.29}$$

The quadratic rise of the m_t term is responsible for the large top mass dependent radiative corrections in case of a heavy top quark (see section 4.3).

4.2.3 The light quark contributions

In all three expressions (4.22,25,28) the leading logarithms from the light fermions enter in terms of the combination

$$\sum_f \frac{\alpha}{3\pi} Q_f^2 \left(\log \frac{M_Z^2}{m_f^2} - \frac{5}{3} \right)$$

which represents the photon vacuum polarization at $k^2 = M_Z^2$. These large logarithmic terms constitute in general the dominant contributions to the self energies resp. to Δr. Their origin is the appearance of two different mass scales where the boson masses and the electric charge have been renormalized. According to the charge renormalization the photon vacuum polarization

$$\Pi^\gamma(0) = -\delta Z_2^\gamma \tag{4.30}$$

has to be evaluated at the exceptional momentum $k^2 = 0$. This includes light quark contributions in a region where non-perturbative strong interaction effects cannot be ignored.

Since reliable theoretical predictions are not available one has to use experimental data for the evaluation of the hadronic part in the vacuum polarization. Instead of a direct perturbative evaluation of (4.30) in terms of quark loops a better strategy is to replace the quantity $\Pi^\gamma_{had}(0)$ by

$$\begin{aligned} \Pi^\gamma_{had}(0) &= \mathrm{Re}\,\Pi^\gamma_{had}(M_Z^2) + \Pi^\gamma_{had}(0) - \mathrm{Re}\,\Pi^\gamma_{had}(M_Z^2) \\ &= \mathrm{Re}\,\Pi^\gamma_{had}(M_Z^2) - \mathrm{Re}\,\hat{\Pi}^\gamma_{had}(M_Z^2) \end{aligned} \tag{4.31}$$

where $\Pi^\gamma_{had}(M_Z^2)$ can be evaluated perturbatively, and the real part of the renormalized vacuum polarization $\hat{\Pi}^\gamma$ satisfies the dispersion relation

$$\mathrm{Re}\,\hat{\Pi}^\gamma_{had}(s) = \frac{\alpha}{3\pi}\, s \int_{4m_\pi^2}^\infty ds' \, \frac{R^\gamma(s')}{s'(s' - s - i\epsilon)} \tag{4.32}$$

with

$$R^\gamma(s) = \frac{\sigma(e^+e^- \to \gamma^* \to hadrons)}{\sigma(e^+e^- \to \gamma^* \to \mu^+\mu^-)} \tag{4.33}$$

as a fairly well known experimental quantity as input.

By this treatment all terms in Π^Z and Δr which are singular in the quark masses are cancelled, and the large log terms are everywhere replaced by the dispersion integral (4.32). The left over terms of order m_f^2/M_Z^2 vanish in the limit $m_f \to 0$ and do not play a practical role for the light quarks. For b and t quarks they are treated perturbatively with free quark fields.

The evaluation of the integral (4.32) for five flavors using e^+e^- data up to an energy $E_1 = 40$ GeV and perturbative field theory for the tail $E > E_1$ has recently been updated by Jegerlehner [63] yielding (for $M_Z = 93$ GeV):

$$\mathrm{Re}\,\Pi^{\gamma(5)}_{had}(M_Z^2) = -0.0286 \pm 0.0007\,. \tag{4.34}$$

The error is due to the experimental error of the e^+e^- data, mainly in the region below the Υ resonance. Earlier evaluations of (4.32) based on the same method have been performed

by various authors [64]. The improvement of the result (4.34) is due to the experimental improvement in the e^+e^- data at high energies from PETRA and PEP.

An independent analysis of (4.32) by evaluating the low energy contributions at a spacelike momentum $k^2 = -79$ GeV^2 [65] yields a slightly different result

$$\mathrm{Re}\,\Pi^{\gamma(5)}_{had}(M_Z^2) = -0.0274 \pm 0.0013\,. \tag{4.35}$$

Quite recently, a re-evaluation of (4.32) by Burckhard et al. [66] yields the value -0.0288 ± 0.0009, which is quite close to the result of [63].

Around the weak boson mass scale the integral (4.32) can sufficiently well be described in analytical form by an expression which is equivalent to the result of a perturbative calculation with quark loop diagrams. The quark mass parameters in that approach are effective quark masses adjusted to fit the numerical value of the dispersion integral (4.32) and have no further physical significance. The values which reproduce the result in (4.34) are:

$$m_u = m_d = 0.041\,GeV\,, \tag{4.36}$$

$$m_s = 0.15\,GeV, \quad m_c = 1.5\,GeV, \quad m_b = 4.5\,GeV\,.$$

The choice of effective quark masses includes QCD effects in the real parts of the vacuum polarization functions automatically. In the imaginary part QCD effects from the 2-loop diagrams

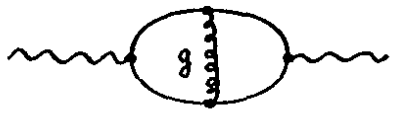

have to be added (see sections 5 and 6).

4.3 The $M_W - M_Z - \sin^2\theta_W$ correlation

After M_Z has been specified the relation (4.20) can formally be solved to give a value for M_W

$$M_W^2 = M_Z^2 \cdot \frac{1}{2}\left(1 + \sqrt{1 - \frac{4A}{M_Z^2(1-\Delta r)}}\right)\,, \tag{4.37}$$

as well as for $\sin^2\theta_W$

$$s_W^2 = 1 - \frac{M_W^2}{M_Z^2} = \frac{1}{2}\left(1 - \sqrt{1 - \frac{4A}{M_Z^2(1-\Delta r)}}\right) \tag{4.38}$$

with

$$A = \frac{\alpha\pi}{\sqrt{2}G_\mu}$$

Since Δr is a function of M_W itself these equations can be solved by iteration. For the calculation of Δr also some values for the until now unknown parameters m_t and M_H have to be specified. For $m_t = 35$ GeV, $M_H = 100$ GeV, $M_Z = 93$ GeV, and the input (4.34) for the hadronic vacuum polarization we find

$$\Delta r = 0.0709 \pm 0.0007 \tag{4.39}$$

in full agreement with [63] [2].

Table 4.1 W mass and $\sin^2\theta_W$ from (4.20) for various Z, Higgs, and top masses.

		M-Higgs = 10		100		1000 GeV	
M-Z	m-top	sin**2	M-W	sin**2	M-W	sin**2	M-W
90.	50.	0.2429	78.31	0.2445	78.23	0.2477	78.06
90.	100.	0.2376	78.59	0.2392	78.50	0.2425	78.33
90.	150.	0.2316	78.89	0.2333	78.81	0.2366	78.63
90.	200.	0.2239	79.29	0.2256	79.20	0.2291	79.02
90.	230.	0.2181	79.58	0.2199	79.49	0.2235	79.31
91.	50.	0.2354	79.57	0.2370	79.49	0.2401	79.33
91.	100.	0.2301	79.85	0.2317	79.77	0.2349	79.60
91.	150.	0.2241	80.16	0.2257	80.07	0.2290	79.90
91.	200.	0.2164	80.56	0.2181	80.47	0.2215	80.29
91.	230.	0.2106	80.85	0.2123	80.76	0.2158	80.58
92.	50.	0.2283	80.82	0.2298	80.74	0.2329	80.58
92.	100.	0.2230	81.09	0.2246	81.01	0.2277	80.85
92.	150.	0.2170	81.41	0.2186	81.33	0.2218	81.16
92.	200.	0.2093	81.81	0.2109	81.72	0.2143	81.55
92.	230.	0.2035	82.11	0.2052	82.02	0.2086	81.84
93.	50.	0.2216	82.05	0.2231	81.97	0.2261	81.81
93.	100.	0.2164	82.33	0.2179	82.25	0.2210	82.08
93.	150.	0.2103	82.65	0.2119	82.56	0.2150	82.40
93.	200.	0.2025	83.05	0.2042	82.97	0.2075	82.79
93.	230.	0.1967	83.35	0.1984	83.27	0.2018	83.09
94.	50.	0.2153	83.27	0.2167	83.19	0.2197	83.03
94.	100.	0.2101	83.55	0.2116	83.47	0.2146	83.30
94.	150.	0.2039	83.87	0.2055	83.79	0.2086	83.62
94.	200.	0.1962	84.28	0.1978	84.19	0.2010	84.02
94.	230.	0.1903	84.58	0.1920	84.50	0.1953	84.32
95.	50.	0.2092	84.48	0.2107	84.40	0.2136	84.24
95.	100.	0.2041	84.75	0.2056	84.67	0.2086	84.51
95.	150.	0.1979	85.08	0.1994	85.00	0.2025	84.84
95.	200.	0.1901	85.49	0.1917	85.41	0.1949	85.24
95.	230.	0.1842	85.80	0.1859	85.72	0.1892	85.54

[2] Note that the final value $\Delta r = 0.0711$ given in [63] is an average over different renormalization schemes

Figure 4.1 : The quantity Δr in (4.18) for $M_Z = 92$ GeV and various M_H (in GeV).

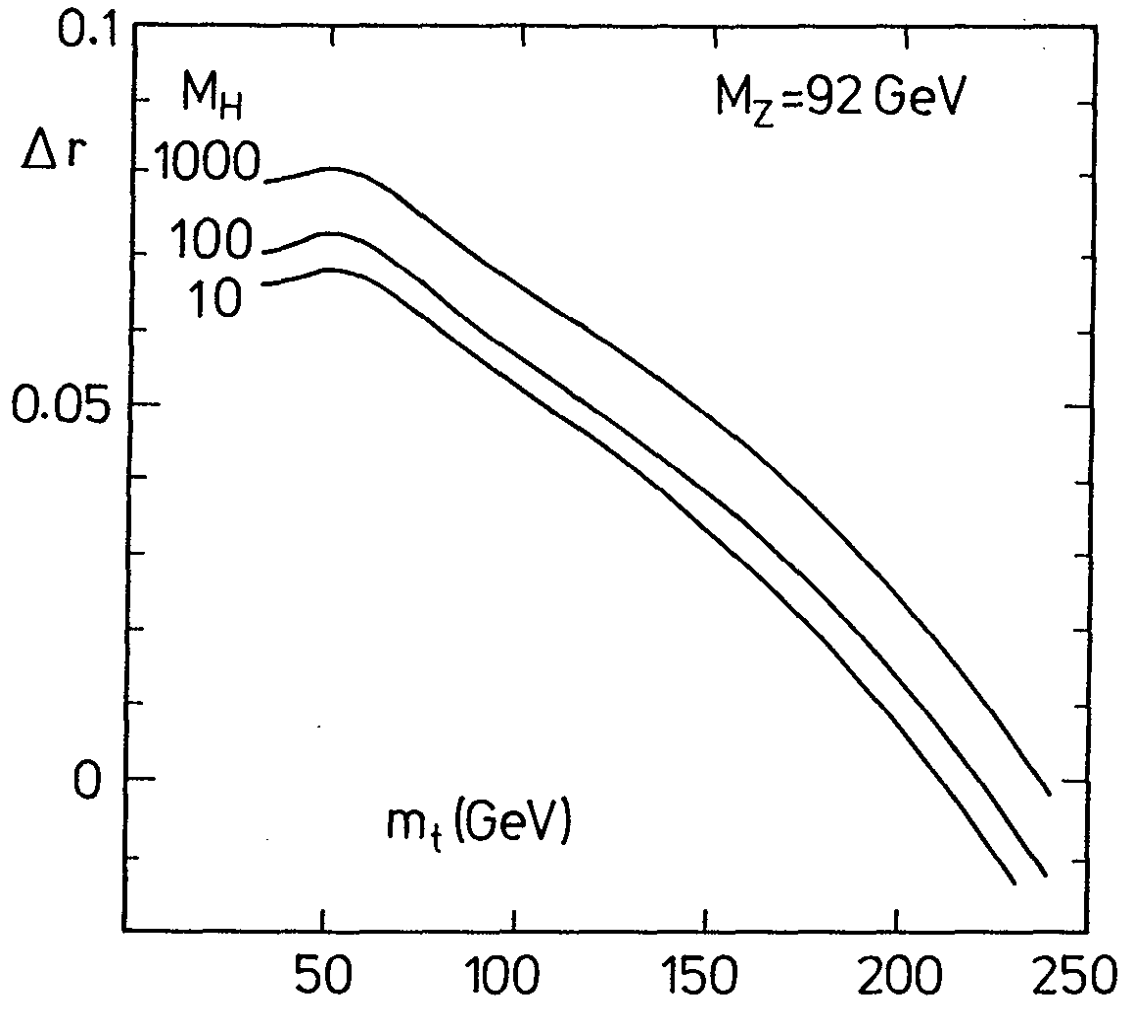

The value for Δr changes if M_Z, M_H, m_t are varied, and so do the corresponding values for M_W and $\sin^2\theta_W$. For a range of input parameters which is of current interest the values for M_W and $\sin^2\theta_W$ are put together in Table 4.1. The quantity Δr is plotted in Figure 4.1.

The strong dependence on a large top mass according to the quadratically rising term (4.30) in Δr can be utilized to derive an upper limit on m_t from the present experimental values for M_W and M_Z [16]: $m_t < 185$GeV at the 1-σ level depending slightly on the Higgs mass. In combination with the information from neutral current neutrino data this limit can be improved [67,68]:

$$m_t < 200\,GeV$$

at the 90% confidence level (depending also on M_H).

Since the top contribution in Δr is negative it tends to cancel the large term from the light fermions with increasing m_t. Around $m_t = 230$ GeV the radiative correction

$$\Delta r \to 0$$

and the tree level formulae (2.34-35) become valid.

The variation with the Higgs mass is much less striking. Changing M_H between 10 GeV and 1 TeV the value for $\sin^2\theta_W$ varies by 0.005, which matches the accuracy obtained in neutrino scattering experiments ($\Delta \sin^2\theta_W \approx 0.005$) and the aimed accuracy from LEP 200 via the measurement of M_W. Estimates for the uncertainties of the various experimental determinations of $\sin^2\theta_W$ are put together in Table 4.2.

Table 4.2

Experiment	$\Delta \sin^2\theta_W$
νN	0.005
νe (CHARM II)	0.005
M_W, M_Z ($p\bar{p}$)	0.003
G_μ, M_Z (LEP)	0.0005
$A_{FB}(\mu^+\mu^-)$ (LEP)	0.001
A_{LR} (LEP)	0.0003
M_W (LEP 200)	0.0006
Theory (hadronic)	0.0002

Our values in Table 4.1 are in complete agreement with the corresponding results of Jegerlehner [63]. The values obtained for $\sin^2\theta_W$ by Lynn and Stuart [33] are systematically lower by an amount of 0.0005. This is due to the slightly smaller value (4.35) for the hadronic QED part of Δr, which has been used as input in [33]. Adjusting this hadronic term numerically (by an additive model independent constant) yields also full agreement between the two calculations. Further checks of these results were performed by Bardin et al. [69] who also find quantitative agreement after adapting the hadronic input.

4.4 Theoretical uncertainties

As far as the standard model parameters m_t, M_H will not be known within a reasonably small range the induced uncertainties will obscure the theoretical predictions for M_W resp. $\sin^2\theta_W$ in terms of the precisely known quantities α, G_μ, and (with LEP/SLC) M_Z. But in principle these errors can be reduced by a discovery of the corresponding particles. Otherwise precision measurements can be used to narrow down the allowed mass range of the outstanding particles.

The error from the hadronic contribution to the vacuum polarization will not improve without higher precision measurements of $\sigma(e^+e^- \to hadrons)$ in the energy range below M_Υ [63]. This error does not exceed the uncertainty expected in the high precision experiments at LEP and SLC.

In addition, a further theoretical uncertainty is due to the unknown effects of higher orders in perturbation theory. Formally, an uncertainty $\delta(\Delta r) \approx (\Delta r)^2 \approx 0.005$ would be estimated from the unknown 2-loop contribution in Δr. However, according to the renormalization group [20] the geometrically summed expression

$$1 + \Delta r + \cdots = \frac{1}{1 - \Delta r}$$

as used in the applications of the previous sections incorporates already all the leading logarithmic terms of order $\sim \alpha^n \log^n m_f/M_Z$ for $n \geq 2$. These terms, which describe the running of α in *QED*

$$\frac{1}{\alpha(\mu^2)} - \frac{1}{\alpha(0)} = \frac{1}{3\pi} \sum_f Q_f^2 \log \frac{m_f^2}{\mu^2} \tag{4.40}$$

constitute the dominant part of the correction factor

$$\frac{1}{1 - \Delta r}\,.$$

This leads to the simple interpretation

$$\frac{\alpha(0)}{1 - \Delta r} \equiv \alpha_W \approx \alpha(\mu^2 = M_W^2)$$

i.e. the leading logarithms can be absorbed in a quantity $\alpha(M_W^2)$ according to (4.40).

Since these leading terms are independent of the electroweak model (and therefore renormalization scheme independent) higher order uncertainties come from those terms not contained in (4.40) which depend explicitly on the chosen renormalization conditions. The renormalization scheme dependence of the one-loop terms in Δr (not those in $\alpha(\mu^2)$) can be used to estimate the higher order uncertainty.

An uncertainty of Δr can be related to a corresponding one in M_W, as derived from (4.37):

$$\frac{\delta M_W}{M_W} = \frac{s_W^2}{c_W^2 - s_W^2} \cdot \frac{\delta(\Delta r)}{2(1 - \Delta r)}\,. \tag{4.41}$$

Applying two different renormalization schemes for fixing the finite parts of the renormalization constants [70] [3] we can estimate the higher order uncertainty in terms of a shift in the W mass, which amounts to (maximum)

$$\delta M_W < 20\ MeV$$

[3] the on-shell scheme as explained in section 3 and a scheme where Σ^W is directly renormalized by τ_μ

or, in terms of Δr:

$$\delta(\Delta r) < 0.0011 \ .$$

By investigation of 4 different renormalization schemes Jegerlehner [71] obtains a similar result:

$$\delta(\Delta r) \approx 0.0011 \ .$$

For realistic estimates this error has to be considered in addition to the error in (4.34) from the experimental data. If we assume that the errors can be added in quadrature we obtain

$$\delta(\Delta r) = 0.0013 \tag{4.42}$$

which we will consider as a reasonable value for the theoretical uncertainty in the $M_W - M_Z - \sin^2\theta_W$ correlation.

Sirlin [72] has estimated the effects coming from the light fermion $\alpha^2 \log M_Z/m_f$ terms in Δr: converted to the W mass shift they are of order 1 MeV.

From the fermion sector large radiative correction effects occur at the one-loop level in the case of a large mass splitting between the members of a SU(2) multiplet [73] (e.g. for $m_t \gg m_b$) and one might worry about large next order contributions. Van der Bij and Hoogeveen [74] have calculated the 2-loop heavy fermion effects to the ρ-parameter $\rho = 1 + \Delta\rho$ with

$$\Delta\rho = \frac{\hat{\Sigma}^Z(0)}{M_Z^2} - \frac{\hat{\Sigma}^W(0)}{M_W^2} \ . \tag{4.43}$$

In the heavy top limit the leading term is given by

$$\Delta\rho^{(2)} = \left(\frac{\alpha}{4\pi}\right)^2 \frac{10 - \pi^2}{8} \cdot 3 \left(\frac{m_t}{M_W}\right)^4 \ .$$

The corresponding contribution to Δr can be roughly estimated in terms of

$$\Delta r^{(2)} \approx - \frac{c_W^2}{s_W^2} \Delta\rho^{(2)} \ ,$$

which is related to a shift in $\sin^2\theta_W$ not negligible for very large m_t. For $m_t < 200$ GeV, favored by present data [67,68] those effects are insignificant.

Effects of a heavy Higgs particle at the one-loop level are much smaller in size since the dependence on M_H is only logarithmic [75]. Although at the 2-loop level a term $\sim M_H^2$ shows up in $\Delta\rho$ its coefficient is small such that it is not significant for Higgs masses below 1 TeV [76].

Chapter 5

The width of the Z boson

One of the basic measurements at the near future colliders LEP and SLC will be the determination of the mass M_Z and the width Γ_Z of the weak neutral gauge boson with an accuracy of 50 MeV, probably 20 MeV [11,14]. This requires an adequate theoretical accuracy on Γ_Z of about 10 MeV.

For this purpose it is necessary to treat next order corrections to the Z width. They are of twofold importance:

- For precision measurements of M_Z it has to be considered that bremsstrahlung emission from the initial state influences the Z resonance line shape significantly. The magnitude of this peak deformation depends on the precise value of Γ_Z; also its s-dependence is of importance, which will be discussed later in chapter 6.
- The partial widths for $Z \to f\bar{f}$ will allow one to study the weak coupling constants for the various types of fermions at the level of quantum corrections.

Calculations of one-loop corrections to $Z \to f\bar{f}$ which mean 2-loop corrections to the imaginary part of Σ^Z have been performed for the leptonic widths in [71,77] and also for $Z \to q\bar{q}$ in [39,40,78]. In [39,40] the accurate discussion of the top quark influence on the $Z \to b\bar{b}$ decays has been performed. The results of various independent calculations agree pretty well within 0.5 MeV.

Electroweak corrections to open top final states in case of $m_t < M_Z/2$, a possibility which is experimentally not completely ruled out, have been considered in [79]. They are less important in view of the uncertainties from the top mass in the phase space factors and from large QCD corrections near threshold [80]. Therefore here we want to study the case $m_t > M_Z/2$.

5.1 Lowest order results

In lowest order the Z propagator has the Breit-Wigner form

$$D_Z^0(s) = \frac{1}{s - M_Z^2 + iM_Z\Gamma_Z^0} \,. \tag{5.1}$$

The lowest order total width Γ_Z^0 is related to the one-loop self energy $\Sigma^Z(s)$ of the Z boson by

$$M_Z \Gamma_Z^0 = \mathrm{Im}\, \Sigma^Z(s = M_Z^2) \,. \tag{5.2}$$

It can be written as the sum of the partial fermionic decay widths $\Gamma_Z^0(f\bar{f})$ with $m_f < M_Z/2$:

$$\Gamma_Z^0 = \sum_f \Gamma_Z^0(f\bar{f}) \,. \tag{5.3}$$

These partial widths can be expressed in terms of the vector and axial vector coupling constants (2.27) of the fermion f to the Z as follows:

$$\Gamma_Z^0(f\bar{f}) = N_C^f \frac{\alpha}{3} M_Z \sqrt{1-4\mu_f} \left(v_f^2(1+2\mu_f) + a_f^2(1-4\mu_f) \right) \tag{5.4}$$

with $N_C^f = 3$ for quarks, $N_C^f = 1$ for leptons, and

$$\mu_f = \frac{m_f^2}{M_Z^2} \,. \tag{5.5}$$

For actual calculations the dependence on s_W^2 resp. M_W is eliminated by utilizing eq. (4.20), as discussed in Section 4.3.

Making use of the relations (2.32) and (2.33) we can write down another possible tree level representation of the partial decay width

$$\bar{\Gamma}_Z^0(f\bar{f}) = N_C^f \frac{G_\mu M_Z^3}{24\pi\sqrt{2}} \sqrt{1-4\mu_f} \left(1 - 4\mu_f + (2I_3^f - 4Q_f s_W^2)^2 (1+2\mu_f) \right) \tag{5.6}$$

leading to the Born total width in the G_μ representation:

$$\bar{\Gamma}_Z^0 = \sum_f \bar{\Gamma}_Z^0(f\bar{f}) \,. \tag{5.7}$$

5.2 QCD corrections

QCD corrections to the hadronic partial widths for $Z \to q\bar{q}$ will not be explicitly incorporated in the numerical results given below in Table 5.1-4. They can easily be included by multiplying each electroweak partial width $\Gamma_{ew}(q\bar{q})$ by the QCD correction factor [81,82] yielding in the massless quark approximation:

$$\Gamma_{ew+QCD}(q\bar{q}) = \Gamma_{ew}(q\bar{q}) \cdot \left\{ 1 + \frac{\alpha_s(M_Z^2)}{\pi} + \left(\frac{\alpha_s(M_Z^2)}{\pi} \right)^2 (1.98 - 0.115\, n_f) \right\} \tag{5.8}$$

with n_f = number of flavors.

Recently also the next order term has been calculated [83] which is even larger than the $0(\alpha_s^2)$ term. For five flavors it is given by

$$+ 64.835 \left(\frac{\alpha_s}{\pi} \right)^3 \,.$$

However, both second and third order terms are not of numerical significance for our aimed accuracy.

For the following discussion in Section 6 this QCD part will always be included with the following value for α_s:

$$\alpha_s(M_Z^2) = 0.12 \pm 0.02\,, \tag{5.9}$$

according to [84]

$$\alpha_s\left((34\,GeV)^2\right) = 0.138 \pm 0.023\,. \tag{5.10}$$

5.3 Electroweak corrections

The partial widths (5.4) in lowest order are influenced by next order corrections in terms of the vector boson 2-point functions, external wave function renormalization of the fermions, and irreducible vertex corrections.

The Z propagator (5.1) is modified replacing the constant width term by the renormalized Z boson self energy $\hat{\Sigma}^Z(s)$ from (3.23):

$$D_Z(s) = \frac{1}{s - M_Z^2 + \mathrm{Re}\hat{\Sigma}^Z(s) + i\,\mathrm{Im}\hat{\Sigma}^Z(s)} \tag{5.11}$$

where $\mathrm{Re}\,\hat{\Sigma}^Z(M_Z^2) = 0$ due to the on-shell renormalization condition (3.14) for the Z boson. Around the Z pole approximately a Breit-Wigner form

$$D_Z(s) = \frac{1}{1 + \hat{\Pi}^Z(M_Z^2)} \cdot \frac{1}{s - M_Z^2 + iM_Z\Gamma_Z^{(1)}} \tag{5.12}$$

is recovered by a re-definition of the total width

$$\Gamma_Z^{(1)} = \frac{\Gamma_Z^0}{1 + \hat{\Pi}^Z(M_Z^2)} \tag{5.13}$$

with Γ_Z^0 from (5.3,4) and

$$\hat{\Pi}^Z(M_Z^2) = \frac{\partial\,\mathrm{Re}\hat{\Sigma}^Z}{\partial s}(M_Z^2)\,. \tag{5.14}$$

This global normalization (5.13) corresponds to the wave function renormalization of the Z line in the decay diagrams 5.1. For each partial width this means that (5.4) has to be multiplied by a common factor:

$$\Gamma_Z^{(1)}(f\bar{f}) = \Gamma_Z^0(f\bar{f}) \cdot \left(1 + \hat{\Pi}^Z(M_Z^2)\right)^{-1}\,. \tag{5.15}$$

Furthermore, the relation (4.20) can be utilized in order to re-express (5.15) in terms of the Fermi constant G_μ, yielding:

$$\Gamma_Z^{(1)}(f\bar{f}) = \tilde{\Gamma}_Z^0(f\bar{f})\,\frac{1 - \Delta r}{1 + \hat{\Pi}^Z(M_Z^2)} \tag{5.16}$$

with $\bar{\Gamma}_Z^0(f\bar{f})$ from (5.6).

Since the large contributions from the light fermions

$$\frac{\alpha}{3\pi}\sum_f Q_f^2 \log\frac{M_Z^2}{m_f^2}$$

in Δr and in $\hat{\Pi}^Z(M_Z^2)$ cancel in the expression (5.16) (see eq.s (4.25) and (4.28)), $\bar{\Gamma}_Z^0$ turns out to be a sufficiently good approximation (for $m_t < 100$ GeV) including already the major part of the one-loop corrections. [1]

In addition to (5.16) we have to incorporate the γ-Z mixing contribution and the vertex corrections together with the external fermion self energies (Figures 3.5,6). Since we do not consider radiative corrections to $Z \to t\bar{t}$ we can neglect all terms of order m_f^2/M_Z^2 ($f \neq t$) in the loop expressions. This means that also Higgs contributions in vertex and fermion self energy diagrams are neglected, except for $f = b$.

In case of the $Z \to b\bar{b}$ decay channel the full top mass dependence coming from the virtual t quarks in Figures 3.5,6 is included. Due to the underlying 't Hooft-Feynman gauge also "unphysical" charged Higgs bosons enter the diagrams as virtual states with poles at $k^2 = M_W^2$.

The final result for the partial width can be written in the following way:

$$\Gamma_Z(f\bar{f}) = \left(\Gamma_Z^0(f\bar{f}) + \Delta\Gamma_Z(f\bar{f})\right)\cdot\left(1+\hat{\Pi}^Z(M_Z^2)\right)^{-1} \tag{5.17}$$

with $\Gamma_Z^0(f\bar{f})$ from (5.4), and

$$\Delta\Gamma_Z(f\bar{f}) = N_C^f\,\frac{2}{3}\,\alpha\,M_Z\,\left\{v_f\,\left(Re\,F_V^{Zf}(M_Z^2) + Q_f\hat{\Pi}^{\gamma Z}(M_Z^2)\right) + a_f\,Re\,F_A^{Zf}(M_Z^2)\right\}\ . \tag{5.18}$$

The γ-Z mixing term is related to the mixing energy $\hat{\Sigma}^{\gamma Z}$, eq. (3.23) :

$$\hat{\Pi}^{\gamma Z}(s) = \mathrm{Re}\,\hat{\Sigma}^{\gamma Z}(s)/s\ . \tag{5.19}$$

The finite vector and axial vector form factors $F_{V,A}^{Zf}$ which include the fermion wave function renormalization factors are listed in the Appendix C for the various types of fermions.

Finally we have to include the QED corrections (Figure 5.2) due to virtual photon exchange and real bremsstrahlung integrated over the full phase space. For light final fermions the result can be simply obtained [85] by multiplying (5.17) with the correction factor $1+\delta_{QED}^f$, with

$$\delta_{QED}^f = \frac{3\alpha}{4\pi}\,Q_f^2\ . \tag{5.20}$$

Its relative influence is $< 0.17\%$.

[1] Others than $Z \to f\bar{f}$ decay channels in higher order of the coupling constant are very small [86], for a light Higgs about 5 MeV from $Z \to Hf\bar{f}$ [87]

Figure 5.1 Non-QED contributions to the partial decay widths $\Gamma_Z(f\bar{f})$

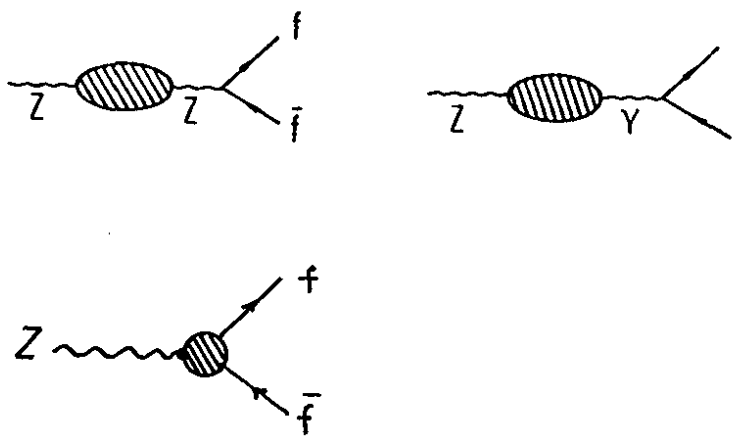

Figure 5.2 QED corrections to the $Z \rightarrow f\bar{f}$ partial widths

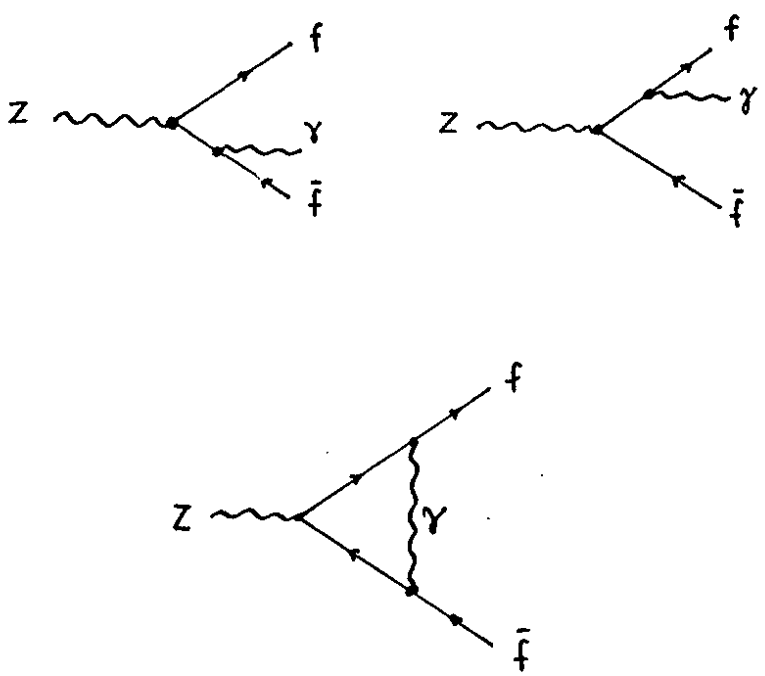

5.4 Results and discussion

Besides the quantities α, G_μ, M_Z, which are sufficient to determine Γ_Z at the tree level, the unknown parameters M_H and m_t enter the higher order result. For our numerical discussion we proceed in the following way:

After specifying the values for M_Z, M_H, m_t we derive from (4.20) the corresponding value for M_W resp. $\sin^2\theta_W$ thus fixing the coupling constants v_f, a_f and the next order terms in (5.17-18).

Table 5.1 contains the total electroweak Z width Γ_Z (including QED corrections) for fixed $M_H = 100$ GeV. The tree level values Γ_Z^0 correspond to the standard parametrization given in (5.3-5), $\bar{\Gamma}_Z^0$ is the tree level width (5.7) in the G_μ representation. For top masses not too large ($m_t < 100$ GeV) $\bar{\Gamma}_Z^0$ gives already an approximation which is good within 5 MeV. For large top masses, however, $\bar{\Gamma}_Z^0$ becomes insufficient as well; in some cases the parametrization Γ_Z^0 in (5.4) is the better approximation.

Table 5.1 Total Z width, no QCD corrections.

M_Z	m_t	Γ_Z^0	$\bar{\Gamma}_Z^0$	Γ_Z
90.	50.	2.1305	2.2936	2.2948
90.	100.	2.1739	2.3056	2.3035
90.	200.	2.2966	2.3386	2.3275
91.	50.	2.2176	2.3889	2.3898
91.	100.	2.2648	2.4019	2.3993
91.	200.	2.3997	2.4379	2.4244
92.	50.	2.3071	2.4869	2.4876
92.	100.	2.3584	2.5010	2.4978
92.	200.	2.5062	2.5401	2.5240
93.	50.	2.3992	2.5878	2.5881
93.	100.	2.4545	2.6029	2.5992
93.	200.	2.6161	2.6451	2.6264
94.	50.	2.4938	2.6914	2.6911
94.	100.	2.5531	2.7075	2.7033
94.	200.	2.7295	2.7531	2.7316
95.	50.	2.5910	2.7978	2.7968
95.	100.	2.6543	2.8149	2.8102
95.	200.	2.8464	2.8639	2.8396
96.	50.	2.6907	2.9070	2.9049
96.	100.	2.7581	2.9250	2.9199
96.	200.	2.9670	2.9776	2.9504

The Higgs and top mass dependences of the total width Γ_Z are put together in Table 5.2 for various Z masses. The variation with m_t is strong enough that it has to be taken into account if one wants a theoretical precision of 10 MeV. For example, the variation of m_t between 50 and 150 GeV leads to an increase in Γ_Z by 21 MeV (for $M_Z = 92$ GeV, $M_H = 100$ GeV). On the other hand, the variation of Γ_Z with the Higgs mass remains smaller than 10 MeV.

Table 5.2 Total Z width for 5 flavors without QCD corrections.

MZ	MT	MH=10	MH=100	MH=1000 GEV
90.	50.	2.2924	2.2948	2.2870
90.	100.	2.3011	2.3035	2.2958
90.	150.	2.3112	2.3137	2.3062
90.	200.	2.3249	2.3275	2.3203
90.	230.	2.3349	2.3376	2.3305
91.	50.	2.3872	2.3898	2.3818
91.	100.	2.3966	2.3993	2.3913
91.	150.	2.4072	2.4099	2.4022
91.	200.	2.4215	2.4244	2.4169
91.	230.	2.4319	2.4349	2.4276
92.	50.	2.4847	2.4876	2.4793
92.	100.	2.4949	2.4978	2.4897
92.	150.	2.5059	2.5090	2.5010
92.	200.	2.5208	2.5240	2.5163
92.	230.	2.5316	2.5349	2.5274
93.	50.	2.5848	2.5880	2.5795
93.	100.	2.5959	2.5992	2.5908
93.	150.	2.6074	2.6108	2.6026
93.	200.	2.6229	2.6264	2.6185
93.	230.	2.6341	2.6377	2.6301
94.	50.	2.6875	2.6911	2.6823
94.	100.	2.6997	2.7033	2.6946
94.	150.	2.7117	2.7154	2.7070
94.	200.	2.7277	2.7316	2.7235
94.	230.	2.7393	2.7433	2.7355
95.	50.	2.7928	2.7968	2.7878
95.	100.	2.8062	2.8102	2.8013
95.	150.	2.8187	2.8228	2.8141
95.	200.	2.8353	2.8396	2.8313
95.	230.	2.8473	2.8517	2.8437
96.	50.	2.9005	2.9049	2.8956
96.	100.	2.9155	2.9199	2.9107
96.	150.	2.9284	2.9330	2.9241
96.	200.	2.9457	2.9504	2.9418
96.	230.	2.9580	2.9629	2.9547

Table 5.3 Partial widths without QED and QCD corrections.

		NEUTRINO			ELECTRON		
MZ	MT	MH=10	100	1000	10	100	1000
90.	50.	0.1592	0.1595	0.1592	0.0795	0.0796	0.0794
90.	100.	0.1597	0.1600	0.1597	0.0797	0.0799	0.0797
90.	150.	0.1603	0.1606	0.1603	0.0800	0.0802	0.0800
90.	200.	0.1612	0.1615	0.1612	0.0804	0.0805	0.0804
90.	230.	0.1618	0.1622	0.1619	0.0806	0.0808	0.0807
91.	50.	0.1645	0.1649	0.1645	0.0823	0.0825	0.0823
91.	100.	0.1650	0.1654	0.1651	0.0826	0.0828	0.0826
91.	150.	0.1657	0.1660	0.1657	0.0830	0.0831	0.0829
91.	200.	0.1666	0.1669	0.1666	0.0834	0.0835	0.0834
91.	230.	0.1672	0.1676	0.1673	0.0837	0.0838	0.0837
92.	50.	0.1700	0.1703	0.1700	0.0854	0.0856	0.0853
92.	100.	0.1705	0.1709	0.1706	0.0858	0.0859	0.0857
92.	150.	0.1712	0.1716	0.1712	0.0861	0.0863	0.0861
92.	200.	0.1721	0.1725	0.1722	0.0866	0.0868	0.0866
92.	230.	0.1728	0.1732	0.1729	0.0869	0.0871	0.0869
93.	50.	0.1755	0.1759	0.1756	0.0887	0.0888	0.0885
93.	100.	0.1761	0.1765	0.1762	0.0891	0.0892	0.0889
93.	150.	0.1768	0.1772	0.1769	0.0895	0.0896	0.0894
93.	200.	0.1778	0.1782	0.1779	0.0900	0.0902	0.0900
93.	230.	0.1785	0.1789	0.1786	0.0904	0.0905	0.0903
94.	50.	0.1812	0.1816	0.1813	0.0921	0.0923	0.0920
94.	100.	0.1818	0.1823	0.1819	0.0926	0.0927	0.0924
94.	150.	0.1825	0.1830	0.1827	0.0930	0.0932	0.0929
94.	200.	0.1835	0.1840	0.1837	0.0936	0.0938	0.0935
94.	230.	0.1843	0.1847	0.1844	0.0940	0.0941	0.0939
95.	50.	0.1870	0.1874	0.1871	0.0958	0.0959	0.0956
95.	100.	0.1877	0.1881	0.1878	0.0963	0.0964	0.0961
95.	150.	0.1884	0.1889	0.1885	0.0967	0.0969	0.0966
95.	200.	0.1894	0.1899	0.1896	0.0974	0.0975	0.0973
95.	230.	0.1902	0.1907	0.1903	0.0978	0.0980	0.0977
96.	50.	0.1928	0.1933	0.1930	0.0995	0.0997	0.0993
96.	100.	0.1936	0.1941	0.1938	0.1001	0.1002	0.0999
96.	150.	0.1944	0.1949	0.1946	0.1006	0.1008	0.1005
96.	200.	0.1954	0.1959	0.1956	0.1013	0.1015	0.1012
96.	230.	0.1962	0.1967	0.1964	0.1018	0.1019	0.1017

HADRONIC DECAY WIDTHS

		D QUARKS			B QUARKS			U QUARKS		
MZ	MT	MH=10	100	1000	10	100	1000	MH=10	100	1000
90.	50.	0.3478	0.3481	0.3468	0.3440	0.3443	0.3430	0.2681	0.2682	0.2670
90.	100.	0.3495	0.3497	0.3484	0.3445	0.3448	0.3435	0.2695	0.2696	0.2684
90.	150.	0.3516	0.3519	0.3506	0.3439	0.3442	0.3430	0.2713	0.2714	0.2703
90.	200.	0.3546	0.3549	0.3536	0.3430	0.3433	0.3422	0.2738	0.2739	0.2728
90.	230.	0.3568	0.3571	0.3558	0.3423	0.3426	0.3415	0.2756	0.2757	0.2746
91.	50.	0.3629	0.3632	0.3619	0.3590	0.3593	0.3580	0.2807	0.2808	0.2796
91.	100.	0.3646	0.3649	0.3636	0.3595	0.3599	0.3586	0.2822	0.2823	0.2811
91.	150.	0.3668	0.3671	0.3658	0.3589	0.3593	0.3580	0.2841	0.2842	0.2830
91.	200.	0.3699	0.3702	0.3689	0.3579	0.3583	0.3571	0.2867	0.2868	0.2857
91.	230.	0.3721	0.3725	0.3712	0.3571	0.3575	0.3564	0.2886	0.2887	0.2876
92.	50.	0.3782	0.3786	0.3772	0.3742	0.3746	0.3733	0.2937	0.2938	0.2925
92.	100.	0.3800	0.3804	0.3791	0.3749	0.3753	0.3740	0.2953	0.2954	0.2942
92.	150.	0.3823	0.3827	0.3814	0.3743	0.3747	0.3734	0.2973	0.2974	0.2962
92.	200.	0.3855	0.3859	0.3846	0.3732	0.3736	0.3724	0.3000	0.3002	0.2990
92.	230.	0.3878	0.3882	0.3869	0.3723	0.3728	0.3717	0.3020	0.3021	0.3010
93.	50.	0.3939	0.3943	0.3929	0.3898	0.3903	0.3889	0.3070	0.3072	0.3059
93.	100.	0.3958	0.3962	0.3949	0.3906	0.3911	0.3897	0.3088	0.3089	0.3077
93.	150.	0.3981	0.3986	0.3973	0.3899	0.3904	0.3891	0.3109	0.3110	0.3098
93.	200.	0.4014	0.4019	0.4005	0.3888	0.3893	0.3881	0.3137	0.3139	0.3126
93.	230.	0.4038	0.4043	0.4030	0.3878	0.3883	0.3872	0.3157	0.3160	0.3147
94.	50.	0.4098	0.4103	0.4089	0.4057	0.4062	0.4048	0.3208	0.3210	0.3196
94.	100.	0.4119	0.4124	0.4110	0.4067	0.4072	0.4058	0.3227	0.3229	0.3215
94.	150.	0.4143	0.4149	0.4135	0.4060	0.4065	0.4052	0.3248	0.3251	0.3238
94.	200.	0.4177	0.4182	0.4169	0.4047	0.4053	0.4041	0.3278	0.3280	0.3268
94.	230.	0.4202	0.4207	0.4194	0.4036	0.4042	0.4031	0.3299	0.3302	0.3289
95.	50.	0.4261	0.4267	0.4253	0.4219	0.4225	0.4211	0.3349	0.3352	0.3338
95.	100.	0.4284	0.4290	0.4275	0.4231	0.4237	0.4223	0.3370	0.3372	0.3358
95.	150.	0.4309	0.4315	0.4301	0.4223	0.4229	0.4216	0.3392	0.3395	0.3381
95.	200.	0.4343	0.4349	0.4336	0.4210	0.4216	0.4204	0.3423	0.3426	0.3413
95.	230.	0.4369	0.4375	0.4362	0.4198	0.4205	0.4194	0.3445	0.3448	0.3435
96.	50.	0.4427	0.4434	0.4419	0.4384	0.4390	0.4376	0.3494	0.3497	0.3483
96.	100.	0.4452	0.4458	0.4444	0.4398	0.4405	0.4391	0.3517	0.3520	0.3505
96.	150.	0.4478	0.4484	0.4470	0.4390	0.4397	0.4384	0.3540	0.3543	0.3529
96.	200.	0.4513	0.4520	0.4506	0.4376	0.4383	0.4371	0.3572	0.3575	0.3562
96.	230.	0.4540	0.4547	0.4533	0.4363	0.4371	0.4360	0.3595	0.3599	0.3585

The hadronic uncertainty from (4.34) is responsible for a hadronic uncertainty in Γ_Z amounting to $(\Delta\Gamma_Z)_{had} = \pm 0.6$ MeV. The somewhat larger hadronic error in the photon vacuum polarization of ± 0.0013, in the result (4.35) [65] results in $(\Delta\Gamma_Z)_{had} = \pm 1$ MeV. In both cases the uncertainty coming from the light quarks is of no practical importance for Γ_Z.

Next we discuss the partial decay widths for $Z \to f\bar{f}$ and their dependence on the model parameters, listed in Table 5.3. Again, the variation with the Higgs mass is not very striking: 0.2 MeV for the leptonic channels, and somewhat more in the hadronic decay modes, but still smaller than 1 MeV.

The dependence on m_t is strongest in the $Z \to u\bar{u}$ and $Z \to d\bar{d}$ decays. In the $Z \to b\bar{b}$ partial width, however, the top mass dependence is much weaker. The reason for this behaviour is the additional top dependence of the vertex corrections in $Z \to b\bar{b}$ which cancels (partly) the top contributions in the gauge boson 2-point functions. This is exhibited in more detail in Table 5.4 (for $M_Z = 92$ GeV, $M_H = 100$ GeV):

The tree level approximations $\bar{\Gamma}^0_Z(f\bar{f})$ as defined in (5.6) are slightly different for d and b quarks due to the finite m_b. The determination of $\sin^2\theta_W$ by means of (4.20) and the dependence of Δr on m_t are responsible for the variation of $\bar{\Gamma}^0_Z(f\bar{f})$ with the value of m_t. The weak corrections $\Delta\Gamma^{weak}_Z(f\bar{f})$ defined as

$$\Delta\Gamma^{weak}_Z(f\bar{f}) = \Gamma_Z(f\bar{f}) - \bar{\Gamma}^0_Z(f\bar{f}) \tag{5.21}$$

with the corrected partial width $\Gamma_Z(f\bar{f})$ from (5.17) induce additional top quark contributions. Those entering via the Z-Z and Z-γ propagators are identical for both d and b, whereas the vertex and quark self energy diagrams (Figures 3.5,6) yield different corrections for d and b final states. For $b\bar{b}$ they tend to cancel the increase of the lowest order term for larger m_t.

Table 5.4 Top dependence of the weak corrections to $Z \to b\bar{b}$, $d\bar{d}$

m_t	$\bar{\Gamma}^0_Z(d\bar{d})$	$\Delta\Gamma^{weak}_Z(d\bar{d})$	$\bar{\Gamma}^0_Z(b\bar{b})$	$\Delta\Gamma^{weak}_Z(b\bar{b})$
50	0.3784	0.0001	0.3748	-0.0002
100	0.3809	-0.0005	0.3773	-0.0020
150	0.3838	-0.0011	0.3801	-0.0055
200	0.3875	-0.0017	0.3839	-0.0102
230	0.3904	-0.0021	0.3867	-0.0139

Finally we want to compare our results with those of the other calculations by Wetzel [78] and Akhundov et al [39]. Wetzel employs a different renormalization scheme ; therefore only a comparison of the corrected values for $\Gamma_Z(f\bar{f})$ is meaningful. For $M_Z = 92$ GeV, $M_H = 100$ GeV and $m_t = 40$ GeV, as specified in [78], we find agreement within 0.5 MeV for the ν, e, u, and d partial widths. Heavy quarks are not discussed in detail in [78].

In order to make our results comparable with those of Akhundov et al [39], obtained in the on-shell scheme and the unitary gauge, we have to put $m_b = 0$ in the tree level formula and to adjust our value for the hadronic QED vacuum polarization in a way that it fits the table for $\sin^2\theta_W$ given by Lynn and Stuart [33] (since their hadronic part was adopted in [39]).

Doing this, we find excellent agreement in all partial widths within 0.1 MeV, sometimes 0.2 MeV, for the whole range of the considered top and Higgs masses.

Concluding this section, our discussion of the Z width has shown that the electroweak corrections play a role for precision experiments, in particular the top mass dependence. The variation with the Higgs mass does not exceed the aimed experimental accuracy.

Chapter 6

e^+e^- annihilation into fermion pairs

In the near future measurements at the e^+e^- colliders LEP and SLC will determine the properties of the Z boson (mass, width, coupling constants) with high accuracy. The basic processes are the annihilation processes into lepton and quark pairs $e^+e^- \to f\bar{f}$, which are described in lowest order by the photon and Z exchange diagrams.

The high precision tests of the standard model require the inclusion of the radiative corrections for an adequate theoretical discussion. Moreover, the observation of new phenomena from ideas beyond the standard model ("new physics") would also be possible [17,18] which makes a careful treatment of the radiative corrections in the minimal model necessary for establishing a solid background. Since polarization effects play an essential role around the Z peak [14] we will discuss the e^+e^- cross section including polarization of the incoming $e^\pm$.

6.1 Cross section for polarized beams and lowest order results

The degrees of longitudinal polarization of $e^\pm$ are denoted by $P_L^\pm$ ($P_L = 1$: right handed, $P_L = -1$: left handed, for both electron and positron), the degrees of transverse polarization by $P_T^\pm$. Since the transverse polarization is the "natural polarization" in a storage ring we want to include this situation for completeness. The principle physical insight gained from transverse polarization does not exceed that from unpolarized beams; information is transfered from the polar angle to the azimuthal angle distributions. Measurements of azimuthal observables, however, are normally less sensitive to systematic uncertainties than polar angle distributions or charge asymmetries which makes also the transverse polarization an interesting and practically important tool.

Without neclecting terms from the final fermion mass m_f the differential cross section can be written in the following way, where the color factor $N_C^f = 1$ (leptons), $N_C^f = 3$ (quarks) distinguishes between the final state fermions: ($\theta = \angle(e^-, f)$, $\mu_f = m_f^2/s$, $s = (p_- + p_+)^2$)

$$\frac{d\sigma}{d\Omega} = \frac{\alpha^2}{4s} N_C^f \sqrt{1-4\mu_f} \left\{ (1 - P_L^+ P_L^-)\, X_U + (P_L^+ - P_L^-)\, X_L + P_T^+ P_T^-\, X_T \right\} \qquad (6.1)$$

with

$$
\begin{aligned}
X_U &= G_1(s)(1+\cos^2\theta) + 4\mu_f G_2(s)\sin^2\theta + \sqrt{1-4\mu_f}\, G_3(s)\cdot 2\cos\theta \qquad (6.2)\\
X_L &= H_1(s)(1+\cos^2\theta) + 4\mu_f H_2(s)\sin^2\theta + \sqrt{1-4\mu_f}\, H_3(s)\cdot 2\cos\theta \\
X_T &= (1-4\mu_f)\,[F_1(s)\cos 2\phi + F_2(s)\sin 2\phi]\sin^2\theta\,.
\end{aligned}
$$

The vector and axial vector coupling constants (2.27) and the propagator in the lowest order Breit-Wigner approximation with Γ_Z^0 from (5.3)

$$
\chi_0(s) = \frac{s}{s - M_Z^2 + iM_Z\Gamma_Z^0} \qquad (6.3)
$$

determine the functions in the expressions (6.2) as follows:

$$
\begin{aligned}
G_1(s) &= Q_f^2 - 2v_e v_f Q_f \,\mathrm{Re}\,\chi_0(s) + (v_e^2+a_e^2)(v_f^2+a_f^2-\mu_f a_f^2)\mid\chi_0(s)\mid^2 \qquad (6.4)\\
G_2(s) &= Q_f^2 - 2v_e v_f Q_f \,\mathrm{Re}\,\chi_0(s) + (v_e^2+a_e^2)v_f^2 \mid\chi_0(s)\mid^2 \\
G_3(s) &= -2a_e a_f Q_f \,\mathrm{Re}\,\chi_0(s) + 4v_e a_e v_f a_f \mid\chi_0(s)\mid^2 \\
\\
H_1(s) &= -2a_e v_f Q_f \,\mathrm{Re}\,\chi_0(s) + 2v_e a_e(v_f^2+a_f^2-\mu_f a_f^2)\mid\chi_0(s)\mid^2 \\
H_2(s) &= -2a_e v_f Q_f \,\mathrm{Re}\,\chi_0(s) + 2v_e a_e v_f^2 \mid\chi_0(s)\mid^2 \\
H_3(s) &= -2v_e a_f Q_f \,\mathrm{Re}\,\chi_0(s) + 2(v_e^2+a_e^2)v_f a_f \mid\chi_0(s)\mid^2 \\
\\
F_1(s) &= Q_f^2 - 2v_e v_f Q_f \,\mathrm{Re}\,\chi_0(s) + (v_e^2-a_e^2)(v_f^2+a_f^2)\mid\chi_0(s)\mid^2 \\
F_2(s) &= 2v_e a_e(v_f^2+a_f^2)\,\mathrm{Im}\,\chi_0(s)
\end{aligned}
$$

6.2 General structure of radiative corrections

As indicated in the description of the on-shell renormalization scheme in section 3.2 the one-loop corrections to the process $e^+e^- \to f\bar{f}$ can be subdivided quite naturally into the following subclasses:

- "QED corrections", which consist of those diagrams with an extra photon added to the Born diagrams either as a real bremsstrahlung photon or a virtual photon loop. They are depicted in Figure 6.1. Although considered not very interesting with respect to the underlying theory they are in general large at LEP energies and hence need a lot of attention for practical purposes.

- "Weak corrections", which collect all other one-loop diagrams: The subset of diagrams which involve corrections to the vector boson propagators γ, Z (Figure 6.2), the set of vertex corrections (where the virtual photon contributions have been removed) and box diagrams with two massive boson exchange (Figure 6.3).

The separation of the QED corrections is sensible since they form a gauge invariant subset and depend on the details of the experiments via the cuts applied to the final state photon.

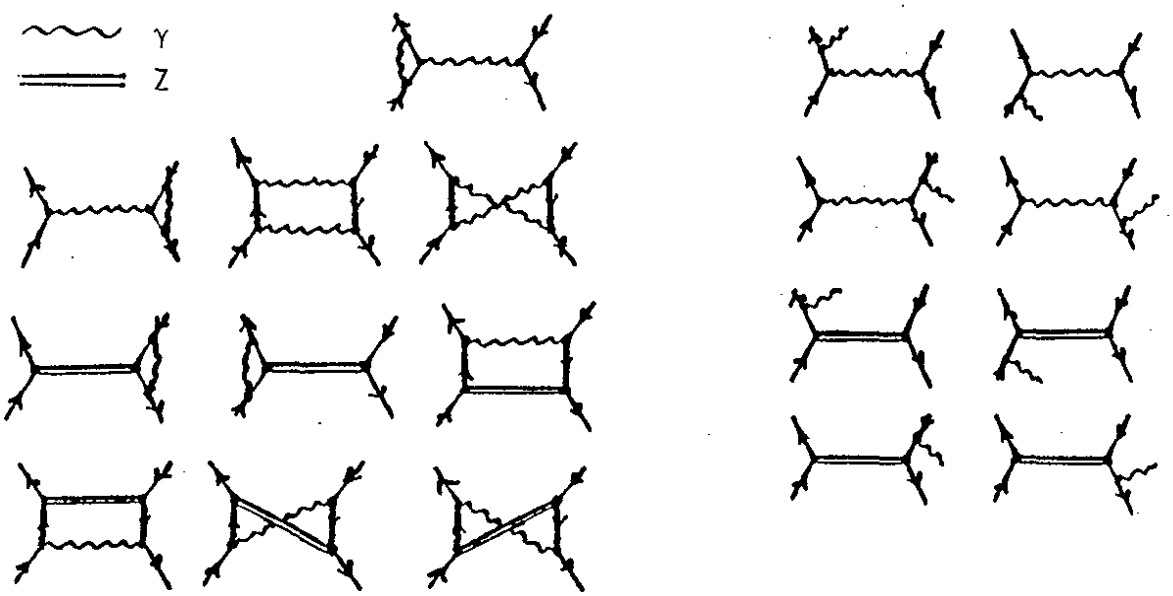

Figure 6.1: QED corrections to $e^+e^- \to f\bar{f}$

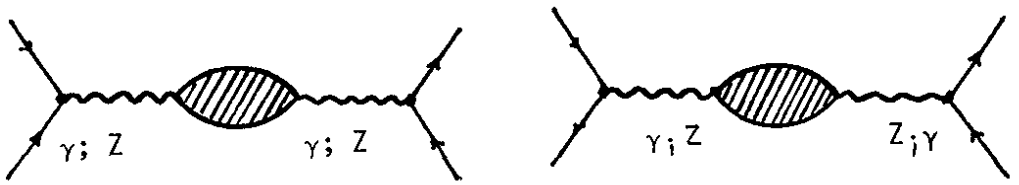

Figure 6.2: Propagator corrections to $e^+e^- \to f\bar{f}$

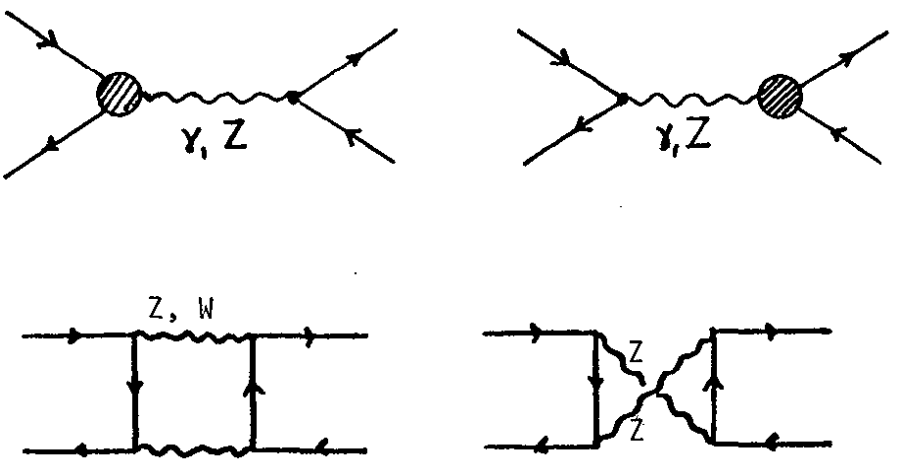

Figure 6.3: Vertex corrections and box contributions to $e^+e^- \to f\bar{f}$

Their proper treatment constitutes the link between data taking and physics analysis. The infrared finite weak corrections are independent of experimental cuts; they include the more subtle part of the electroweak theory beyond the tree level and are also sensitive to "new physics" objects.

Due to the smallness of the electron mass the lowest order Higgs exchange diagram can be neglected. For the same reason also diagrams with Higgs - gauge boson mixing and box diagrams where one or both of the internal vector bosons of Figure 6.3 are replaced by Higgs scalars are negligible; they are suppressed by at least a factor $\frac{\alpha}{\pi}\frac{m_e}{M_W}$. The propagator corrections, however, involve all particles of the model, in particular the as yet unknown Higgs boson and the top quark, and thus depend on M_H and m_t. For light final fermions ($f \neq b, t$) the vertex corrections of Figure 6.3 contain only W and Z in virtual states. Vertex corrections to heavy fermions depend also on the Higgs-fermion Yukawa couplings.

The tree level formulae of 6.1 are valid also for a $t\bar{t}$ final state. The complete treatment of the radiative corrections for such a heavy fermion production process, however, is rather lengthy and will therefore be presented elsewhere [88]. In the present article we want to restrict ourselves to the situation where only the known fermions appear as external particles for which the one-loop corrections can be cast into a compact and transparent form. Since the m_f terms give only a very small contribution already at the tree level we can neglect all fermion mass effects in the next order vertex and box diagrams with two exceptions:
• mass terms from a virtual top quark are always treated without approximation in vertex corrections involving the (t, b) doublet and the WW box contribution for $b\bar{b}$ final states;
• in the QED corrections all mass terms (also from light fermions) are kept which would lead to mass singularities for $m_f \to 0$.

In this approximation the vertex corrections can be represented in terms of form factors $F_{V,A}^{Z(\gamma)f}(k^2)$ for the vector and axial vector currents only. Also the box diagrams can be written as a sum over terms like

$$\text{(initial current)} \cdot \text{(final current)} \cdot \text{(formfactor)}.$$

where the currents have only vector and axial vector contributions. This simple structure arises from helicity conservation at the vector boson - fermion vertices in the small mass limit. It allows to express the corrected cross section in the same way as given in (6.1) and (6.2); only the invariant functions in (6.2) which are not already suppressed by a front factor m_f^2/s have to be substituted by their corrected versions.

According to our general strategy outlined in section 3 all the ingredients in the cross section (6.1) are expressed in terms of the physical masses. Once M_Z will be known the differential cross section and all derived observable quantities (total cross section, all kind of asymmetries, ...) are functions of M_W or synonymously of $\sin^2\theta_W$ (after specifying values for M_H and m_t). Those observables can therefore provide measurements of $\sin^2\theta_W$ which are supplementary to the determination from the low energy processes μ decay and neutrino scattering. In addition, the $\sin^2\theta_W$ dependence of the e^+e^- observables if formulated in terms of $\sin^2\theta_W$, M_Z, ..., is preserved also in the case that $\sin^2\theta_W$ is not only a convenient bookkeeping device but an independent parameter. Such a structure is encountered e.g. in a non-minimal SU(2)×U(1) model with additional Higgs bosons in non-standard representations with dimension ≥ 3. This, however, under the assumption that the loop contributions are dominated by the standard model radiative corrections and new bosons give only negligible effects in the loop diagrams.

On the other hand, if we take the minimal model seriously, all the neutral current coupling constants (via $\sin^2\theta_W$) and M_W are fixed after the other masses have been specified: their values follow from the solution of the equations (4.37), (4.38), as done in section 4.3. After inserting these values into (6.1,2) the auxiliary quantity $\sin^2\theta_W$ has completely disappeared from the final result. Then the measurable quantities in $e^+e^- \to f\bar{f}$ are predictions, dependent on M_H and m_t only (assuming that M_Z is well known). A possible mismatch with experiment would become visible in a disagreement between data and these predictions from M_H, m_t within a reasonable range. Additional structures like non-standard Higgs representations can be allowed for if the tight relations (4.37,38) are softened by means of the replacement

$$M_Z \to \sqrt{\rho}\, M_Z \,,$$

with a further independent parameter ρ.

6.3 The (γ, Z) propagator

In lowest order, after diagonalization of the neutral boson mass matrix, the propagator matrix is diagonal. But mixing due to quantum corrections prohibits the photon and Z boson from propagating independently of each other in higher orders. Consequently, the propagator of the $\gamma\, Z$ system has to be considered as a 2×2 matrix. The radiative corrections to the propagator system can be obtained by inversion of the matrix (transverse parts only)

$$(\mathbf{D}_{\mu\nu})^{-1} = i\, g_{\mu\nu} \begin{pmatrix} k^2 + \hat{\Sigma}^\gamma(k^2) & \hat{\Sigma}^{\gamma Z}(k^2) \\ \hat{\Sigma}^{\gamma Z}(k^2) & k^2 - M_Z^2 + \hat{\Sigma}^Z(k^2) \end{pmatrix} \tag{6.5}$$

with the 1-particle irreducible (1PI) renormalized self energies specified in (3.23) to one-loop order, yielding:

$$\mathbf{D}_{\mu\nu} = -i\, g_{\mu\nu} \begin{pmatrix} D_\gamma & D_{\gamma Z} \\ D_{\gamma Z} & D_Z \end{pmatrix} \tag{6.6}$$

where $(s = k^2)$

$$D_\gamma(s) = \frac{1}{s + \hat{\Sigma}^\gamma(s) - \frac{\hat{\Sigma}^{\gamma Z}(s)^2}{s - M_Z^2 + \hat{\Sigma}^Z(s)}} \tag{6.7}$$

$$D_Z(s) = \frac{1}{s - M_Z^2 + \hat{\Sigma}^Z(s) - \frac{\hat{\Sigma}^{\gamma Z}(s)^2}{s + \hat{\Sigma}^\gamma(s)}} \tag{6.8}$$

$$D_{\gamma Z}(s) = -\frac{\hat{\Sigma}^{\gamma Z}(s)}{[s + \hat{\Sigma}^\gamma(s)]\,[s - M_Z^2 + \hat{\Sigma}^Z(s)] - \hat{\Sigma}^{\gamma Z}(s)^2} \,. \tag{6.9}$$

Obviously the matrix (6.5) can be diagonalized only for one specific value of k^2. This has been done by fixing the mixing counter term in such a way that (6.5) is diagonal for $k^2 = 0$ (Section 3.4).

Expansion in terms of the Σ's allows to interpret (6.7-9) as a summation of the 1PI contributions to the vector boson 2-point functions to all orders (see also the discussions in

[43,89]):

$$D_\gamma = \frac{1}{s+\hat{\Sigma}^\gamma} + \frac{1}{s+\hat{\Sigma}^\gamma}\hat{\Sigma}^{\gamma Z}\frac{1}{s-M_Z^2+\hat{\Sigma}^Z}\hat{\Sigma}^{\gamma Z}\frac{1}{s+\hat{\Sigma}^\gamma} + \cdots$$

$$D_Z = \frac{1}{s-M_Z^2+\hat{\Sigma}^Z} + \frac{1}{s-M_Z^2+\hat{\Sigma}^Z}\hat{\Sigma}^{\gamma Z}\frac{1}{s+\hat{\Sigma}^\gamma}\hat{\Sigma}^{\gamma Z}\frac{1}{s-M_Z^2+\hat{\Sigma}^Z} + \cdots$$

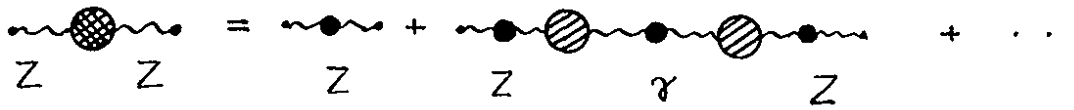

$$D_{\gamma Z} = -\frac{1}{s+\hat{\Sigma}^\gamma}\hat{\Sigma}^{\gamma Z}\frac{1}{s-M_Z^2+\hat{\Sigma}^Z} - \frac{1}{s+\hat{\Sigma}^\gamma}\hat{\Sigma}^{\gamma Z}\frac{1}{s-M_Z^2+\hat{\Sigma}^Z}\hat{\Sigma}^{\gamma Z}\frac{1}{s+\hat{\Sigma}^\gamma}\hat{\Sigma}^{\gamma Z}\frac{1}{s-M_Z^2+\hat{\Sigma}^Z} - \cdots$$

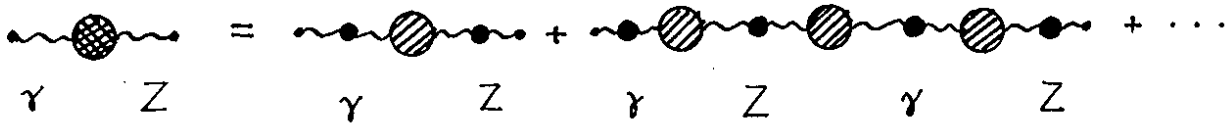

In the graphical representation the lines with the double-shaded blobs denote the full propagators (6.7-9) and the single-shaded blobs the 1PI self energies; the dot at the lines indicates that all the diagonal 1PI contributions to the γ and$Z$ propagators are included:

In $O(\alpha)$, with the leading log terms resummed to all orders, the propagators are simplified to

$$D_\gamma = \frac{1}{s+\hat{\Sigma}^\gamma(s)} \tag{6.10}$$

$$D_Z = \frac{1}{s-M_Z^2+\hat{\Sigma}^Z(s)}$$

$$D_{\gamma Z} = -\frac{1}{s}\hat{\Sigma}^{\gamma Z}(s)\frac{1}{s-M_Z^2+i\mathrm{Im}\hat{\Sigma}^Z(s)}$$

The further approximaton of the Z propagator in (6.10)

$$\text{Re}\ \hat{\Sigma}^Z \approx 0, \quad \text{Im}\ \hat{\Sigma}^Z(s) \approx \text{Im}\ \hat{\Sigma}^Z(M_Z^2)$$

leads to the lowest order Breit-Wigner form

$$D_Z^0(s) = \frac{1}{s - M_Z^2 + i M_Z \Gamma_Z^0}$$

which has been used in the Born formulae (6.4).

Off resonance, in the continuum region, the approximation (6.10) is adequate. Around the Z peak, however, (6.10) becomes insufficient:

1. The on-resonance value of the amplitude for $e^+e^- \to f\bar{f}$ in lowest order is of $O(1)$ and not of $O(\alpha)$ as in the continuum: The tree level width which is given by the imaginary part of the one-loop Z self energy Im $\Sigma^Z(M_Z^2)$ cancels the coupling constants in the numerator of the matrix element. For the next order corrections to the cross section around the Z peak the $O(\alpha^2)$ contributions to the Z width have to be included. One part of them is given by the imaginary part of the $\left(\hat{\Sigma}^{\gamma Z}\right)^2$ term in (6.8).

2. The real part of $\left(\hat{\Sigma}^{\gamma Z}\right)^2$ in (6.8) gives a $O(\alpha^2)$ correction to the resonance amplitude. In a systematic expansion up to $O(\alpha)$ it would therefore not appear. A numerical study shows that it is indeed negligible if the top quark is not too heavy (< 150 GeV). For a large mass splitting in the (t,b) doublet, however, the $O(\alpha^2)$ term matches the experimental accuracy aimed in LEP experiments. For practical reasons it is desirable to have a handle on the effects induced in the physically interesting observables.

For an appropriate discussion in view of the questions raised above we proceed as follows:

Ad 1:
The resummed form (6.8) is still insufficient for the imaginary part of the Z propagator: besides the reducible $O(\alpha^2)$ term Im $\left(\hat{\Sigma}^{\gamma Z}\right)^2$ we need also the 2-loop irreducible part $\text{Im}\hat{\Sigma}^Z_{(2)}$ of the diagonal Z self energy contributing to the $O(\alpha^2)$ width as well. Both the reducible and irreducible terms have been included in our discussion of the on-resonance Z width ($s = M_Z^2$) in Section 5.3. Note that the s-dependence of the imaginary part is also significant: the replacement

$$M_Z\,\Gamma_Z(M_Z^2) \to \sqrt{s}\,\Gamma_Z(s) = \text{Im}\ \hat{\Sigma}^Z(s)$$

causes a shift of the resonance peak on the energy scale of about 35 MeV [41,52] to lower values.

Altogether, we have to replace the imaginary part of the denominator in (6.8) by the proper expression

$$\text{Im}\left[\hat{\Sigma}^Z(s) - \frac{\left(\hat{\Sigma}^{\gamma Z}(s)\right)^2}{s + \hat{\Sigma}^\gamma(s)}\right] + \frac{s}{M_Z^2} \cdot \text{Im}\ \hat{\Sigma}^Z_{(2)}(M_Z^2) \tag{6.11}$$

where $\hat{\Sigma}^Z$ still denotes the 1PI one-loop part (a similar discussion has been given by Wetzel in [32]).

The term $\mathrm{Im}\ \hat{\Sigma}^Z_{(2)}(M_Z^2)$ is related by unitarity to the Z width and has been calculated in chapter 5. The electroweak next order corrections to the fermion loops yield:

$$\mathrm{Im}\ \hat{\Sigma}^{Z\ ew}_{(2)}(M_Z^2) = M_Z \sum_{f\neq t} \left(\Delta\Gamma_Z(f\bar{f}) + \Gamma^0_Z(f\bar{f}) \cdot \frac{3\alpha}{4\pi} Q_f^2 \right) \tag{6.12}$$

with $\Gamma^0_Z(f\bar{f})$ from (5.4) and $\Delta\Gamma_Z(f\bar{f})$ from (5.18) with the mixing term removed (since it is already contained in the first part of (6.11)).

In addition to (6.12) there are still other contributions to $\mathrm{Im}\ \hat{\Sigma}^Z_{(2)}$: 3-body decays, and QCD corrections to the fermion loops. Among the 3-body decays of the Z only the decay mode $Z \to Hf\bar{f}$ for a light Higgs boson is numerically of some significance, although only marginally [87]. For $M_H = 10$ GeV the sum contributes

$$\sum_f \Gamma_Z(Z \to Hf\bar{f}) \approx 5 \text{ MeV}$$

to the total Z width. This decay mode has not been included in our discussion of the Z width in chapter 5. For completeness we will keep it in (6.11) as

$$\mathrm{Im}\ \hat{\Sigma}^{Z\ 3-body}_{(2)} = M_Z \sum_f \Gamma_Z(Z \to Hf\bar{f}) \tag{6.13}$$

for the further discussion, based on the results of [87]. Other decay modes give only negligible contributions [86].

More important are the effects from QCD: strong corrections increase the total Z width by about 70 MeV. For the light quarks they can easily be incorporated in (6.11) by adding the term

$$\mathrm{Im}\ \hat{\Sigma}^{Z\ QCD}_{(2)}(M_Z^2) = M_Z \sum_q \Gamma^0_Z(q\bar{q}) \cdot (R_{QCD} - 1) \tag{6.14}$$

where R_{QCD} is the correction factor in (5.8) with the value of α_s in (5.9). For the $Z \to t\bar{t}$ partial width in case of a "light" top quark the mass dependent QCD corrections have to be used instead of (5.8) which differ significantly from the zero mass approximation. We do not list them here but refer to the literature [80,81]. In view of the uncertainties associated with the values of α_s and m_t the 2-loop 1PI electroweak contributions are of minor importance [79]. For this article we restrict ourselves to the case $2m_t > M_Z$ and postpone the detailed discussion of open top production to another place [88].

After specifying the 1PI 2-loop term in (6.11) as the sum

$$\mathrm{Im}\ \hat{\Sigma}^Z_{(2)}(M_Z^2) = \mathrm{Im}\ \hat{\Sigma}^{Z\ ew}_{(2)}(M_Z^2) + \mathrm{Im}\ \hat{\Sigma}^{Z\ QCD}_{(2)}(M_Z^2) + \mathrm{Im}\ \hat{\Sigma}^{Z\ 3-body}_{(2)}(M_Z^2) \tag{6.15}$$

of the various contributions in (6.12,13,14) we have completed our discussion of the imaginary part (6.11) of the Z propagator. The remaining uncertainty from the experimental error in α_s as given in (5.9) can be estimated to be of order 10 MeV in the Z width. For a comprehensive discussion of the ingredients in the Z propagator see also the contribution by Burgers [42] to the CERN report on Polarization at LEP [14] It should be noted that the available computer programs [90] for numerical studies include also the case $m_t < M_Z/2$ together with the mass dependent QCD corrections based on the results of [81].

Ad 2:

The inclusion of also the real part of the $\left(\hat{\Sigma}^{\gamma Z}\right)^2$ term in (6.8) takes care of the fact that the physical Z mass gets a contribution in higher order from mixing with the photon. A rigorous treatment would require a proper 2-loop renormalization and is related to the question what the meaning of the Z mass is at the 2-loop level. For a discussion at the present stage the most natural possibility is to define M_Z by the condition

$$\mathrm{Re}\left[\hat{\Sigma}^Z(M_Z^2) - \frac{\left(\hat{\Sigma}^{\gamma Z}(M_Z^2)\right)^2}{s+\hat{\Sigma}^\gamma(M_Z^2)}\right] = 0\,. \tag{6.16}$$

With this definition (and in the constant width approximation) we recover an approximate Breit-Wigner form around M_Z^2, quite in analogy to (5.12):

$$D_Z(s) \approx \frac{1}{1+\hat{\Pi}^Z(M_Z^2)} \cdot \frac{1}{s - M_Z^2 + i\,M_Z\Gamma_Z} \tag{6.17}$$

but now with

$$\hat{\Pi}^Z(M_Z^2) = \frac{\partial}{\partial s}\,\mathrm{Re}\left[\hat{\Sigma}^Z(s) - \frac{\left(\hat{\Sigma}^{\gamma Z}(s)\right)^2}{s+\hat{\Sigma}^\gamma(s)}\right]_{s=M_Z^2} \tag{6.18}$$

and

$$\Gamma_Z = \frac{1}{1+\hat{\Pi}^Z(M_Z^2)} \cdot \frac{1}{M_Z}\left(\mathrm{Im}\left[\hat{\Sigma}^Z(M_Z^2) - \frac{\left(\hat{\Sigma}^{\gamma Z}(M_Z^2)\right)^2}{M_Z^2+\hat{\Sigma}^\gamma(M_Z^2)}\right] + \mathrm{Im}\,\hat{\Sigma}^Z_{(2)}(M_Z^2)\right) \tag{6.19}$$

where also the results of the foregoing discussion have been implemented.

In order to fulfil the requirement (6.16) we have to modify the renormalization condition which fixes the Z mass counter term δM_Z^2 in section 3.5. Instead of (3.16) the condition leading to (6.16) reads:

$$\delta M_Z^2 = \mathrm{Re}\left[\Sigma^Z(M_Z^2) - \frac{\left(\hat{\Sigma}^{\gamma Z}(M_Z^2)\right)^2}{M_Z^2+\hat{\Sigma}^\gamma(M_Z^2)}\right]\,. \tag{6.20}$$

The condition for the W mass counter term δM_W^2 is unchanged and so are all the other renormalization conditions formulated in 3.4. Now the set of equations (3.16-17) defining the renormalization constants and the renormalized 2-point functions (3.23) are implicit equations since they contain the renormalized mixing on the r.h.s. However, it is straightforward to solve them for the renormalized quantities in terms of the non-renormalized ones.

Writing the photon propagator (6.7) in the form

$$D_\gamma(s) = \frac{1}{s+\hat{\Sigma}^\gamma(s)} + \left(\frac{\hat{\Sigma}^{\gamma Z}(s)}{s+\hat{\Sigma}^\gamma(s)}\right)^2 \cdot \frac{1}{s - M_Z^2 + \hat{\Sigma}^Z(s) - \frac{\left(\hat{\Sigma}^{\gamma Z}(s)\right)^2}{s+\hat{\Sigma}^\gamma(s)}}\,, \tag{6.21}$$

graphically depicted as

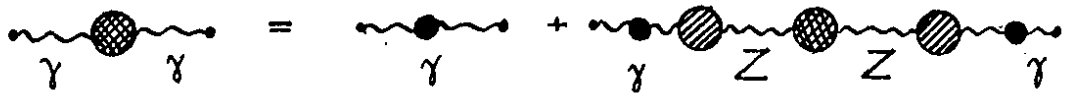

shows the presence of a second pole which is exactly the Z pole of (6.8). The pole of the mixing propagator (6.9) at $s = 0$ is cancelled by the $\hat{\Sigma}^{\gamma Z}$ in the numerator. The photon propagator (6.7) near its "conventional"pole at $s = 0$ still behaves like

$$D_\gamma(s) \approx \frac{1}{s} \cdot \frac{1}{1 + (\hat{\Sigma}^\gamma)'(0) + \hat{\Sigma}^{\gamma Z}(0) \cdot (\hat{\Sigma}^{\gamma Z})'(0)/(M_Z^2 - \hat{\Sigma}^Z(0))} = \frac{1}{s}$$

because of our renormalization conditions for $\hat{\Sigma}^\gamma$ and $\hat{\Sigma}^{\gamma Z}$ in (3.15). The photon field renormalization constant δZ_2^γ (and also the charge renormalization constant δZ_1^γ) thus is not changed by the mixing with the Z boson.

For Z and W the additional mass counter term in (6.20) appears in the field and coupling renormalization constants (3.17) and hence in the 2-point functions (3.23) involving massive bosons. In other places like the boson-fermion vertices this additional term does not show up since the corresponding counter terms contain only differences $\delta Z_1 - \delta Z_2$ which are independent of $\delta M_{Z,W}^2$. Vertex renormalization is therefore not affected.

The modification of the W propagator via δZ_2^W has a further consequence:
The quantity Δr in (4.18), which (together with M_Z) determines the numerical value for $\sin^2\theta_W$, is modified according to

$$\begin{aligned} \Delta r &\rightarrow \Delta r + \frac{c_W^2}{s_W^2} \mathrm{Re} \left(\frac{\left(\hat{\Sigma}^{\gamma Z}(M_Z^2)\right)^2 / M_Z^2}{M_Z^2 + \hat{\Sigma}^\gamma(M_Z^2)} \right) \\ &\equiv \Delta r + \Delta r_{(2)} \,. \end{aligned} \tag{6.22}$$

$\Delta r_{(2)}$ is responsible for a small shift in $\sin^2\theta_W$ if the top mass becomes large. For many physically interesting quantities like the width, peak cross section, and line shape of the Z, the effect of this shift in $\sin^2\theta_W$ is almost cancelled by the modification of the Z propagator discussed above such that the combined net effects are tiny.

To make this statement more quantitative we list a comparison of the following quantities calculated with and without the real part of the mixing term in (6.8): the integrated cross section for $e^+e^- \rightarrow \mu^+\mu^-$ at the resonance peak (without QED corrections), the total Z width, and $\sin^2\theta_W$ as well as M_W. The upper values are those derived without the mixing term. The table contains the results for $M_Z = 92$ GeV, $M_H = 100$ GeV, and for various top masses.

As one can see from the table there is practically no difference in σ and in Γ_Z for all values of m_t: the changes in σ are well below 0.1%, and the variation of Γ_Z is < 3 MeV and therefore smaller than the uncertainty induced by the error of α_s. For M_W as well, the shift remains below the experimental accuracy of 100 MeV, although it can come very close to it.

m-top	sigma [nb]	Z width [GeV]	sin**2 theta	W-mass [GeV]
50	1.9505	2.5589	0.22983	80.739
	1.9503	2.5593	0.22981	80.740
100	1.9497	2.5699	0.22458	81.013
	1.9500	2.5694	0.22457	81.014
150	1.9515	2.5820	0.21859	81.326
	1.9518	2.5807	0.21884	81.313
200	1.9553	2.5982	0.21092	81.724
	1.9550	2.5961	0.21187	81.675
230	1.9591	2.6101	0.20516	82.022
	1.9577	2.6074	0.20692	81.931

The changes in $\sin^2\theta_W$ are also only marginal for not too high top quark masses; for $m_t = 200$ GeV the difference is of the order 0.001. Thus, $\sin^2\theta_W$ is the only quantity which is affected by the mixing term, with measurable consequences on the on-resonance asymmetries to be discussed later. It is worth to note that our results on $\sin^2\theta_W$ agree within 0.0002 with the corresponding values of Kennedy et al. [91] (they have the slightly smaller values). This has to be compared with the uncertainty in $\sin^2\theta_W$ of 0.0004 from other sources (see section 4.4). The values for Γ_Z given in [91] are not for the physical width and cannot directly be compared with ours. Moreover, in [91] not the complete vertex corrections have been included. As pointed out by Burgers [42] the results of [91] are in agreement with ours after correcting for these inadequacies.

We want to conclude this discussion with a few critical remarks how to classify the listed additional small shifts in $\sin^2\theta_W$ in the light of further next order contributions not included at the present stage:

1. The modification of Δr by (6.21) leads to a sizable change in $\sin^2\theta_W$ only if m_t is large. For small m_t this variation is covered by the hadronic error in $\sin^2\theta_W$ with its source in the data entering the dispersion relation (4.32) for the light quarks. For a heavy top the leading contribution to Δr, eq. (4.29), rises proportional to m_t^2/M_W^2 and hence can become very large. Strong corrections to the (t,b) contribution to Δr can be estimated from their effects in the ρ parameter shift $\Delta\rho$ (defined in (4.43)) which is in leading order related to Δr by

$$\Delta r \approx -\frac{c_W^2}{s_W^2}\Delta\rho\,.$$

The $O(\alpha_s)$ strong corrections to $\Delta\rho$ have been calculated by Djouadi and Verzegnassi [92] and are reported to be large, in the heavy top limit given by

$$\Delta\rho \to \Delta\rho\cdot\left(1-\frac{\alpha_s}{\pi}\frac{2\pi^2+6}{9}\right)\,.$$

This leads to an increase in $\sin^2\theta_W$ of 0.002 for $m_t = 230$ GeV. Since the leading top approximation is not accurate enough for Δr preference would be given to a full calculation of the strong corrections. Without restriction to the leading term Kniehl et al. [93] have investigated the strong interaction effects in $\Delta r_{(t,b)}$ by the method of dispersion relations. They found smaller corrections but instead of the on-shell top mass an effective constituent top mass is used which is related to the mass M_T of the toponium ground state by $m_t \approx M_T - 400$ MeV (the precise relation is also affected by QCD corrections). The effect of the strong corrections can be expressed in terms of a change in the predictions for M_W by 25 - 60 MeV if m_t varies from 60 to 250 GeV. Both calculations [92,93] yield positive corrections to Δr. For $m_t > 150$ GeV also the choice of the scale where α_s has to be evaluated becomes of some significance, but still below the experimental sensitivity (estimates in [93] report an uncertainty in the left-right asymmetry which is about 1/3 of the aimed experimental error). A systematic study to get rid of this uncertainty would require a $O(\alpha_s^2)$ calculation. At present there seems not yet a sufficient consensus on the strong interaction effects from heavy quarks. In the results given in the following sections we use the lowest order expressions for the (t,b) doublet without incorporating the results of [92,93], having in mind, however, that our values for very large m_t may not give the ultimate answer.

2. We do not consider our strategy outlined above for the purely electroweak part as reliable enough for extrapolating to top masses much higher than about 250 GeV. The confidence in the reliability of the results is essentially based on the negligibility of 2-loop irreducible effects, which is safely true if m_t is small enough. As has been shown for $\Delta\rho$ [74] those effects are small also for heavy fermions in the absence of large isospin mass splitting. For a very heavy top, however, Yukawa couplings become strong and irreducible contributions involving Higgs bosons may become also large: for $m_t > 220$ GeV the corresponding coupling constant

$$\alpha_{Yukawa} = \frac{1}{4\pi}\left(\frac{g_2}{\sqrt{2}}\frac{m_t}{M_W}\right)^2 > \alpha_s$$

is of the same order as α_s. For the imaginary parts we have shown in [40] (see also chapter 5) that 2-loop irreducible effects are of the same size as the $O(\alpha^2)$ reducible ones in case of a heavy top. Therefore we would estimate that the limit of the present method is reached when the changes of $\sin^2\theta_W$ from the next order term in (6.22) exceed the $O(\alpha\alpha_s)$ corrections. This applies also to the method of Kennedy and Lynn in [43] since their "starred" objects are constructed on the basis of one-loop 1PI graphs only. Without a closer inspection of the 1PI 2-loop contributions involving strong Yukawa couplings the extrapolation to very high top masses as done in [43] has to be considered with some reservation.

6.4 Weak corrections

In this section we specify the complete set of the one-loop non-QED corrections (weak corrections in the sense of 6.2) to the polarization dependent differential cross section for $e^+e^- \to f\bar{f}$. Before doing this, however, we want to give a simple interpretation of the involved looking propagator corrections discussed in the preceding section which allows a better qualitative understanding and a simplified treatment in terms of an "improved Born approximation".

6.4.1 Improved Born amplitude

The matrix element for $e^+e^- \to f\bar{f}$ with the dressed propagators (6.7-9), (6.21) can be expressed graphically by use of the notation of section 6.2:

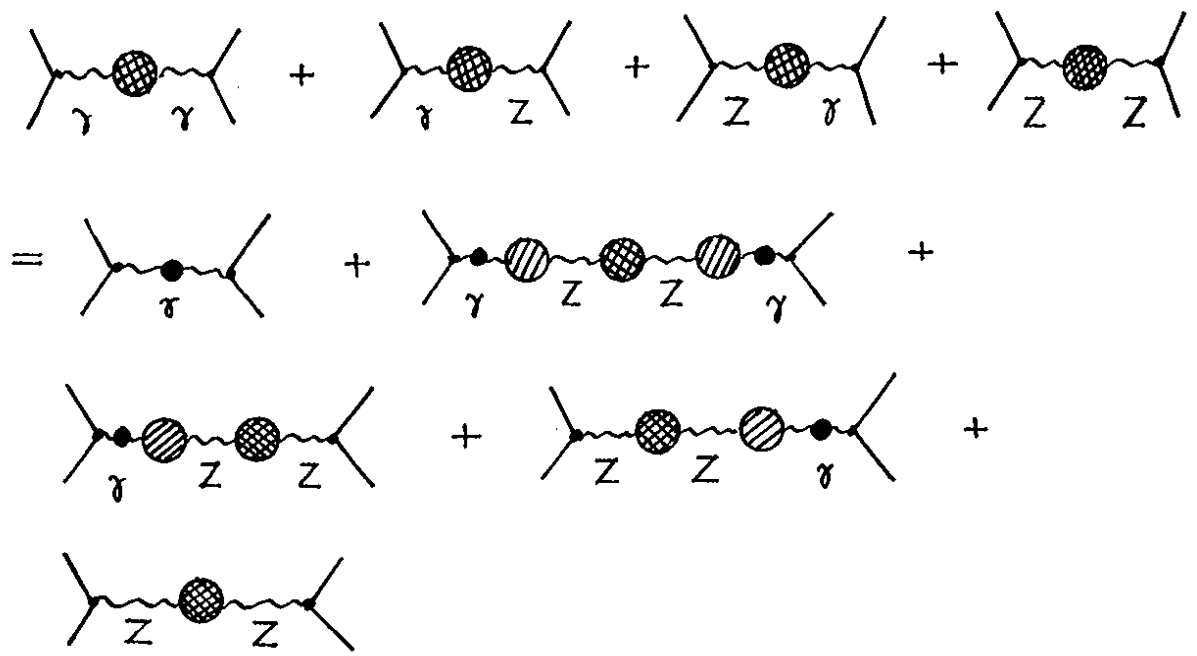

Neglecting the small imaginary parts except that of the Z propagator and replacing the full s dependence around the Z to a very good approximation by

$$\begin{aligned} \hat{\Sigma}^{\gamma}(s) &= s\,\hat{\Pi}^{\gamma}(M_Z^2) \\ \hat{\Sigma}^{\gamma Z}(s) &= s\,\hat{\Pi}^{\gamma Z}(M_Z^2) \end{aligned} \tag{6.23}$$

where

$$\begin{aligned} \hat{\Pi}^{\gamma}(s) &= \mathrm{Re}\,\frac{\hat{\Sigma}^{\gamma}(s)}{s} \\ \hat{\Pi}^{\gamma Z}(s) &= \mathrm{Re}\,\frac{\hat{\Sigma}^{\gamma Z}(s)}{s} \end{aligned} \tag{6.24}$$

and introducing the symbol

$$\gamma_\mu \otimes \gamma^\mu \equiv \bar{v}_e \gamma_\mu u_e \cdot \bar{u}_f \gamma^\mu v_f$$

for the spinor contractions we can write the amplitude in the following way:

$$\begin{aligned}\mathbf{M} &= \frac{e^2}{1+\hat{\Pi}^\gamma(M_Z^2)}\,Q_e Q_f\,\frac{1}{s}\,\gamma_\mu\otimes\gamma^\mu \\ &+ \frac{e^2}{4s_W^2 c_W^2}\,\frac{1}{1+\hat{\Pi}^Z(M_Z^2)}\,\frac{1}{s-M_Z^2+i\frac{s}{M_Z}\Gamma_Z}\cdot \\ &+ \gamma_\mu\left[I_3^e - 2\bar{s}_W^2 Q_e - I_3^e\gamma_5\right]\otimes\gamma^\mu\left[I_3^f - 2\bar{s}_W^2 Q_f - I_3^f\gamma_5\right]\end{aligned} \tag{6.25}$$

Thereby Γ_Z denotes the physical width (6.19), and

$$\bar{s}_W^2 = s_W^2 - s_W c_W \frac{\hat{\Pi}^{\gamma Z}(M_Z^2)}{1+\hat{\Pi}^\gamma(M_Z^2)}\,. \tag{6.26}$$

$\hat{\Pi}^Z(M_Z^2)$ is defined in eq. (6.18); it differs from the one-loop expression in (5.13) just by the quantity $\Delta r_{(2)}$ in (6.22). Making use of the relation (4.19) and its modification (6.22), together with

$$e(M_Z^2)^2 = \frac{e^2}{1+\hat{\Pi}^\gamma(M_Z^2)} \tag{6.27}$$

which is practically identical to the QED running α in (4.40), we find for the amplitude (6.25) the Born like expression

$$\begin{aligned}\mathbf{M} &= Q_e Q_f\,\frac{e(M_Z^2)^2}{s}\,\gamma_\mu\otimes\gamma^\mu \\ &+ \frac{G_\mu}{\sqrt{2}}\,\kappa\,\frac{M_Z^2}{s-M_Z^2+i\frac{s}{M_Z}\Gamma_Z}\cdot \\ &+ \gamma_\mu\left[I_3^e - 2\bar{s}_W^2 Q_e - I_3^e\gamma_5\right]\otimes\gamma^\mu\left[I_3^f - 2\bar{s}_W^2 Q_f - I_3^f\gamma_5\right]\end{aligned} \tag{6.28}$$

with

$$\kappa = \frac{1-\overline{\Delta r}}{1+\hat{\Pi}^Z(M_Z^2)}\,. \tag{6.29}$$

In this correction factor the formally higher order terms cancel as well as the leading log terms from the light fermions. It is therefore very close to 1, except for a heavy top. The leading top term yields

$$\kappa \approx 1 + \frac{3\alpha}{16\pi s_W^2}\cdot\frac{m_t^2}{M_W^2} \approx 1+\Delta\rho\,; \tag{6.30}$$

it behaves for large m_t like the ρ parameter defined in (4.43). (6.26) defines an effective mixing angle which deviates from s_W^2 also in case of a heavy top only, to leading order given by

$$\bar{s}_W^2 \approx s_W^2 + \frac{\alpha(M_Z^2)}{4\pi}\cdot\frac{3c_W^2}{4s_W^2}\cdot\frac{m_t^2}{M_W^2}\,. \tag{6.31}$$

The amplitude (6.28) together with the approximations (6.30) and (6.31) contains all (potentially) large effects from fermions, either light or heavy. The quality of the approximate formulae for κ and $\bar{s}_W^2$ is depicted in Figure 6.4. The residual terms of the full expressions are of the same size as the vertex (and box) corrections to be included next.

Figure 6.4:
Full (——) and approximate (- - - -) form of κ and the effective $\bar{s}^2_W$.
$M_Z = 92$ GeV, $M_H = 100$ GeV.

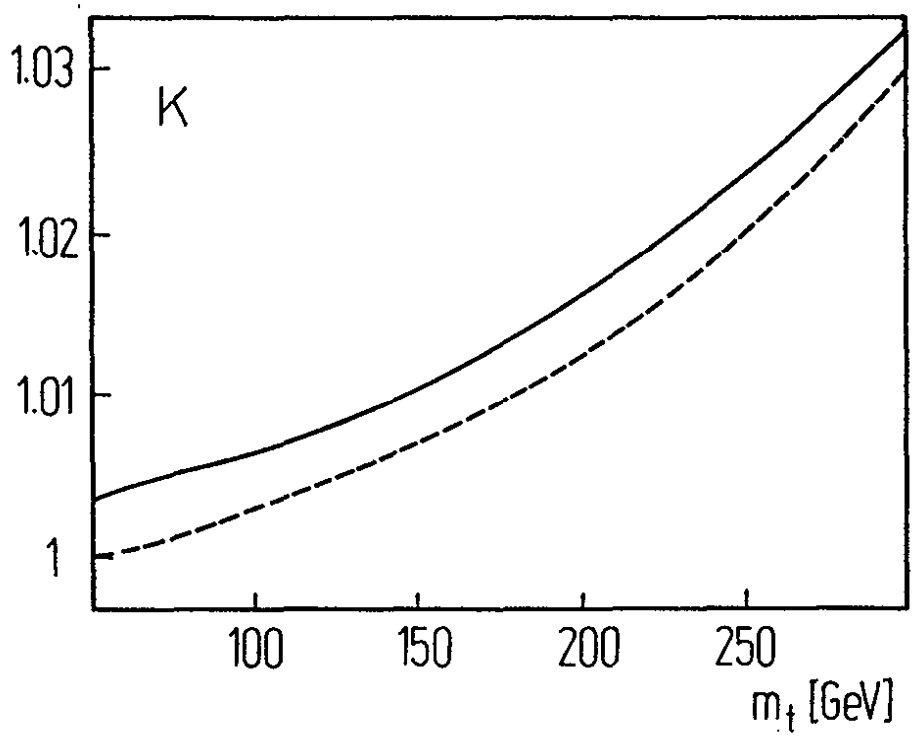

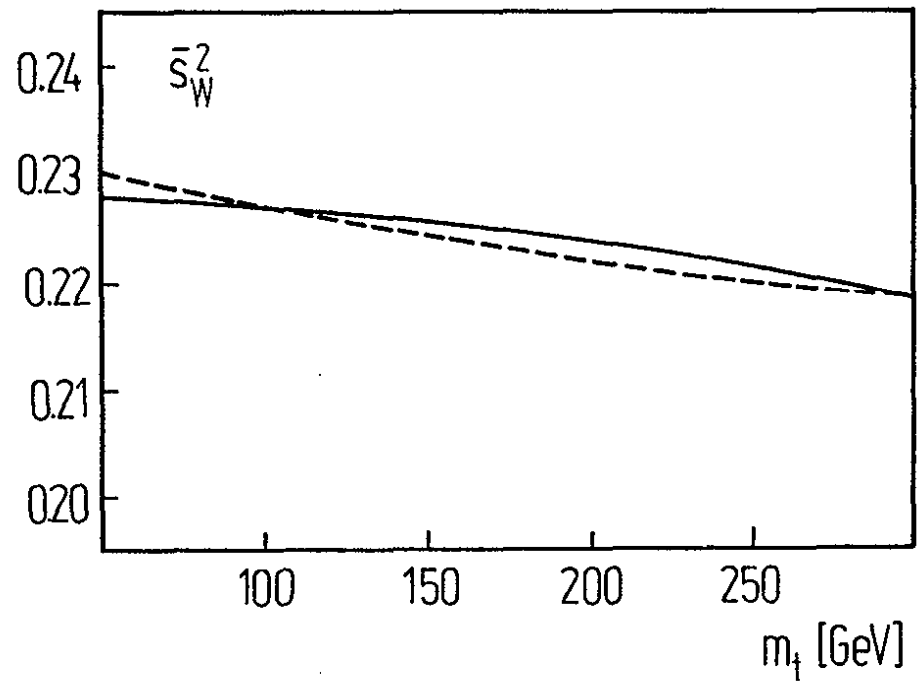

6.4.2 The complete expressions

In order to obtain the full result for the differential cross section (6.1) we have to specify only the invariant functions in (6.2), which are listed to lowest order in (6.4). We do this by introducing a compact notation in terms of s-dependent coupling constants and propagator functions according to the following table:

j	V_j^e	A_j^e	V_j^f	A_j^f	χ_j
1	Q_e	0	Q_f	0	$\chi_1 = \chi_\gamma$
2	v_e	a_e	v_f	a_f	$\chi_2 = \chi_Z$
3	Q_e	0	v_f	a_f	$\chi_3 = \chi_{\gamma Z}$
4	v_e	a_e	Q_f	0	$\chi_4 = \chi_{\gamma Z}$
5	$F_V^{\gamma e}(s)$	$F_A^{\gamma e}(s)$	Q_f	0	$\chi_5 = \chi_\gamma$
6	Q_e	0	$F_V^{\gamma f}(s)$	$F_A^{\gamma f}(s)$	$\chi_6 = \chi_\gamma$
7	$F_V^{Ze}(s)$	$F_A^{Ze}(s)$	v_f	a_f	$\chi_7 = \chi_Z$
8	v_e	a_e	$F_V^{Zf}(s)$	$F_A^{Zf}(s)$	$\chi_8 = \chi_Z$
9	$(v_e^2 + a_e^2)$	$2v_e a_e$	$(v_f^2 + a_f^2)$	$2v_f a_f$	χ_9
10	$2v_e a_e$	$(v_e^2 + a_e^2)$	$2v_f a_f$	$(v_f^2 + a_f^2)$	χ_{10}
11	$\frac{1}{2s_W}$	$\frac{1}{2s_W}$	$\frac{1}{2s_W}$	$\frac{1}{2s_W}$	χ_{11}

The coupling constants are those of (2.27); the form factors $F_V^{\gamma e} \cdots F_A^{Zf}$ from the vertex corrections are listed in Appendix C.

The functions χ are defined as follows:

$$\begin{aligned} \chi_\gamma &= s\, D_\gamma(s) \\ \chi_Z &= s\, D_Z(s) \\ \chi_{\gamma Z} &= -s\, D_{\gamma Z}(s) \end{aligned} \tag{6.32}$$

with the propagators $D_{\gamma,Z,\gamma Z}$ from (6.7-9). $\chi_{9,10}$ belong to the box diagrams with ZZ exchange and χ_{11} to that with WW exchange. The box contributions depend also on the scattering

angle resp. the Mandelstam variables

$$t = -\frac{s}{2}(1-\cos\theta), \quad u = -\frac{s}{2}(1+\cos\theta)\,.$$

They can be expressed in terms of functions I and I_5 given in Appendix D: [1]

$$\begin{aligned}
\chi_9 &= \frac{\alpha}{2\pi}\left[I(s,t,M_Z) - I(s,u,M_Z)\right] \qquad (6.33)\\
\chi_{10} &= \frac{\alpha}{2\pi}\left[I_5(s,t,M_Z) + I_5(s,u,M_Z)\right]\\
\chi_{11} &= \frac{\alpha}{2\pi}\begin{cases}\left[I(s,t,M_W) + I_5(s,t,M_W\right] & \text{for } I_3^f = -\frac{1}{2} \text{ fermions}\\ \left[-I(s,u,M_W) + I_5(s,u,M_W\right] & \text{for } I_3^f = +\frac{1}{2} \text{ fermions.}\end{cases}
\end{aligned}$$

The result can be summarized in terms of a matrix element

$$\mathbf{M} = \sum_j \gamma_\mu \left(V_j^e - A_j^e\gamma_5\right) \otimes \gamma^\mu \left(V_j^f - A_j^f\gamma_5\right) \chi_j\,.$$

Now we have collected everything for specifying the invariant functions as to be inserted into the cross section formulae (6.2):

$$\begin{aligned}
G_1(s,t) &= \mathrm{Re}\sum_{j,k=1}^{11}(V_j^e V_k^{e*} + A_j^e A_k^{e*})(V_j^f V_k^{f*} + A_j^f A_k^{f*})\,\chi_j\chi_k^* \qquad (6.34)\\
G_3(s,t) &= \mathrm{Re}\sum_{j,k=1}^{11}(V_j^e A_k^{e*} + A_j^e V_k^{e*})(V_j^f A_k^{f*} + A_j^f V_k^{f*})\,\chi_j\chi_k^*\\
H_1(s,t) &= \mathrm{Re}\sum_{j,k=1}^{11}(V_j^e A_k^{e*} + A_j^e V_k^{e*})(V_j^f V_k^{f*} + A_j^f A_k^{f*})\,\chi_j\chi_k^*\\
H_3(s,t) &= \mathrm{Re}\sum_{j,k=1}^{11}(V_j^e V_k^{e*} + A_j^e A_k^{e*})(V_j^f A_k^{f*} + A_j^f V_k^{f*})\,\chi_j\chi_k^*\\
F_1(s,t) &= \mathrm{Re}\sum_{j,k=1}^{11}(V_j^e V_k^{e*} - A_j^e A_k^{e*})(V_j^f V_k^{f*} + A_j^f A_k^{f*})\,\chi_j\chi_k^*\\
F_2(s,t) &= -\mathrm{Im}\sum_{j,k=1}^{11}(V_j^e A_k^{e*} - A_j^e V_k^{e*})(V_j^f V_k^{f*} + A_j^f A_k^{f*})\,\chi_j\chi_k^*\,.
\end{aligned}$$

For the functions G_2 and H_2 the lowest order expressions, if any, in (6.4) are sufficient; the same applies to the small mass term in G_1, H_1.

The cross section for unpolarized beams requires only G_1 and G_3. H_1, H_3 yield the longitudinal and F_1, F_2 the transverse polarization part of the cross section.

[1] In case of WW exchange either the direct or the crossed box diagram contributes depending on the isospin of the final fermion f

6.5 QED corrections

The distinguishing feature of the weak corrections is their independence of the specific experimental set up. The last piece completing our discussion at the one-loop level consists of the QED corrections which are the result of an incoherent superposition of 2-particle and (inclusive) 3-particle final states. In order to obtain an infrared finite result it is sufficient to deal with the soft photon part of the real bremsstrahlung cross section. The soft photon approximation means that the radiated photon energy $k^0 \leq \Delta E$ is restricted to a maximum energy ΔE which is small compared to the energy of the scattering process: $\Delta E \ll \sqrt{s} = 2E$. In this approximation the QED corrections can be cast into a form quite similar to that of the weak part. Since the photons radiated from the initial state need not necessarily be soft with respect to the resonance shape, however, the energy loss in the Z propagator has to be taken into account.

In real experiments the restriction to small values of $\Delta E/E$ is often not applicable due to the geometrical layout of a realistic detector. Then also hard photons with $k^0 > \Delta E$ become important and the definition of the final state may depend on other restrictions like accollinearity cuts to the outgoing fermion. These have usually been applied for μ pair production, conveniently treated by Monte Carlo simulations [28,44]. The proper hard photon part is IR and UV finite; it can be treated as decoupled from the rest of the electroweak cross section. The electroweak properties of the Z boson enter only globally in terms of the characterizing quantities mass, width, and coupling constants. For the adaptation between the soft and hard part, however, it has to be ensured that they are consistent with each other.

The abelian structure of the electromagnetic $U(1)_{em}$ symmetry implies that the virtual photonic corrections are UV finite already without the full SU(2)×U(1) renormalizability. After a complete renormalization of the full theory the photonic part of the corrections is recovered, but the separation within the whole set of radiative corrections is not unambigous and, in general, scheme dependent. It is a nice feature of the on-shell renormalization that we are left with the same QED corrections which would be obtained from a restriction to the $U(1)_{em}$ gauge structure only [29].

For completing our renormalized one-loop corrections in the on-shell scheme we list this class of virtual and soft real QED corrections. Differently from the weak corrections, the results cannot be presented at the level of amplitudes; we put them together as additive contributions to the functions in (6.34) with the same notations for the propagators:

$$\begin{aligned} G_1^{QED} &= Q_f^2 \mid \chi_1 \mid^2 C_{11}^V \\ &\quad + Q_e Q_f \, 2\,\mathrm{Re}\left\{\chi_1 \chi_2^* (v_e v_f C_{12}^V + a_e a_f C_{12}^A)\right\} \\ &\quad + \mid \chi_2 \mid^2 \left\{(v_e^2 + a_e^2)(v_f^2 + a_f^2) C_{22}^V + 4 v_e a_e v_f a_f C_{22}^A)\right\} \end{aligned} \tag{6.35}$$

$$\begin{aligned} G_3^{QED} &= Q_f^2 \mid \chi_1 \mid^2 C_{11}^A \\ &\quad + Q_e Q_f \, 2\,\mathrm{Re}\left\{\chi_1 \chi_2^* (a_e a_f C_{12}^V + v_e v_f C_{12}^A)\right\} \\ &\quad + \mid \chi_2 \mid^2 \left\{4 v_e a_e v_f a_f C_{22}^V + (v_e^2 + a_e^2)(v_f^2 + a_f^2) C_{22}^A\right\} \end{aligned}$$

$$
\begin{aligned}
H_1^{QED} &= Q_e Q_f \, 2\,\mathrm{Re}\left\{\chi_1 \chi_2^* (a_e v_f \, C_{12}^V + v_e a_f \, C_{12}^A)\right\} \\
&\quad + \mid \chi_2 \mid^2 \left\{2 v_e a_e (v_f^2 + a_f^2) \, C_{22}^V + 2(v_e^2 + a_e^2) v_f a_f \, C_{22}^A\right\}
\end{aligned}
$$

$$
\begin{aligned}
H_3^{QED} &= Q_e Q_f \, 2\,\mathrm{Re}\left\{\chi_1 \chi_2^* (v_e a_f \, C_{12}^V + a_e v_f \, C_{12}^A)\right\} \\
&\quad + \mid \chi_2 \mid^2 \left\{2(v_e^2 + a_e^2) v_f a_f \, C_{22}^V + 2 v_e a_e (v_f^2 + a_f^2) \, C_{22}^A\right\}
\end{aligned}
$$

$$
\begin{aligned}
F_1^{QED} &= Q_f^2 \mid \chi_1 \mid^2 \, C_{11}^V \\
&\quad + Q_e Q_f \, 2\,\mathrm{Re}\left\{\chi_1 \chi_2^* (v_e v_f \, C_{12}^V + a_e a_f \, C_{12}^A)\right\} \\
&\quad + \mid \chi_2 \mid^2 \, (v_e^2 - a_e^2)(v_f^2 + a_f^2) \, C_{22}^V
\end{aligned}
$$

$$
F_2^{QED} \approx 0 \, .
$$

The coefficients are defined as follows:

$$
\begin{aligned}
C_{11}^V &= \gamma_{IR} + \gamma_{fin} + Q_e Q_f (X + 2\,\mathrm{Re} V^{\gamma\gamma}) \qquad (6.36) \\
C_{11}^A &= 2\,\mathrm{Re}\, A^{\gamma\gamma} \\
C_{12}^V &= \gamma_{IR}^{int} + \gamma_{fin} + Q_e Q_f (X + V^{\gamma\gamma} + V^{\gamma Z}) \\
C_{12}^A &= Q_e Q_f \, (A^{\gamma\gamma} + A^{\gamma Z}) \\
C_{22}^V &= \gamma_{IR}^{res} + \gamma_{tail} + \gamma_{fin} + Q_e Q_f (X + 2\,\mathrm{Re} V^{\gamma Z}) \\
C_{22}^A &= Q_e Q_f \cdot 2\,\mathrm{Re}\, A^{\gamma Z} \, .
\end{aligned}
$$

For convenience we make use of the abbreviations

$$
\beta_e = \log\left(\frac{s}{m_e^2}\right) - 1, \quad \beta_{int} = 2 \log \frac{t}{u}, \quad \epsilon = \frac{\Delta E}{E} \qquad (6.37)
$$

and of the complex Z mass with the physical width Γ_Z

$$
M^2 = M_Z^2 - i M_Z \Gamma_Z \qquad (6.38)
$$

and specify the ingredients in (6.36) in the following way:

$$
\gamma_{IR} = \frac{2\alpha}{\pi} \left\{\beta_e + Q_f^2 \beta_f + Q_e Q_f \beta_{int}\right\} \log(\epsilon) \qquad (6.39)
$$

$$
\begin{aligned}
\gamma_{IR}^{int} &= \frac{2\alpha}{\pi} \left\{\beta_e \log\left(\epsilon \frac{M^2 - s}{M^2 - s + s\epsilon}\right) + Q_f^2 \beta_f \log(\epsilon)\right. \\
&\quad \left. + \frac{1}{2} Q_e Q_f \beta_{int} \log\left(\epsilon^2 \frac{s}{M^2 - s + s\epsilon}\right)\right\}
\end{aligned}
$$

$$
\begin{aligned}
\gamma_{IR}^{res} &= \frac{2\alpha}{\pi}\left\{\beta_e \log\mid \epsilon\frac{M^2-s}{M^2-s+s\epsilon}\mid + Q_f^2\beta_f\,\log(\epsilon)\right. \\
&\left. + Q_eQ_f\beta_{int}\log\mid \epsilon\frac{s}{M^2-s+s\epsilon}\mid\right\} \\
\gamma_{tail} &= \frac{2\alpha}{\pi}\beta_e\frac{s-M_Z^2}{M_Z\Gamma_Z}\left(\arctan\frac{M_Z^2-s+s\epsilon}{M_Z\Gamma_Z} - \arctan\frac{M_Z^2-s}{M_Z\Gamma_Z}\right) \\
\gamma_{fin} &= \frac{3\alpha}{2\pi}(\beta_e+Q_f^2\beta_f) + \frac{\alpha}{\pi}(1+Q_f^2)(\frac{\pi^2}{3}-\frac{1}{2})\,.
\end{aligned}
\tag{6.40}
$$

The quantity X is the finite part of the initial - final state bremsstrahlung interference

$$
X = \frac{\alpha}{\pi}\left[\log^2\left(-\frac{t}{s}\right) - 2\,\mathrm{Li}_2\left(-\frac{t}{s}\right) - \log^2\left(-\frac{u}{s}\right) + 2\,\mathrm{Li}_2\left(-\frac{u}{s}\right)\right]\,, \tag{6.41}
$$

and the following functions are the finite parts of the $\gamma\gamma$, γZ box diagrams:

$$
\begin{aligned}
V^{\gamma\gamma} &= \frac{\alpha}{2\pi}\left[G(s,t) - G(s,u) + 2\pi i\log\left(\frac{t}{u}\right)\right] \\
A^{\gamma\gamma} &= \frac{\alpha}{2\pi}\left[G(s,t) + G(s,u)\right] \\
V^{\gamma Z} &= \frac{\alpha}{2\pi}\left[V(s,t) - V(s,u)\right] \\
A^{\gamma Z} &= \frac{\alpha}{2\pi}\left[A(s,t) + A(s,u)\right]
\end{aligned}
\tag{6.42}
$$

with

$$
\begin{aligned}
G(s,t) &= \frac{s}{2(s+t)}\log\frac{t}{s+i\epsilon} - \frac{s(s+2t)}{4(s+t)^2}\left[\log^2\frac{t}{s+i\epsilon} + \pi^2\right]\,, \\
A(s,t) &= \frac{s-M^2}{s+t}\left\{\log\frac{t}{s-M^2} + \frac{M^2}{s}\log\left(1-\frac{s}{M^2}\right)\right. \\
&\left. + \frac{s+2t+M^2}{s+t}\left[\log\left(-\frac{t}{M^2}\right)\log\left(\frac{M^2-s}{M^2+t}\right) + \mathrm{Li}_2\left(\frac{s}{M^2}\right) - \mathrm{Li}_2\left(-\frac{t}{M^2}\right)\right]\right\}\,, \\
V(s,t) &= A(s,t) + 2\,\mathrm{Li}_2\left(1+\frac{M^2}{t}\right)\,.
\end{aligned}
\tag{6.43}
$$

Li_2 denotes the dilogarithm

$$
\mathrm{Li}_2(z) = -\int_0^1 dx\,\frac{\log(1-xz)}{x}\,.
$$

With this soft photon part our description of the one-loop renormalization is completed. The missing hard photon part, which is important for practical reasons, will not be given here. It has been treated extensively in the literature [28,29,44,50-53,94,101] and exists also in form of Monte Carlo programs [28,44,91,99,101]. In this place we only give an overview on the

present status; the influence of the QED corrections on the various measurable quantities, including hard photons, will be addressed in the following sections in each case seperately.

The soft photon part (in various approximations) has been calculated by several authors [26-29,95] for unpolarized beams; general beam polarization is discussed in [29]. The formulae given in this report are the most complete ones for the single photon case given in the literature up to now. They differ slightly from those of [29] where multi-photon radiation was included via exponentiation, similarly to [27]. Also vacuum polarizations are removed here since they have been treated already in the context of the preceding section. The restriction to the single photon case is required for the combination with the hard photon part in the Monte Carlo generator [44]. Multi photon emission can be restored analytically by exponentiating the infrared terms in (6.35). The discussions in [28,44] include the hard photon part in the unpolarized case. In [44] the helicity amplitudes are given for the radiative processes $e^+e^- \to \mu^+\mu^-\gamma, e^+e^-\gamma$ allowing to extend the existing Monte Carlo program also to beam polarization. The Monte Carlo generators based on [44] contain in addition the full weak part for unpolarized beams, that of [91] also for longitudinal polarization. Independent analytical calculations for total cross section and forward-backward asymmetry in $e^+e^- \to \mu^+\mu^-$ have been performed by Bardin et al. [50-52], for the cross section with longitudinal beam polarization by Jadach at al. [53].

The major part of the quoted work is concerned with the single bremsstrahlung process. An analytical calculation of the $O(\alpha^2)$ initial state corrections to the integrated cross section has been performed by Berends et al. [36], resummation of the leading log terms to all orders by various authors [27,29,35,37]. A Monte carlo approach to generate multi-photon final states based on the strategy of Yennie et al. [96] has been developped by Jadach and Ward [38].

6.6 The Z line shape

Besides α and G_μ we need the Z mass M_Z as an experimental quantity for completion of our input to fix the theory. M_Z will be measured from the shape of the resonance, in particular from the location of the maximum. The relation between $\sqrt{s_{max}}$ and M_Z is influenced sizably by the initial state bremsstrahlung. Since the $O(\alpha)$ QED corrections are large around the Z peak (typically -40%) a careful study of the next order contributions becomes necessary for precision measurements of the mass and width of the Z boson. The main source for large negative corrections is the initial state bremsstrahlung where both soft and hard photons lead to a reduction of the peak cross section: soft photons because of the absence of the ideal elastic process, and hard photons because of the energy loss in the resonance propagator. The reduction of the peak height of the integrated cross section is roughly given by the factor

$$1 - \frac{2\alpha}{\pi} \log(\frac{M_Z}{\Gamma_Z}) \log(\frac{M_Z^2}{m_e^2}) = 0.6$$

as can be seen from the IR term in (6.35).

A partial summation of multiple photon emission consists of exponentiation of the leading log terms with the main effect:

$$1 - \frac{2\alpha}{\pi} \log(\frac{M_Z}{\Gamma_Z}) \log(\frac{M_Z^2}{m_e^2}) \quad \longrightarrow \quad \left(\frac{M_Z}{\Gamma_Z}\right)^{-\frac{2\alpha}{\pi}\log(M_Z^2/m_e^2)}$$

A comparison with and without exponentiation shows that the position of the maximum in $O(\alpha)$ is significantly too high. The exact treatment of the $O(\alpha^2)$ initial state QED corrections to the integrated $e^+e^- \rightarrow \mu^+\mu^-$ cross section has been performed in [36]: The displacement of the resonance peak of +184 MeV from $O(\alpha)$ is reduced by -88 MeV due to the $O(\alpha^2)$ contributions if $M_Z = 93$ GeV is taken (Figure 6.5). The remaining uncertainty can be estimated from

$$O(\alpha^2)\ exponentiated - O(\alpha^2)\ non\ exponentiated$$

to be about 15 MeV.

Figure 6.5

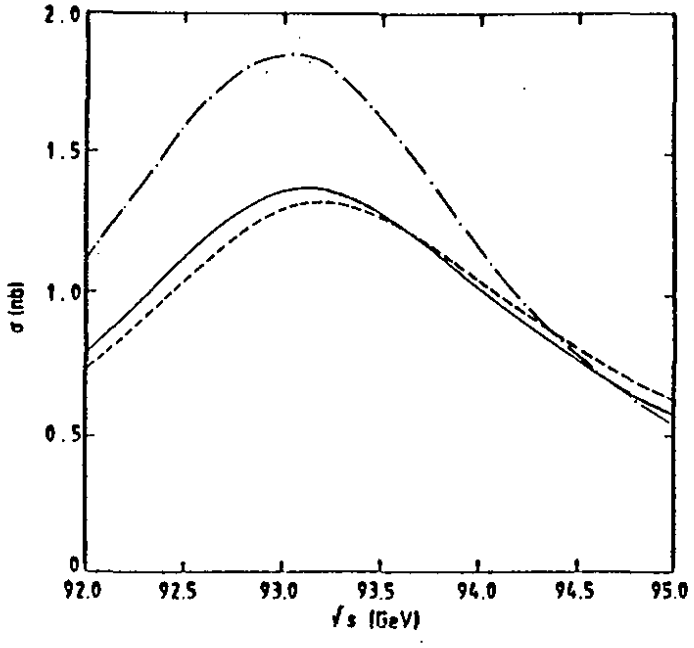

Total cross section for $e^+e- \longrightarrow \mu^+\mu^-$
—·—·— Born approximation
– – – – – – $O(\alpha)$ corrected
———— $O(\alpha^2)$ corrected

The effect of final state radiation amounts to a factor $1 + \frac{3\alpha}{4\pi}Q_f^2$ for each fermion type contribution to the total cross section which means a correction of less than 0.2%. Also the interference of initial-final state radiation together with $\gamma\gamma$, γZ box diagrams does not influence the maximum position in a significant way [42,53].

For a final answer also the weak corrections have to be incorporated. This has been done by Berends et al. [41] with the following main results:

- The position of the peak maximum is shifted to lower values by about 35 MeV. This shift is due to the s-dependence of the width and was confirmed by Bardin et al. [52].
- The dependence of the maximum position on the unknown standard model parameters M_H, m_t is insignificant. This is important for an experimental determination of M_Z which is required to be free of model assumptions.

This last point is substantiated in Figure 6.6 which presents the Z line shape as depending on M_H, m_t, and in the values of table 6.1. The results include the higher order QED corrections; they are an update of [41] (which are only very little changed) based on the most recent version of the weak part in 6.4, and were figured out by Burgers [42] using [90].

Table 6.1: Peak maximum and position in $e^+e^- \rightarrow \mu^+\mu^-$. $M_Z = 92$ GeV, $\alpha_s = 0.12$.

m_t[GeV]	M_H[GeV]	σ_{max}[nb]	$\sqrt{s_{max}}$ [GeV]
40	100	1.369	92.094
60	100	1.452	92.094
90	10	1.446	92.094
90	100	1.453	92.094
90	1000	1.454	92.094
230	10	1.454	92.096
230	100	1.461	92.096
230	1000	1.461	92.095

Figure 6.6

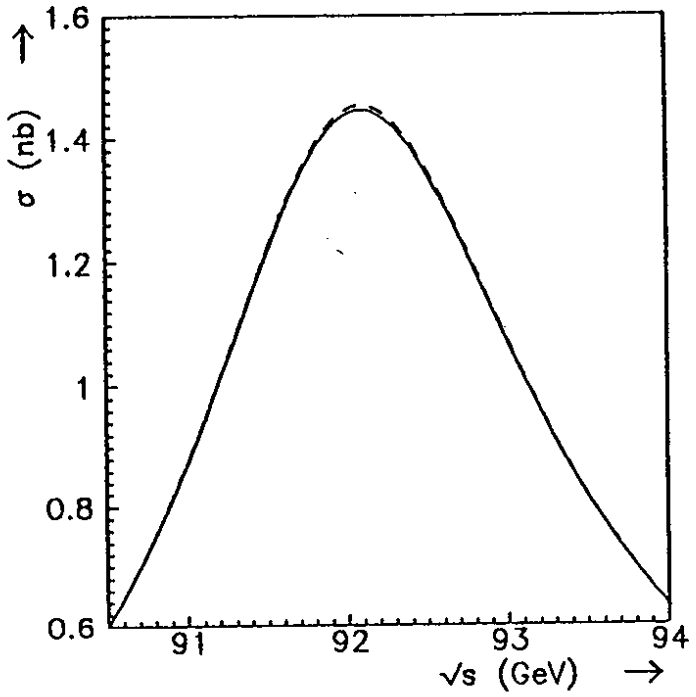

Higgs-mass dependence of the Z peak in muon-pair production. $M_Z = 92\text{GeV}$, $m_t = 90\text{GeV}$, $\alpha_s = 0.12$. Dashed line $M_H = 1000\text{GeV}$, solid line $M_H = 10\text{GeV}$.

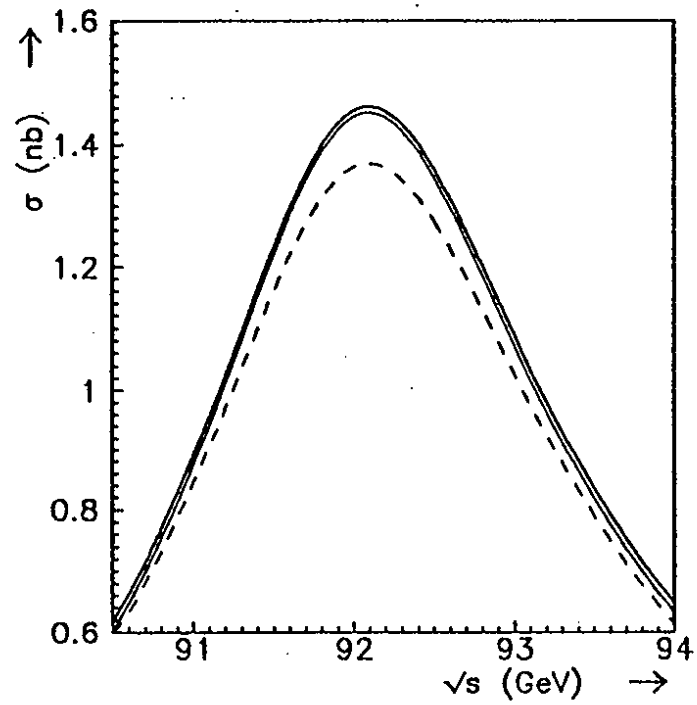

Top-mass dependence of the Z peak in muon-pair production. $M_Z = 92\text{GeV}$, $M_H = 100\text{GeV}$, $\alpha_s = 0.12$. Upper solid line $m_t = 230\text{GeV}$, lower solid line $m_t = 60\text{GeV}$, dashed line $m_t = 40\text{GeV}$.

6.7 On-resonance asymmetries

The measurement of the Z mass from the resonance shape completes our set of input parameters α, G_μ, M_Z for fixing the theory.

For testing the theory further precisely measurable quantities are necessary. From the Z line shape one can determine, besides M_Z, the following quantities:

- the total cross section
$$\sigma_T = \sum_f \sigma(e^+e^- \to f\bar{f})$$
- the total Z width Γ_Z

which have already been addressed in the previous sections. The hadronic cross section will be discussed later. Without beam polarization the further observables are accessible:

- the partial widths $\Gamma_Z(Z \to f\bar{f})$;
- the forward-backward asymmetries
$$A_{FB}(e^+e^- \to f\bar{f}) = \frac{\sigma^{for} - \sigma^{back}}{\sigma^{for} + \sigma^{back}} \; ; \tag{6.44}$$
with
$$\sigma^{for} = \int_{\theta<\pi/2} d\Omega \, \frac{d\sigma}{d\Omega}, \quad \sigma^{back} = \int_{\theta>\pi/2} d\Omega \, \frac{d\sigma}{d\Omega}$$

The instrument of longitudinal polarization for the incident e^- beam offers the polarization dependent asymmetries

- the left-right asymmetry
$$A_{LR} = \frac{\sigma_L - \sigma_R}{\sigma_L + \sigma_R} \tag{6.45}$$
where $\sigma_{L(R)}$ denotes the integrated cross section for left (right) handed electrons;
- the polarized forward-backward asymmetry
$$A_{FB}^{pol}(e^+e^- \to f\bar{f}) = \frac{\sigma_L^{for} - \sigma_L^{back} - (\sigma_R^{for} - \sigma_R^{back})}{\sigma_L^{for} + \sigma_L^{back} + \sigma_R^{for} + \sigma_R^{back}} \tag{6.46}$$

In this section we want to discuss these asymmetries in some detail. In lowest order the on-resonance asymmetries are simple combinations of the fermionic coupling constants [2] :

$$\begin{aligned} A_{FB} &= \frac{3}{4} \cdot \frac{2v_e a_e}{v_e^2 + a_e^2} \cdot \frac{2v_f a_f}{v_f^2 + a_f^2} \\ A_{LR} &= \frac{2v_e a_e}{v_e^2 + a_e^2} \\ A_{FB}^{pol} &= \frac{3}{4} \cdot \frac{2v_f a_f}{v_f^2 + a_f^2} \; . \end{aligned} \tag{6.47}$$

[2] up to small terms $\sim (\Gamma_Z/M_Z)^2$ coming from the pure γ exchange

The ingredients in all these asymmetries are the combinations

$$A_f := \frac{2v_f a_f}{v_f^2 + a_f^2} = \frac{2 \mid 2I_3^f - 4Q_f \sin^2\theta_W \mid}{1 + (2I_3^f - 4Q_f \sin^2\theta_W)^2} \; ; \tag{6.48}$$

for a given species of fermions they are functions of $\sin^2\theta_W$ only. Note that $A_{FB}^{pol}(e^+e^- \to f\bar{f})$ measures the same quantity A_f as the final state polarization of the fermion f in $e^+e^- \to f\bar{f}$. A_f is displayed in Figure 6.7 for various fermions.

The ϕ-dependence of the cross section (6.1) in case of transverse polarization gives rise to an azimuthal asymmetry, which is determined by the quantity

$$A_T = \frac{F_1}{G_1} \; . \tag{6.49}$$

On-resonance it reduces to

$$A_T \approx -1 + \frac{v_e^2}{a_e^2} \; ,$$

which measures essentially the same information as the unpolarized leptonic forward-backward asymmetry if the lepton couplings are universal. We will therefore skip a more elaborate discussion, but refer to $A_{FB}(e^+e^- \to \mu^+\mu^-)$. The following general features of A_T are of practical importance: full ϕ acceptance, independence of the final state, insensitivity to QED corrections [29].

Figure 6.7: The quantity A_f for quarks and leptons.

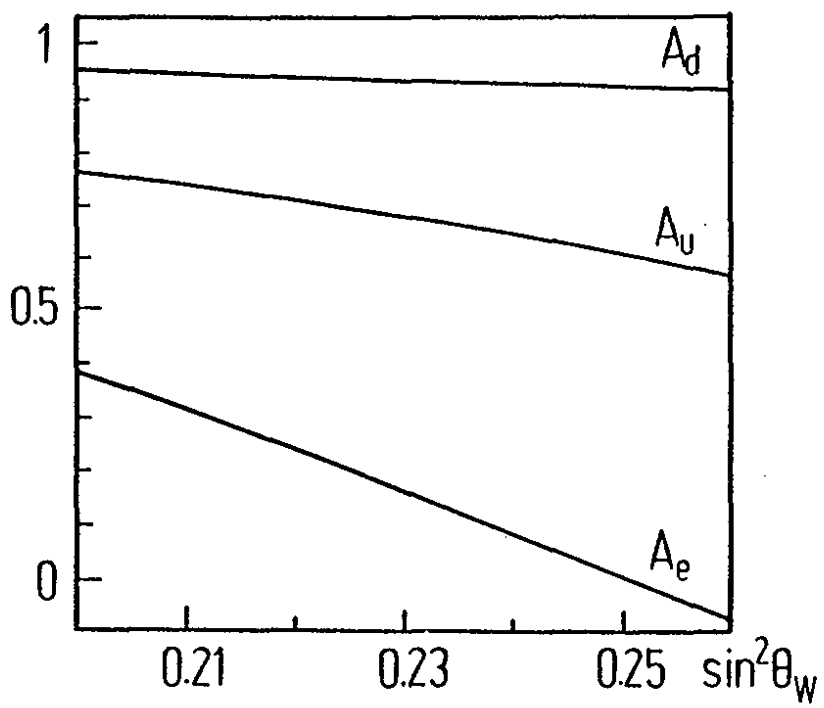

Since a sensitivity to $\sin^2\theta_W$ means also a sensitivity to the details of the weak part of the model the structure of (6.47) suggests A_{LR} and A_{FB}^{pol} to be the best candidates for electroweak tests: A_{LR} measures the initial state and A_{FB}^{pol} the final state coupling constants, allowing simultanously tests of the fermion universality. The particular sensitivity of A_{LR} to $\sin^2\theta_W$ will allow a measurement of this parameter with an error of ± 0.0004 if an accuracy $(\Delta A_{LR})_{exp} = 0.003$ can be achieved [14] (see Figure 6.8).

Figure 6.8: $\sin^2\theta_W$ from α, G_μ, M_Z, and from A_{LR}. $M_Z = 93$ GeV, $m_t = 60$ GeV.

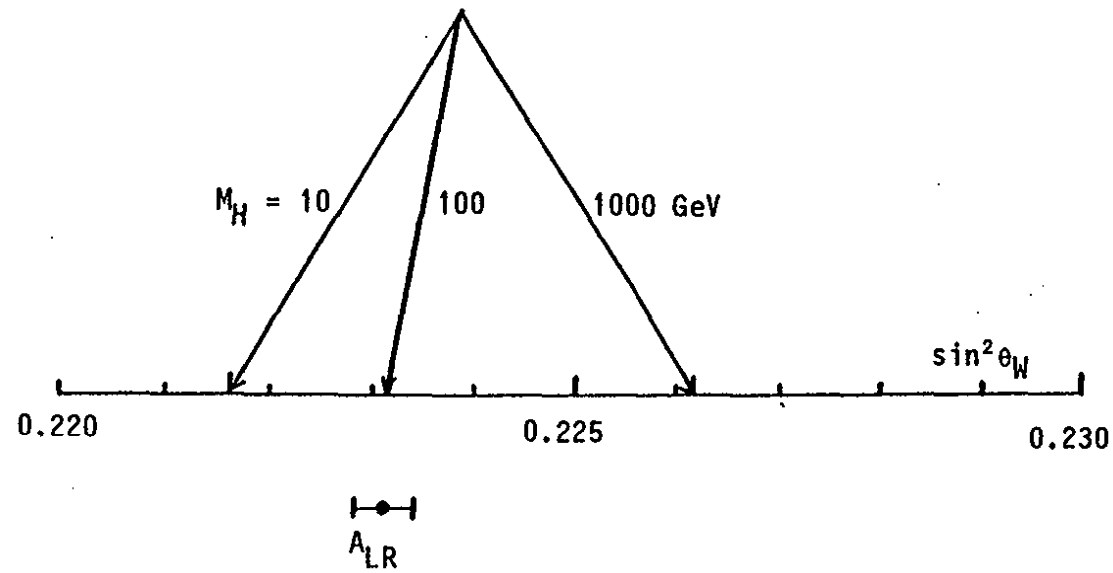

A_{LR} is practically independent of the final state fermion species which allows an inclusive measurement without loss of statistics. Another important advantage of A_{LR} is the property that it is only very little influenced by QED corrections. This was first pointed out in 1982 by Böhm and Hollik [29] for the soft photon part, and was later confirmed also for the inclusion of hard photons, analytically by Jadach et al. [53], and numerically via Monte Carlo simulation by Kennedy et al. [91]. At the Trieste Workshop on radiative corrections in 1983 [23] the author emphasized the unique possibility of testing the non-QED part of the electroweak theory in terms of A_{LR} [97] which was followed by a closer inspection of the weak contributions by Lynn and Stuart [33] and Hollik [34]. A_{LR} is only very little influenced also by QCD corrections in case of quark pair production [80,98] as far as the quark masses are small. Moreover, also A_{FB}^{pol} has been shown to get only very small QED corrections [99], allowing the conjecture that the next order contributions do not play a practical role. For a discussion of the QED corrections to the unpolarized forward-backward asymmetry and their cut dependence we refer to [100]. The weak corrections to $A_{FB}(e^+e^- \to \mu^+\mu^-)$ have been treated by many authors [26,30-34,95,101].

The explicit sensitivity of A_{LR} and $A_{FB}(e^+e^- \to \mu^+\mu^-)$ to $\sin^2\theta_W$ allows to use these quantities for measurements of $\sin^2\theta_W$. From this point of view $\sin^2\theta_W$ (resp. M_W) is considered as an independent parameter, not yet fixed in terms of G_μ. Figure 6.9 shows the

on-resonance asymmetries A_{LR}, A_{FB}, in lowest order from (6.47), and with the weak corrections included. Although for a "light" top quark the Born approximation is very close to the full one-loop prediction, the differences of ~ 0.005 in A_{LR} (and even larger fore other Higgs masses) and ~ 0.004 in A_{FB} are not negligible in view of the experimental accuracy.

Whereas the Born term is a function of $\sin^2\theta_W$ only, the complete expressions depend also on m_t (and to a less extent on M_H). The determination of $\sin^2\theta_W$ from a measured value of A_{LR} or A_{FB} hence is not free of assumptions on m_t and M_H. This, however, is not surprising since also the determination of $\sin^2\theta_W$ from M_Z, G_μ yields values dependent on m_t, M_H, and both results have to agree if the minimal model is correct. The asymmetries which correspond to those "correct" $\sin^2\theta_W$ values are marked by a dot in Figure 6.9

Figure 6.9: A_{LR} and A_{FB} in $e^+e^- \to \mu^+\mu^-$. $M_Z = 92$ GeV, $M_H = 100$ GeV.

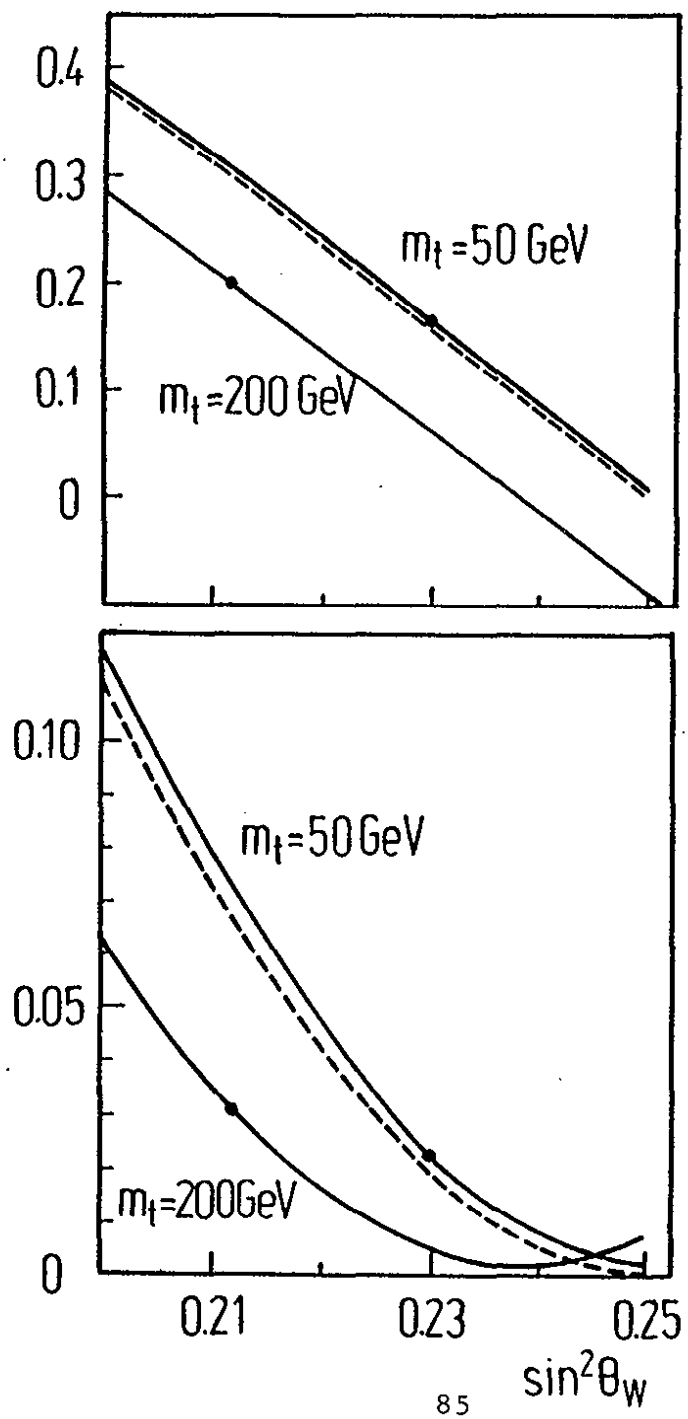

This brings us to the second point of view: Given M_Z (together with m_t, M_H), $\sin^2\theta_W$ and M_W are fixed in the minimal model, and so are the asymmetries. The lowest order values are obtained from the Born formulae (6.47) together with $\sin^2\theta_W$ as derived from G_μ and M_Z. The effect of the propagator corrections can be summarized by a shift in $\sin^2\theta_W$, yielding the effective $\bar{s}^2_W$ of (6.26) which is independent of the final fermion species. The residual contributions are almost completely due to the weak vertex corrections. Both types of corrections are significant for A_{LR} in view of precision experiments. The results are put together in the following table (for $M_Z = 92$ GeV, $M_H = 100$ GeV, $m_t = 50$ GeV):

	A_{LR}	A_{FB}
Born term	0.1596	0.0192
with propagator corrections	0.1727	0.0248
with full weak corrections	0.1668	0.0230

Next we want to describe the influence of the $O(\alpha^2)$ term in the Z propagator, as discussed in section 6.3: The upper values in the table are those derived without the mixing term. As one can see A_{LR} is slightly changed for large m_t, whereas A_{FB} is not influenced in a way exceeding the experimental accuracy. (Input: $M_Z = 92$ GeV, $M_H = 100$ GeV)

m_t [GeV]	A_{LR}	A_{FB}
50	0.1663	0.0229
	0.1668	0.0230
100	0.1760	0.0253
	0.1745	0.0249
150	0.1891	0.0280
	0.1850	0.0276
200	0.2068	0.0310
	0.1990	0.0315
230	0.2200	0.0328
	0.2089	0.0345

In the following tables we collect the predictions for A_{LR}, A_{FB} in $e^+e^- \to \mu^+\mu^-$ for a wide range of the model parameters. As can be seen, the variation with M_H in A_{LR} is about five times as big as the expected experimental error. This means that A_{LR} becomes sensitive to the Higgs mass; probably it is the only quantity which can probe indirectly the Higgs sector of the minimal model. The variation in A_{FB} is somewhat less striking, about twice the experimental error.

Table 6.3: A_{LR} for $e^+e^- \to \mu^+\mu^-$ (masses in GeV)

		M-Higgs		
M-Z	m-top	10	100	1000
90.	50.	0.0585	0.0510	0.0404
90.	100.	0.0669	0.0595	0.0491
90.	150.	0.0787	0.0714	0.0612
90.	200.	0.0943	0.0871	0.0772
90.	230.	0.1055	0.0984	0.0886
91.	50.	0.1181	0.1110	0.1009
91.	100.	0.1261	0.1190	0.1092
91.	150.	0.1372	0.1302	0.1206
91.	200.	0.1519	0.1450	0.1357
91.	230.	0.1624	0.1556	0.1465
92.	50.	0.1736	0.1668	0.1573
92.	100.	0.1812	0.1745	0.1652
92.	150.	0.1917	0.1850	0.1760
92.	200.	0.2055	0.1990	0.1901
92.	230.	0.2154	0.2089	0.2003
93.	50.	0.2252	0.2188	0.2098
93.	100.	0.2325	0.2261	0.2173
93.	150.	0.2423	0.2360	0.2275
93.	200.	0.2553	0.2491	0.2408
93.	230.	0.2646	0.2584	0.2503
94.	50.	0.2732	0.2671	0.2586
94.	100.	0.2802	0.2741	0.2658
94.	150.	0.2894	0.2834	0.2753
94.	200.	0.3015	0.2956	0.2878
94.	230.	0.3102	0.3044	0.2967
95.	50.	0.3178	0.3119	0.3040
95.	100.	0.3244	0.3186	0.3108
95.	150.	0.3331	0.3274	0.3198
95.	200.	0.3445	0.3389	0.3315
95.	230.	0.3526	0.3471	0.3398
96.	50.	0.3591	0.3536	0.3461
96.	100.	0.3655	0.3600	0.3526
96.	150.	0.3737	0.3682	0.3610
96.	200.	0.3843	0.3790	0.3720
96.	230.	0.3919	0.3866	0.3798

Table 6.4 : $\hat{A_{FB}}$ for $e^+e^- \to \mu^+\mu^-$ (masses in GeV)

		M-Higgs		
M-Z	m-top	10	100	1000
90.	50.	0.0043	0.0037	0.0030
90.	100.	0.0050	0.0043	0.0035
90.	150.	0.0062	0.0054	0.0044
90.	200.	0.0081	0.0071	0.0059
90.	230.	0.0097	0.0086	0.0072
91.	50.	0.0124	0.0112	0.0096
91.	100.	0.0138	0.0125	0.0108
91.	150.	0.0159	0.0145	0.0127
91.	200.	0.0189	0.0174	0.0155
91.	230.	0.0213	0.0197	0.0176
92.	50.	0.0248	0.0230	0.0208
92.	100.	0.0267	0.0249	0.0226
92.	150.	0.0295	0.0276	0.0252
92.	200.	0.0335	0.0315	0.0290
92.	230.	0.0365	0.0345	0.0319
93.	50.	0.0404	0.0383	0.0354
93.	100.	0.0428	0.0406	0.0377
93.	150.	0.0462	0.0440	0.0410
93.	200.	0.0509	0.0486	0.0456
93.	230.	0.0545	0.0520	0.0490
94.	50.	0.0586	0.0561	0.0528
94.	100.	0.0614	0.0588	0.0555
94.	150.	0.0652	0.0626	0.0593
94.	200.	0.0705	0.0678	0.0644
94.	230.	0.0744	0.0717	0.0682
95.	50.	0.0785	0.0757	0.0721
95.	100.	0.0816	0.0788	0.0752
95.	150.	0.0858	0.0830	0.0793
95.	200.	0.0915	0.0886	0.0849
95.	230.	0.0957	0.0927	0.0890
96.	50.	0.0997	0.0967	0.0928
96.	100.	0.1031	0.1001	0.0962
96.	150.	0.1075	0.1045	0.1006
96.	200.	0.1135	0.1104	0.1065
96.	230.	0.1178	0.1147	0.1108

Finally we want to compare our results with those of Lynn and Stuart [33]. To this end we have to restrict ourselves to the $O(\alpha)$ contributions and to adjust our hadronic part of Δr to $\Delta r_{had}^{QED} = -0.0274$, which was used in [33]. Doing this, we find agreement in A_{LR} within < 0.0004 for the whole parameter range. The values for A_{FB} are also in very good agreement for $m_t < 130$ GeV (differences smaller than 0.001); for $m_t = 180$ GeV our values are slightly higher (by about 0.002).

The following tables for the hadronic forward-backward asymmetries with and without longitudinal beam polarization complete the results of this section. In $e^+e^- \to b\bar{b}$, $c\bar{c}$ they are expected to be measurable with an error of about 0.02. For a detailed experimental discussion see the contribution by Drees et al. [102] to the CERN report on Polarization at LEP [14].

Table 6.5: $A_{FB}(e^+e^- \to b\bar{b})$ (masses in GeV)

		M-Higgs		
M-Z	m-top	10	100	1000
90.	50.	0.0423	0.0371	0.0297
90.	100.	0.0481	0.0429	0.0357
90.	150.	0.0561	0.0510	0.0439
90.	200.	0.0664	0.0614	0.0546
90.	230.	0.0737	0.0687	0.0621
91.	50.	0.0842	0.0792	0.0721
91.	100.	0.0898	0.0849	0.0779
91.	150.	0.0975	0.0925	0.0858
91.	200.	0.1072	0.1024	0.0959
91.	230.	0.1140	0.1093	0.1029
92.	50.	0.1237	0.1189	0.1121
92.	100.	0.1291	0.1243	0.1177
92.	150.	0.1363	0.1316	0.1252
92.	200.	0.1455	0.1409	0.1347
92.	230.	0.1519	0.1473	0.1413
93.	50.	0.1608	0.1561	0.1497
93.	100.	0.1660	0.1613	0.1551
93.	150.	0.1728	0.1682	0.1621
93.	200.	0.1814	0.1770	0.1711
93.	230.	0.1874	0.1830	0.1773
94.	50.	0.1954	0.1910	0.1849
94.	100.	0.2004	0.1960	0.1900
94.	150.	0.2068	0.2025	0.1967
94.	200.	0.2150	0.2107	0.2051
94.	230.	0.2206	0.2164	0.2110
95.	50.	0.2279	0.2236	0.2178
95.	100.	0.2327	0.2284	0.2228
95.	150.	0.2387	0.2345	0.2290
95.	200.	0.2463	0.2423	0.2370
95.	230.	0.2516	0.2476	0.2424
96.	50.	0.2582	0.2541	0.2486
96.	100.	0.2628	0.2587	0.2534
96.	150.	0.2685	0.2645	0.2593
96.	200.	0.2756	0.2717	0.2667
96.	230.	0.2805	0.2767	0.2718

Table 6.6: $A_{FB}(e^+e^- \to c\bar{c})$ (masses in GeV)

		M-Higgs		
M-Z	m-top	10	100	1000
90.	50.	0.0295	0.0258	0.0207
90.	100.	0.0336	0.0299	0.0248
90.	150.	0.0394	0.0358	0.0307
90.	200.	0.0474	0.0437	0.0386
90.	230.	0.0531	0.0494	0.0444
91.	50.	0.0601	0.0563	0.0511
91.	100.	0.0643	0.0606	0.0554
91.	150.	0.0703	0.0665	0.0614
91.	200.	0.0783	0.0745	0.0694
91.	230.	0.0841	0.0804	0.0753
92.	50.	0.0907	0.0869	0.0816
92.	100.	0.0950	0.0912	0.0860
92.	150.	0.1010	0.0972	0.0920
92.	200.	0.1090	0.1052	0.1001
92.	230.	0.1148	0.1110	0.1059
93.	50.	0.1210	0.1171	0.1118
93.	100.	0.1253	0.1214	0.1162
93.	150.	0.1312	0.1274	0.1222
93.	200.	0.1391	0.1353	0.1302
93.	230.	0.1448	0.1410	0.1360
94.	50.	0.1505	0.1466	0.1414
94.	100.	0.1548	0.1510	0.1458
94.	150.	0.1607	0.1568	0.1517
94.	200.	0.1684	0.1646	0.1596
94.	230.	0.1740	0.1702	0.1653
95.	50.	0.1791	0.1753	0.1701
95.	100.	0.1835	0.1796	0.1746
95.	150.	0.1891	0.1853	0.1804
95.	200.	0.1967	0.1929	0.1880
95.	230.	0.2021	0.1983	0.1935
96.	50.	0.2067	0.2029	0.1979
96.	100.	0.2110	0.2072	0.2023
96.	150.	0.2165	0.2128	0.2079
96.	200.	0.2238	0.2201	0.2154
96.	230.	0.2291	0.2254	0.2207

Table 6.7: $A_{FB}^{pol}(e^+e^- \to c\bar{c})$ (masses in GeV)

		M-Higgs		
M-Z	m-top	10	100	1000
90.	50.	0.4698	0.4672	0.4635
90.	100.	0.4727	0.4702	0.4665
90.	150.	0.4768	0.4743	0.4707
90.	200.	0.4821	0.4797	0.4763
90.	230.	0.4859	0.4835	0.4802
91.	50.	0.4902	0.4878	0.4844
91.	100.	0.4929	0.4905	0.4872
91.	150.	0.4966	0.4943	0.4910
91.	200.	0.5014	0.4992	0.4961
91.	230.	0.5049	0.5027	0.4997
92.	50.	0.5086	0.5063	0.5032
92.	100.	0.5110	0.5089	0.5058
92.	150.	0.5144	0.5123	0.5093
92.	200.	0.5189	0.5168	0.5139
92.	230.	0.5221	0.5200	0.5172
93.	50.	0.5252	0.5231	0.5203
93.	100.	0.5275	0.5255	0.5227
93.	150.	0.5306	0.5286	0.5259
93.	200.	0.5347	0.5328	0.5301
93.	230.	0.5376	0.5357	0.5331
94.	50.	0.5403	0.5384	0.5358
94.	100.	0.5425	0.5406	0.5380
94.	150.	0.5453	0.5435	0.5410
94.	200.	0.5491	0.5473	0.5448
94.	230.	0.5517	0.5499	0.5476
95.	50.	0.5540	0.5523	0.5498
95.	100.	0.5561	0.5543	0.5519
95.	150.	0.5587	0.5570	0.5547
95.	200.	0.5622	0.5605	0.5582
95.	230.	0.5646	0.5629	0.5608
96.	50.	0.5666	0.5649	0.5626
96.	100.	0.5685	0.5668	0.5646
96.	150.	0.5709	0.5693	0.5672
96.	200.	0.5741	0.5725	0.5704
96.	230.	0.5764	0.5748	0.5728

Table 6.8: $A_{FB}^{pol}(e^+e^- \to b\bar{b})$ (masses in GeV)

		M-Higgs		
M-Z	m-top	10	100	1000
90.	50.	0.6925	0.6921	0.6914
90.	100.	0.6929	0.6924	0.6917
90.	150.	0.6932	0.6927	0.6921
90.	200.	0.6936	0.6931	0.6925
90.	230.	0.6939	0.6934	0.6928
91.	50.	0.6963	0.6959	0.6953
91.	100.	0.6966	0.6962	0.6956
91.	150.	0.6969	0.6965	0.6959
91.	200.	0.6973	0.6968	0.6963
91.	230.	0.6975	0.6971	0.6965
92.	50.	0.6997	0.6993	0.6988
92.	100.	0.7000	0.6996	0.6991
92.	150.	0.7003	0.6999	0.6993
92.	200.	0.7006	0.7002	0.6997
92.	230.	0.7008	0.7004	0.6999
93.	50.	0.7028	0.7024	0.7019
93.	100.	0.7031	0.7027	0.7022
93.	150.	0.7033	0.7030	0.7025
93.	200.	0.7036	0.7032	0.7028
93.	230.	0.7038	0.7034	0.7029
94.	50.	0.7056	0.7053	0.7048
94.	100.	0.7059	0.7056	0.7051
94.	150.	0.7061	0.7058	0.7053
94.	200.	0.7063	0.7060	0.7056
94.	230.	0.7065	0.7061	0.7057
95.	50.	0.7082	0.7079	0.7074
95.	100.	0.7085	0.7081	0.7077
95.	150.	0.7086	0.7083	0.7079
95.	200.	0.7088	0.7085	0.7081
95.	230.	0.7090	0.7087	0.7083
96.	50.	0.7105	0.7102	0.7098
96.	100.	0.7108	0.7105	0.7101
96.	150.	0.7110	0.7107	0.7103
96.	200.	0.7111	0.7108	0.7105
96.	230.	0.7112	0.7110	0.7106

6.8 The total hadronic cross section

Besides the hadronic partial widths and the hadronic asymmetries of the previous section the cross section

$$\sigma(e^+e^- \to \text{hadrons}) = \sum_q \sigma(e^+e^- \to q\bar{q}) \tag{6.50}$$

is a hadronic quantity of special interest since it is large and can be measured with high precision. It constitutes the major part of the total e^+e^- cross section in the vicinity of the Z and hence fills sizably the Z resonance shape from which M_Z will be measured. In section 6.4 it was emphasized that the peak cross section is insensitive to the detailed values of the unknown parameters of the model, which was demonstrated explicitly in terms of the cross section for $e^+e^- \to \mu^+\mu^-$. Here we want to make this statement quantitative also for the hadronic part. The QED corrections, which are left out here, can be incorporated by convoluting the non-QED cross section with the initial state radiation spectrum [42]; other QED corrections are negligible (see the discussion in 6.4).

Following the general convention to express the (unpolarized) hadronic cross section in terms of the dimensionless quantity

$$R = \frac{\sigma(e^+e^- \to \text{hadrons})}{\sigma_0} \tag{6.51}$$

with the pointlike muon cross section

$$\sigma_0 = \sigma_0(e^+e^- \to \gamma^* \to \mu^+\mu^-) = \frac{4\pi\alpha^2}{3s} \tag{6.52}$$

we list the on-resonance values for R in table 6.9, again varying the model parameters in a wide range. For b, c final states finite mass terms have been kept. As can be seen, the cross section is almost completely stable against changes in the internal parameters. This stability is a consequence of cancellations between the corrections to the Z width in the denominator and the corrections to the coupling constants in the numerator of the matrix element. For the same reason R is also insensitive to QCD corrections and therefore to the uncertainty in α_s.

It may also be of advantage to normalize the hadronic cross section in terms of the real muon cross section instead of the fictitious σ_0 in (6.52). Such a modified R ratio

$$R^* = \frac{\sigma(e^+e^- \to \text{hadrons})}{\sigma(e^+e^- \to \mu^+\mu^-)} \tag{6.53}$$

can be measured without the requirement of an absolute normalization. (In this case, however, QCD corrections are present). We list also the values for R^* in table 6.10.

The on-resonance R^* is only a ratio of coupling constants and is determined essentially by the actual value of $\sin^2\theta_W$, in lowest order (and neglecting finite mass terms) given by

$$R^* = 3\,\frac{5 + 2(1 - \frac{8}{3}s_W^2)^2 + 3(1 - \frac{4}{3}s_W^2)^2}{1 + (1 - 4s_W^2)^2}\,. \tag{6.54}$$

The dependence on $\sin^2\theta_W$ is displayed in Figure 6.10 (QCD corrections included), together with the effect of the weak corrections. The strategy is the same as for Figure 6.9: to consider

$\sin^2\theta_W$ as an independenet parameter, not yet fixed via G_μ. This again offers a possibility to measure $\sin^2\theta_W$ which remains also valid for the more general situation beyond the minimal model with

$$\frac{M_W^2}{M_Z^2\cos^2\theta_W} \neq 1 .$$

The sensitivity to $\sin^2\theta_W$, however, is much weaker than in case of the left-right asymmetry A_{LR}.

Figure 6.10 :
$\sin^2\theta_W$ dependence of R^* in lowest order (- - - -) and with weak corrections (——).
$M_Z = 92$ GeV, $M_H = 100$ GeV.

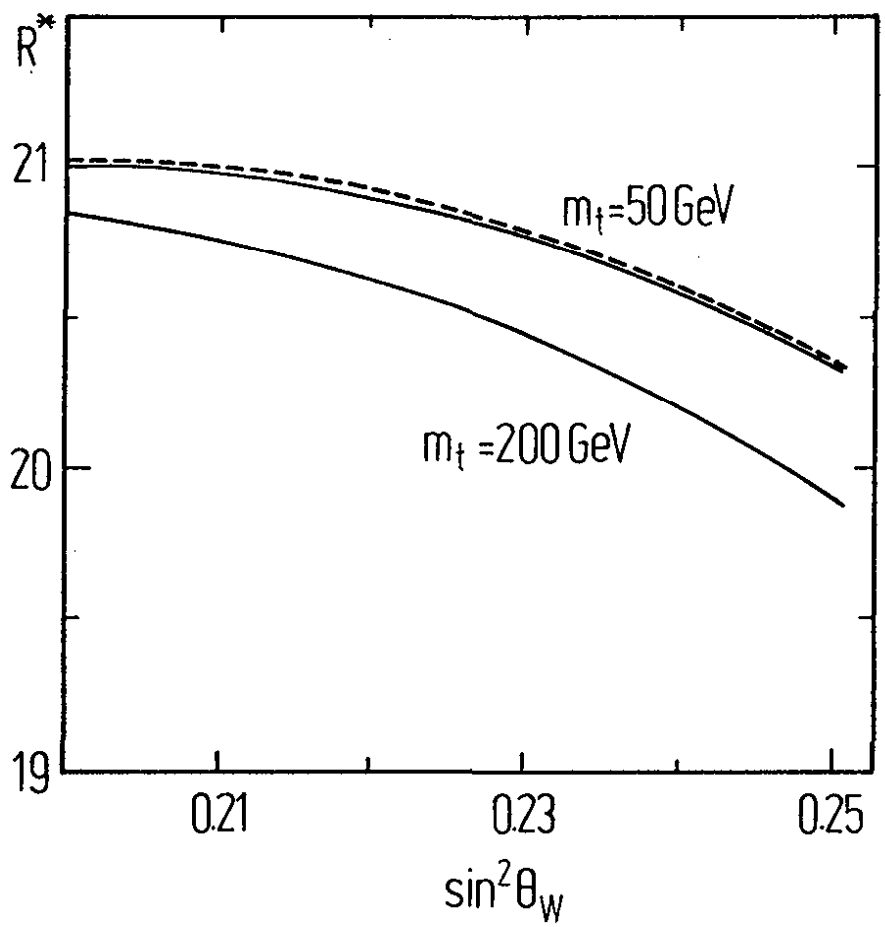

Table 6.9: Total hadronic cross section R on resonance (masses in GeV)

		M-Higgs		
M-Z	m-top	10	100	1000
90.	50.	3952.	3969.	3971.
90.	100.	3950.	3967.	3970.
90.	150.	3949.	3966.	3968.
90.	200.	3949.	3966.	3968.
90.	230.	3949.	3966.	3968.
91.	50.	3944.	3960.	3962.
91.	100.	3942.	3959.	3961.
91.	150.	3942.	3959.	3960.
91.	200.	3943.	3960.	3961.
91.	230.	3944.	3961.	3962.
92.	50.	3940.	3957.	3957.
92.	100.	3940.	3956.	3957.
92.	150.	3940.	3957.	3958.
92.	200.	3942.	3959.	3960.
92.	230.	3944.	3961.	3961.
93.	50.	3941.	3957.	3958.
93.	100.	3941.	3958.	3958.
93.	150.	3942.	3959.	3959.
93.	200.	3945.	3962.	3962.
93.	230.	3947.	3965.	3964.
94.	50.	3946.	3962.	3962.
94.	100.	3946.	3963.	3962.
94.	150.	3948.	3965.	3964.
94.	200.	3951.	3969.	3968.
94.	230.	3954.	3972.	3971.
95.	50.	3953.	3970.	3969.
95.	100.	3954.	3971.	3970.
95.	150.	3956.	3973.	3972.
95.	200.	3960.	3978.	3977.
95.	230.	3963.	3982.	3980.
96.	50.	3963.	3980.	3978.
96.	100.	3964.	3981.	3980.
96.	150.	3967.	3984.	3983.
96.	200.	3971.	3989.	3988.
96.	230.	3975.	3993.	3992.

Table 6.10: Total hadronic cross section R^* on resonance (masses in GeV)

		M-Higgs		
M-Z	m-top	10	100	1000
90.	50.	20.50	20.48	20.44
90.	100.	20.51	20.49	20.46
90.	150.	20.51	20.49	20.46
90.	200.	20.50	20.49	20.46
90.	230.	20.50	20.48	20.46
91.	50.	20.66	20.64	20.62
91.	100.	20.66	20.65	20.62
91.	150.	20.66	20.64	20.62
91.	200.	20.64	20.63	20.61
91.	230.	20.63	20.62	20.60
92.	50.	20.78	20.77	20.75
92.	100.	20.78	20.77	20.75
92.	150.	20.77	20.76	20.74
92.	200.	20.75	20.74	20.72
92.	230.	20.73	20.72	20.71
93.	50.	20.87	20.86	20.85
93.	100.	20.87	20.86	20.85
93.	150.	20.85	20.84	20.83
93.	200.	20.82	20.81	20.80
93.	230.	20.80	20.79	20.78
94.	50.	20.94	20.93	20.92
94.	100.	20.93	20.93	20.92
94.	150.	20.91	20.90	20.89
94.	200.	20.87	20.87	20.86
94.	230.	20.84	20.84	20.83
95.	50.	20.98	20.97	20.97
95.	100.	20.97	20.97	20.96
95.	150.	20.94	20.94	20.93
95.	200.	20.90	20.90	20.89
95.	230.	20.86	20.86	20.86
96.	50.	21.00	20.99	20.99
96.	100.	20.99	20.99	20.98
96.	150.	20.95	20.95	20.95
96.	200.	20.91	20.91	20.91
96.	230.	20.87	20.87	20.87

Chapter 7

Summary

The fundamental processes in high energy e^+e^- annihilation are the 4-fermion processes $e^+e^- \to f\bar{f}$. In lowest order they are of pure electroweak origin, in the standard model mediated by the exchange of photons and Z bosons.

Experiments at the e^+e^- colliders LEP and SLC will determine the mass and width of the Z boson with high accuracy as well as a series of on-resonance asymmetries with and without beam polarization. Together with W mass measurements and with the precisely known muon decay constant G_μ these experiments provide precision tests of the standard model where the inclusion of radiative corrections is not only a necessity but also a benefit: providing a unique chance to test the quantum structure of the standard model and to probe its empirically unknown part. The values for all the total and partial Z widths and for all the asymmetries can be calculated in terms of the few input parameters α, G_μ, M_Z, together with the as yet unknown Higgs and top masses entering the results at the level of radiative corrections. If the minimal model is correct all these calculations have to reproduce the experimental results with a choice of M_H and m_t within a reasonable domain ($50\,\mathrm{GeV} < m_t < 200\,\mathrm{GeV}$, as favored by present experimental data; $10\,\mathrm{GeV} < M_H < 1\,\mathrm{TeV}$, as favored by theoretical consistency arguments). If agreement is found the measurements with high accuracy will restrict the parameter range to an area substantially smaller than allowed by present days' data.

As a quantity with small systematic errors (experimentally and theoretically) the left-right asymmetry is the most sensitive probe not only of quantum effects in the standard model but also of possible new physics beyond the minimal model, in particular of new particles which are too heavy to be produced directly. By this feature longitudinal beam polarization considerably improves the physics potential of the e^+e^- colliders.

In this paper we have presented the standard model results for the quantitities measurable in e^+e^- collisions around the Z pole with high accuracy, and outlined the path how these results come about. The detailed presentation of the formulae provides the basis for practical applications, also in other energy domains below and above the Z resonance, and can be considered a guide through the analytic part of the corresponding computer programs for the Z line shape [90] and Monte Carlo generators [44]. The way of presentation allows in addition to easily incorporate all kinds of new objects in SU(2)×U(1) with couplings to the gauge bosons but not to the external fermions ("oblique corrections" in the terminology of [17]). Moreover, our set of formulae for the weak part is sufficiently complete as to produce theoretical results with the required accuracy, in particular with the leading fermionic contributions resummed to all orders. Not listed are the expressions for the higher order QED results which have meanwhile been calculated for the initial state QED corrections :

explicit 2-loop calculations [36], and resummation of the dominant infrared photon terms to all orders, either analytically [27,29,35,37] or by Monte Carlo event-by-event generation [38], being in nice agreement with each other within the required accuracy. Together with these higher order QED terms the basic ingredients for precision tests of the electroweak theory are reliably calculated, and the generally dominating QED corrections are under control.

Uncertainties in the radiative corrections come from the uncertainty in the hadronic contribution to the vacuum polarization. Also the unknown Higgs and top mass may be considered as a source of uncertainties preventing at present the numerical predictions from being unique. The error in the theoretical predictions induced by the hadronic uncertainty matches the experimental error of the future experiments. For the goal of revealing signals from new physics and identifying their origin our ignorance of the top mass remains an obstacle which can be circumvented only by more restrictive experimental information on the top quark.

Acknowledgement

I would like to thank W. Beenakker, F. Berends, M. Böhm, G. Burgers, A. Denner, R. Kleiss, H. Spiesberger, W. van Neerven for a pleasant and fruitful collaboration and for innumerable stimulating and clarifying discussions. I want to thank also D. Bardin, J. Fleischer, S. Jadach, F. Jegerlehner, H. Kühn, T. Riemann, R. Stuart, B. Ward for many helpful discussions and for supplying me with detailed informations on the actual status of their work, and the MARK II group for the kind hospitality offered to me at SLAC. In particular I want to express my gratitude to G. Burgers, whose effort in constructing efficient computer programs, updating the input parameters and performing all kinds of cross checks played an essential role for the final evaluation, and to M. Böhm, whose permanent encouragement during all phases of this work was decisive for accomplishing this paper.

Appendix A

Counter terms

Here we collect the formal relations for the renormalized 2- and 3-point functions as composed by the unrenormalized quantities and their corresponding counter terms.

A.1 Vector boson self energies

We expand the renormalization constants according to

$$Z_i = 1 + \delta Z_i \,.$$

It is convenient to introduce the following linear combinations of the SU(2) and the U(1) field renormalization constants $\delta Z_2^{W,B}$ and the coupling renormalization constants $\delta Z_1^{W,B}$ $(i = 1,2)$:

$$\begin{pmatrix} \delta Z_i^\gamma \\ \delta Z_i^Z \end{pmatrix} = \begin{pmatrix} s_W^2 & c_W^2 \\ c_W^2 & s_W^2 \end{pmatrix} \begin{pmatrix} \delta Z_i^W \\ \delta Z_i^B \end{pmatrix} , \tag{A.1}$$

From the unrenormalized vector boson self energies Σ^γ, $\Sigma^{\gamma Z}$, Σ^Z, Σ^W the corresponding renormalized ones are obtained via

$$\begin{aligned} \hat{\Sigma}^\gamma(k^2) &= \Sigma^\gamma(k^2) + \delta Z_2^\gamma\, k^2 \\ \hat{\Sigma}^Z(k^2) &= \Sigma^Z(k^2) - \delta M_Z^2 + \delta Z_2^Z\,(k^2 - M_Z^2) \\ \hat{\Sigma}^W(k^2) &= \Sigma^W(k^2) - \delta M_W^2 + \delta Z_2^W\,(k^2 - M_W^2) \\ \hat{\Sigma}^{\gamma Z}(k^2) &= \Sigma^{\gamma Z}(k^2) - \delta Z_2^{\gamma Z}\, k^2 + (\delta Z_1^{\gamma Z} - \delta Z_2^{\gamma Z})\, M_Z^2 \,. \end{aligned} \tag{A.2}$$

In the last line the combinations $(i = 1,2)$

$$\delta Z_i^{\gamma Z} = \frac{c_W s_W}{c_W^2 - s_W^2} (\delta Z_i^Z - \delta Z_i^\gamma) \tag{A.3}$$

have been introduced.

The mass counter terms $\delta M_{W,Z}^2$ are related to the fundamental renormalization constants by

$$\frac{\delta M_Z^2}{M_Z^2} - \frac{\delta M_W^2}{M_W^2} = \frac{s_W}{c_W} (3\,\delta Z_2^{\gamma Z} - 2\,\delta Z_1^{\gamma Z}) \,. \tag{A.4}$$

This relation allows to express finally the $\delta Z_i^{Z,W}$ in terms of the unrenormalized on-shell vector boson self energies.

A.2 Fermion self energies

In section 3.4 we have decomposed the unrenormalized self energy of a fermion f into V, A, S parts with invariant functions $\Sigma^f_{V,A,S}(k^2)$. The renormalized fermion self energy can be written as follows

$$\begin{aligned}\hat{\Sigma}^f(k) &= \not{k}\left(\Sigma^f_V(k^2) + \delta Z^f_V\right) + \not{k}\gamma_5\left(\Sigma^f_A(k^2) - \delta Z^f_A\right) \\ &\quad + m_f\left(\Sigma^f_S(k^2) - \delta Z_V - \frac{\delta m_f}{m_f}\right)\end{aligned} \tag{A.5}$$

with

$$\delta Z^f_V = \frac{\delta Z_L + \delta Z^f_R}{2}, \quad \delta Z^f_A = \frac{\delta Z_L - \delta Z^f_R}{2}. \tag{A.6}$$

δZ_L is the left-handed renormalization constant for the whole doublet; therefore not all of the $\delta Z^f_{V,A}$ are independent for the members of a family. We have dropped the family index in the formulae.

A.3 Vertex corrections

With the coupling constants v_f, a_f of the fermion f to the Z we get the renormalized electromagnetic vertex as

$$\begin{aligned}\hat{\Gamma}^{\gamma ff}_\mu &= \Gamma^{\gamma ff}_\mu - ie\,Q_f\,\gamma_\mu\,(\delta Z^\gamma_1 - \delta Z^\gamma_2 + \delta Z^f_V - \delta Z^f_A\,\gamma_5) \\ &\quad - ie\,\gamma_\mu(v_f - a_f\gamma_5)(\delta Z^{\gamma Z}_1 - \delta Z^{\gamma Z}_2)\end{aligned} \tag{A.7}$$

with the unrenormalized vertex $\Gamma^{\gamma ff}_\mu$.

The renormalized weak neutral current vertex has the form

$$\begin{aligned}\hat{\Gamma}^{Zff}_\mu &= \Gamma^{Zff}_\mu + ie\,\gamma_\mu(v_f - a_f\gamma_5)(\delta Z^Z_1 - \delta Z^Z_2) \\ &\quad + ie\,Q_f\,\gamma_\mu\,(\delta Z^{\gamma Z}_1 - \delta Z^{\gamma Z}_2) \\ &\quad + ie\,\gamma_\mu\,(v_f\delta Z^f_V + a_f\delta Z^f_A) \\ &\quad - ie\,\gamma_\mu\gamma_5\,(v_f\delta Z^f_A + a_f\delta Z^f_V).\end{aligned} \tag{A.8}$$

For the muon decay matrix element we need also the charged current vertex

$$\hat{\Gamma}^{Wl\nu}_\mu = \Gamma^{Wl\nu}_\mu + i\frac{e}{2\sqrt{2}s_W}\gamma_\mu(1-\gamma_5)(1 + \delta Z^W_1 - \delta Z^W_2 + \delta Z_L) \tag{A.9}$$

with δZ_L for the corresponding lepton doublet.

Γ_μ denotes always the unrenormalized vertices.

Appendix B

Unrenormalized vector boson self energies

Here we list the functions $\Sigma^{\gamma,\gamma Z,Z,W}$ in terms of the on-shell parameters and in dimensional regularization. With the dimension D and the mass scale μ we introduce the symbol for the singular term

$$\Delta_j = \frac{2}{4-D} - \gamma + \log 4\pi - \log \frac{m_j^2}{\mu^2} \tag{B.1}$$

for a given kind of mass m_j (γ is the Euler constant).

In [45] the formulae were listed in a compact form for leptons and quarks together. This form, however, cannot be used for the incorporation of a heavy lepton from a next generation if it is accompanied by a massless neutrino. [1] The formulae given here are free of this restriction.

We make use of the abbreviations

$$s = k^2, \quad z = M_Z^2, \quad w = M_W^2, \quad h = M_H^2 \, .$$

Then the functions read as follows (fermion summation extends also over color in case of quarks):

$$\begin{aligned} \Sigma^{\gamma}(s) &= \frac{\alpha}{4\pi}\left\{\frac{4}{3}\sum_f Q_f^2\left[s\Delta_f + (s+2m_f^2)\,F(s,m_f,m_f) - \frac{s}{3}\right]\right. \\ &\quad \left. -(3s\Delta_W + 3s + 4w)\,F(s,M_W,M_W)\right\} \, , \end{aligned} \tag{B.2}$$

$$\begin{aligned} \Sigma^{\gamma Z}(s) &= \frac{\alpha}{4\pi}\left\{-\frac{4}{3}\sum_f Q_f v_f\left[s\Delta_f + (s+2m_f^2)\,F(s,m_f,m_f) - \frac{s}{3}\right]\right. \\ &\quad + \frac{1}{c_W s_W}\left[\left(3c^2+\frac{1}{6}\right)s + 2w\right]\Delta_W \\ &\quad \left. + \frac{1}{c_W s_W}\left[\left(3c_W^2+\frac{1}{6}\right)s + \left(4c_W^2+\frac{4}{3}\right)w\right]F(s,M_W,M_W) + \frac{s}{9c_W s_W}\right\} \, , \end{aligned} \tag{B.3}$$

[1] the same applies to [49]

$$
\begin{aligned}
\Sigma^Z(s) \;=\; & \frac{\alpha}{4\pi}\left\{\frac{4}{3}\sum_{l=e,\mu,\tau} 2a_l^2\, s\left(\Delta_l + \frac{5}{3} - \log(-\frac{s}{m_l^2} - i\epsilon)\right)\right. \\
& + \frac{4}{3}\sum_{f\neq\nu}\left[(v_f^2+a_f^2)\left(s\Delta_f + (s+2m_f^2)\,F(s,m_f,m_f) - \frac{s}{3}\right)\right. \\
& \left.\left. - \frac{3}{8c_W^2 s_W^2} m_f^2\, F(s,m_f,m_f)\right]\right. \\
& + \left[\left(3 - \frac{19}{6s_W^2} + \frac{1}{6c_W^2}\right)s + \left(4 + \frac{1}{c_W^2} - \frac{1}{s_W^2}\right)M_Z^2\right]\Delta_W \\
& + \left[\left(-c_W^4(40s+80w) + (c_W^2-s_W^2)^2(8w+s) + 12w\right)F(s,M_W,M_W)\right. \\
& + \left(10z - 2h + s + \frac{(h-z)^2}{s}\right)F(s,M_H,M_Z) - 2h\log\frac{h}{w} - 2z\log\frac{z}{w} \\
& + (10z - 2h + s)\left(1 - \frac{h+z}{h-z}\log\frac{M_H}{M_Z} - \log\frac{M_H M_Z}{w}\right) \\
& \left. + \frac{2}{3}s\left(1 + (c_W^2-s_W^2)^2 - 4c_W^4\right)\right]\frac{1}{12c_W^2 s_W^2}\Bigg\}\,,
\end{aligned}
\tag{B.4}
$$

$$
\begin{aligned}
\Sigma^W(s) \;=\; & \frac{\alpha}{4\pi}\frac{1}{3s_W^2}\left\{\sum_{l=e,\mu,\tau}\left[(s - \frac{3}{2}m_l^2)\,\Delta_l\right.\right. \\
& \left. + \left(s - \frac{m_l^2}{2} - \frac{m_l^4}{2s}\right)F(s,0,m_l) + \frac{2}{3}s - \frac{m_l^2}{2}\right] \\
& + \sum_{q-doublets}\left[\frac{\Delta_+}{2}\left(s - \frac{5}{2}m_+^2 - \frac{m_-^2}{2}\right) + \frac{\Delta_-}{2}\left(s - \frac{5}{2}m_-^2 - \frac{m_+^2}{2}\right)\right. \\
& + \left(s - \frac{m_+^2+m_-^2}{2} - \frac{(m_+^2-m_-^2)^2}{2s}\right)F(s,m_+,m_-) \\
& \left. + \left(s - \frac{m_+^2+m_-^2}{2}\right)\left(1 - \frac{m_+^2+m_-^2}{m_+^2-m_-^2}\log\frac{m_+}{m_-}\right) - \frac{s}{3}\right] \\
& - \left[\frac{19}{2}s + 3w\left(1 - \frac{s_W^2}{c_W^2}\right)\right]\Delta_W \\
& + \left[s_W^4 z - \frac{c_W^2}{3}\left(7z + 7w + 10s - 2\frac{(z-w)^2}{s}\right)\right. \\
& \left. \quad - \frac{1}{6}\left(w + z - \frac{s}{2} - \frac{(z-w)^2}{2}\right)\right]F(s,M_Z,M_W) \\
& + \frac{s_W^2}{3}\left(-4w - 10s + \frac{2w^2}{s}\right)F(s,0,M_W) \\
& + \frac{1}{6}\left(5w - h + \frac{s}{2} - \frac{(h-w)^2}{2s}\right)F(s,M_H,M_W) \\
& + \left[\frac{c_W^2}{3}(7z + 7w + 10s - 4(z-w)) - s_W^4 z + \frac{1}{6}\left(2w - \frac{s}{2}\right)\right]\frac{z}{z-w}\log\frac{z}{w}
\end{aligned}
\tag{B.5}
$$

$$
\begin{aligned}
&- \left(\frac{2}{3}w + \frac{s}{12}\right) \frac{h}{h-w} \log \frac{h}{w} \\
&- \frac{c_W^2}{3}\left(7z + 7w + \frac{32}{3}s\right) + s_W^4 z + \frac{1}{6}\left(\frac{5}{3}s + 4w - z - h\right) - \frac{s_W^2}{3}\left(4w + \frac{32}{3}\right)\Bigg\} \ .
\end{aligned}
$$

The function F can be defined via the integral representation

$$
\begin{aligned}
F(s, m_1, m_2) \ &= \ -1 + \frac{m_1^2 + m_2^2}{m_1^2 - m_2^2} \log \frac{m_1}{m_2} \\
&\quad - \int_0^1 dx \, \log \frac{x^2 - x(s + m_1^2 - m_2^2) + m_1^2 - i\varepsilon}{m_1 m_2} \ .
\end{aligned} \tag{B.6}
$$

F has the property $F(0, m_1, m_2) = 0$. The analytical form can be found in [45]. In this place we want to give only some simpler expressions for special situations:

One mass zero:

$$
F(s, 0, m) \ = \ 1 + \left(\frac{m^2}{s} - 1\right) \log\left(1 - \frac{s}{m^2} - i\varepsilon\right)
$$

Small s ($\ll m_1^2, m_2^2$):

$$
\begin{aligned}
F(s, m_1, m_2) \ &= \ \frac{s}{(m_1^2 - m_2^2)^2}\left(\frac{m_1^2 + m_2^2}{2} - \frac{m_1^2 + m_2^2}{m_1^2 - m_2^2} \log \frac{m_1^2}{m_2^2}\right) + \cdots \\
F(s, m, m) \ &= \ \frac{s}{6m^2} + \cdots
\end{aligned}
$$

Large s ($\gg m_1^2, m_2^2$):

$$
F(s, m_1, m_2) \ = \ 1 - \log \frac{|\, s \,|}{m_1 m_2} + \frac{m_1^2 + m_2^2}{m_1^2 - m_2^2} \log \frac{m_1^2}{m_2^2} + i\pi\, \theta(s) + \cdots
$$

Appendix C

Vertex form factors

In this appendix we list the non-QED parts of the renormalized form factors for the electromagnetic and the neutral current vertex of the known fermions (on-shell fermions). The form factors given here deviate from those of ref. [45] in a threefold respect:

(i) They include the finite wave function renormalization of the external fermions and are therefore not irreducible;

(ii) they contain the complete m_t mass dependence when the top quark appears in internal lines as well as the unphysical Higgs bosons;

(iii) the QED part (virtual photon contribution) has been removed. It is instead incorporated in the QED corrections of section 6.5.

C.1 Weak neutral current vertex

For momentum transfer $s = k^2$ large compared to m_f^2 the finite result for the Zff vertex after renormalization can be summarized in terms of vector and axial vector form factors:

$$\hat{\Gamma}_\mu^{Zff} = ie\gamma_\mu(v_f - a_f\gamma_5) + ie\gamma_\mu\left(F_V^{Zf}(s) - \gamma_5 F_A^{Zf}(s)\right) . \tag{C.1}$$

The explicit expressions for the form factors read for

neutrinos:

$$\begin{aligned} F_V^{Z\nu} &= F_A^{Z\nu} \\ &= \frac{\alpha}{4\pi}\frac{1}{4c_W s_W}\left[\frac{1}{4c_W^2 s_W^2}\Lambda_2(s,M_Z) + \frac{2s_W^2-1}{2s_W^2}\Lambda_2(s,M_W) + \frac{3c_W^2}{s_W^2}\Lambda_3(s,M_W)\right] \end{aligned} \tag{C.2}$$

and for the charged fermions:

$$\begin{aligned} F_V^{Zf} &= \frac{\alpha}{4\pi}\left[v_f(v_f^2+3a_f^2)\Lambda_2(s,M_Z) + F_L^f\right] \\ F_A^{Zf} &= \frac{\alpha}{4\pi}\left[a_f(3v_f^2+a_f^2)\Lambda_2(s,M_Z) + F_L^f\right] \end{aligned} \tag{C.3}$$

with

$$F_L^l = \frac{1}{8s_W^3 c_W}\Lambda_2(s,M_W) - \frac{3c_W}{4s_W^3}\Lambda_3(s,M_W) \tag{C.4}$$

$$F_L^u = -\frac{1-\frac{2}{3}s_W^2}{8s_W^3 c_W}\Lambda_2(s,M_W) + \frac{3c_W}{4s_W^3}\Lambda_3(s,M_W)$$
$$F_L^d = \frac{1-\frac{4}{3}s_W^2}{8s_W^3 c_W}\Lambda_2(s,M_W) - \frac{3c_W}{4s_W^3}\Lambda_3(s,M_W)\,.$$

Note that (C.4) is not valid for the (t,b) doublet.
The functions Λ_2, Λ_3 have the form [1] ($w = M^2/s$ with $M = M_Z$ or M_W, $s > 0$)

$$\begin{aligned}\Lambda_2(s,M) &= -\frac{7}{2} - 2w - (2w+3)\log(w) \\ &\quad +2(1+w)^2\left[\log(w)\log(\frac{1+w}{w}) - \mathrm{Li}_2(-\frac{1}{w})\right] \\ &\quad -i\pi\left[3+2w-2(w+1)^2\log\left(\frac{1+w}{w}\right)\right]\end{aligned} \tag{C.5}$$

$$\begin{aligned}\Lambda_3(s,M) &= \frac{5}{6} - \frac{2w}{3} + \frac{2}{3}(2w+1)\sqrt{4w-1}\,\arctan\frac{1}{\sqrt{4w-1}} \\ &\quad -\frac{8}{3}w(w+2)\left(\arctan\frac{1}{\sqrt{4w-1}}\right)^2.\end{aligned}$$

The situation for the b-quark vertex is more complicated due to the presence of the top quark and the charged Goldstone Higgs bosons in virtual states. The general form (C.1) and (C.3) is also valid for $f = b$; only the left-handed contribution F_L^b has to be calculated separately.

F_L^b is the sum of the top dependent vertex diagrams (see Figure 3.6) and the counter term in (A.8) (without the Z contribution to the b quark self energy). The result is

$$F_L^b = \sum_{i=b}^{g} F_i + \frac{\frac{2}{3}s_W^2 - 1}{4s_W c_W}\delta Z_L^{fin} \tag{C.6}$$

where

$$\delta Z_L^{fin} = \frac{1}{2s_W^2}(2+\frac{m_t^2}{M_W^2})\left(\bar{B}_1(m_b^2,m_t,M_W) + m_b^2\bar{B}_1'(m_b^2,m_t,M_W)\right). \tag{C.7}$$

For the function $\bar{B}_1$ see equation (C.16); $\bar{B}_1'$ denotes the derivative

$$\bar{B}_1'(s,m_1,m_2) = \frac{\partial}{\partial s}\bar{B}_1(s,m_1,m_2)\,.$$

The F_i in (C.6) are the expressions corresponding to the diagrams in Figure 3.6 after subtracting those (divergent) parts which are cancelled by the vertex counter term after renormalization:

$$\begin{aligned}F_b &= \frac{v_t+a_t}{4s_W^2}\left\{-\frac{3}{2} + 2\log\frac{M_W}{m_t} + 4\,C_2^0(s,m_t,m_t,M_W)\right. \\ &\quad -2s\left[C_2^+(s,m_t,m_t,M_W) - C_2^-(s,m_t,m_t,M_W)\right] \\ &\quad \left.+4s\,C_1^+(s,m_t,m_t,M_W) - 2s\,C_0(s,m_t,m_t,M_W)\right\} \\ &\quad -\frac{v_t-a_t}{4s_W^2}\,2m_t^2\,C_0(s,m_t,m_t,M_W),\end{aligned} \tag{C.8}$$

[1] Λ_3 only for $s < 4M_W^2$

$$
\begin{aligned}
F_c &= -\frac{c_W}{4s_W^3}\left\{-\frac{3}{2}+12\,C_2^0(s,M_W,M_W,m_t)\right.\\
&\quad -2s\left[C_2^+(s,M_W,M_W,m_t)-C_2^-(s,M_W,M_W,m_t)\right]\\
&\quad \left.+4s\,C_1^+(s,M_W,M_W,m_t)\right\},\\
F_d &= \frac{v_t-a_t}{4s_W^2}\left(\frac{m_t}{M_W}\right)^2\left\{-\frac{3}{4}+\log\frac{M_W}{m_t}+2\,C_2^0(s,m_t,m_t,M_W)\right.\\
&\quad \left.-s\left[C_2^+(s,m_t,m_t,M_W)-C_2^-(s,m_t,m_t,M_W)\right]\right\}\\
&\quad -\frac{v_t+a_t}{4s_W^2}\left(\frac{m_t}{M_W}\right)^2 m_t^2\,C_0(s,m_t,m_t,M_W),\\
F_e &= \frac{s_W^2-c_W^2}{8s_W^3c_W}\left(\frac{m_t}{M_W}\right)^2\left\{-\frac{1}{4}+2\,C_2^0(s,M_W,M_W,m_t)\right\},\\
F_f &= F_g = -\frac{m_t^2}{4s_Wc_W}\,C_0(s,M_W,M_W,m_t).
\end{aligned}
$$

The functions C_1^+, C_2^+, C_2^-, C_2^0 are specified in terms of the scalar 3-point integral C_0 and the finite parts of the 2-point integrals $\bar{B}_0$, $\bar{B}_1$ defined below in sect. C.3:

$$
\begin{aligned}
(4m_b^2-s)\,C_1^+(s,M,M,M') &= \log\frac{M'}{M}+\bar{B}_0(s,M,M)-\bar{B}_0(m_b^2,M,M') \qquad \text{(C.9)}\\
&\quad +(M'^2-M^2+m_b^2)\,C_0(s,M,M,M'),\\
C_2^0(s,M,M,M') &= \frac{1}{4}\left[\bar{B}_0(s,M,M)+1\right]\\
&\quad +\frac{1}{2}(M^2-M'^2-m_b^2)\,C_1^+(s,M,M,M')\\
&\quad +\frac{1}{2}M'^2\,C_0(s,M,M,M'),\\
(4m_b^2-s)\,C_2^+(s,M,M,M') &= \frac{1}{2}\,\bar{B}_0(s,M,M)+\frac{1}{2}\left[\bar{B}_1(m_b^2,M',M)-\frac{1}{4}\right]\\
&\quad +(M'^2-M^2+m_b^2)\,C_1^+(s,M,M,M')\\
&\quad -C_2^0(s,M,M,M'),\\
s\,C_2^-(s,M,M,M') &= -\frac{1}{2}\left[\bar{B}_1(m_b^2,M',M)-\frac{1}{4}\right]-C_2^0(s,M,M,M').
\end{aligned}
$$

C.2 Electromagnetic vertex

The renormalized γff vertex can be written in a way similar to the Zff vertex in (C.1) (the global $-$ sign is due to our conventions in section 2.3):

$$\hat{\Gamma}_\mu^{\gamma ff} = -i\,e\,Q_f\,\gamma_\mu - i\,e\,\gamma_\mu\left(F_V^{\gamma f}(s) - \gamma_5 F_A^{\gamma f}(s)\right) \tag{C.10}$$

with the electromagnetic form factors

$$\begin{aligned} F_V^{\gamma f} &= \frac{\alpha}{4\pi}\left[Q_f(v_f^2+a_f^2)\Lambda_2(s,M_Z) + G_L^f\right] \\ F_A^{\gamma f} &= \frac{\alpha}{4\pi}\left[Q_f\,2v_f a_f\,\Lambda_2(s,M_Z) + G_L^f\right] \end{aligned} \tag{C.11}$$

and

$$\begin{aligned} G_L^l &= -\frac{3}{4s_W^2}\Lambda_3(s,M_W) \\ G_L^u &= -\frac{1}{12s_W^2}\Lambda_2(s,M_W) + \frac{3}{4s_W^2}\Lambda_3(s,M_W) \\ G_L^d &= \frac{1}{6s_W^2}\Lambda_2(s,M_W) - \frac{3}{4s_W^2}\Lambda_3(s,M_W)\,. \end{aligned} \tag{C.12}$$

Again the form (C.12) is not valid for the (t,b) doublet.

For the γbb vertex we have to use the following G_L^b, calculated in analogy to C.1:

$$G_L^b = \sum_{i=b}^{g} G_i - \frac{1}{6}\delta Z_L^{fin} \tag{C.13}$$

with δZ_L^{fin} from (C.7) and

$$\begin{aligned} G_b &= \frac{1}{6s_W^2}\left\{-\frac{3}{2} + 2\log\frac{M_W}{m_t} + 4\,C_2^0(s,m_t,m_t,M_W)\right. \\ &\quad -2s\left[C_2^+(s,m_t,m_t,M_W) - C_2^-(s,m_t,m_t,M_W)\right] \\ &\quad +4s\,C_1^+(s,m_t,m_t,M_W) - 2s\,C_0(s,m_t,m_t,M_W) \\ &\quad \left.-2m_t^2\,C_0(s,m_t,m_t,M_W)\right\}, \end{aligned} \tag{C.14}$$

$$\begin{aligned} G_c &= -\frac{1}{4s_W^2}\left\{-\frac{3}{2} + 12\,C_2^0(s,M_W,M_W,m_t)\right. \\ &\quad -2s\left[C_2^+(s,M_W,M_W,m_t) - C_2^-(s,M_W,M_W,m_t)\right] \\ &\quad \left.+4s\,C_1^+(s,M_W,M_W,m_t)\right\}, \end{aligned}$$

$$\begin{aligned} G_d &= \frac{1}{6s_W^2}\left(\frac{m_t}{M_W}\right)^2\left\{-\frac{3}{4} + \log\frac{M_W}{m_t} + 2\,C_2^0(s,m_t,m_t,M_W)\right. \\ &\quad -s\left[C_2^+(s,m_t,m_t,M_W) - C_2^-(s,m_t,m_t,M_W)\right] \\ &\quad \left.-m_t^2\,C_0(s,m_t,m_t,M_W)\right\}, \end{aligned}$$

$$G_e = -\frac{1}{4s_W^2}\left(\frac{m_t}{M_W}\right)^2 \left\{-\frac{1}{4} + 2\,C_2^0(s, M_W, M_W, m_t)\right\},$$

$$G_f = G_g = \frac{m_t^2}{4s_W^2}\,C_0(s, M_W, M_W, m_t).$$

The C functions are the same as in (C.9)

C.3 Two- and three-point integrals

Finally we have to specify the functions $\bar{B}_0$, $\bar{B}_1$ and C_0.

$\bar{B}_0$ is the finite part of the scalar 2-point integral B_0

$$\frac{i}{16\pi^2}\,B_0(q^2, M, M') = \mu^{4-D}\int \frac{d^Dk}{(2\pi)^D}\,\frac{1}{(k^2-M^2)\,((q+k)^2-M'^2)}$$

and is defined as

$$B_0(s, M, M') = \frac{1}{2}(\Delta_M + \Delta_{M'}) + \bar{B}_0(s, M, M')$$

with Δ_M defined in (B.1). In terms of the function F in (B.6) it is given by

$$\bar{B}_0(s, M, M') = 1 - \frac{M^2+M'^2}{M^2-M'^2}\log\frac{M}{M'} + F(s, M, M'). \qquad \text{(C.15)}$$

The function $\bar{B}_1$ is related to F in the following way:

$$\bar{B}_1(s, M, M') = -\frac{1}{4} + \frac{M^2}{M^2-M'^2}\log\frac{M}{M'} + \frac{M'^2-M^2-s}{2s}\,F(s, M, M'). \qquad \text{(C.16)}$$

It is the finite part of the vector 2-point integral

$$\frac{i}{16\pi^2}\,q_\mu\,B_1(q^2, M, M') = \mu^{4-D}\int \frac{d^Dk}{(2\pi)^D}\,\frac{k_\mu}{(k^2-M^2)\,((q+k)^2-M'^2)}$$

defined with the following subtraction:

$$B_1(s, M, M') = -\frac{1}{2}(\Delta_{M'} + \frac{1}{2}) + \bar{B}_1(s, M, M').$$

The scalar 3-point integral for equal external masses m_f

$$\frac{i}{16\pi^2}\,C_0(s, M, M, M') = \int \frac{d^4k}{(2\pi)^4}\,\frac{1}{(k^2-M'^2)\,((k-p_f)^2-M^2)\left((k+p_{\bar{f}})^2-M^2\right)} \qquad \text{(5.10)}$$

where

$$s = (p_f + p_{\bar{f}})^2, \quad p_f^2 = p_{\bar{f}}^2 = m_f^2$$

is equivalent to the parameter integral

$$C_0(s,M,M,M') = -\int_0^1 dy \int_0^y dx \left(ay^2 + bx^2 + cxy + dy + ex + f\right)^{-1}$$

with

$$a = m_f^2, \quad b = -c = s, \quad d = M^2 - M'^2 - m_f^2, \quad e = 0, \quad f = M'^2 - i\varepsilon.$$

Applying the method of 't Hooft and Veltman [103] it can expressed in terms of dilogarithms

$$C_0(s,M,M,M') = \frac{1}{c+2\alpha b}\sum_{l=1}^{3}\sum_{j=1}^{2}(-1)^l \left\{\mathrm{Li}_2\left(\frac{x_l}{x_l - y_{lj}}\right) - \mathrm{Li}_2\left(\frac{x_l - 1}{x_l - y_{lj}}\right)\right\} \qquad \text{(C.17)}$$

together with

$$\alpha = \frac{1}{2}\left(1 - \sqrt{1 - \frac{4m_f^2}{s}}\right)$$

and

$$x_1 = -\frac{d + 2a + c\alpha}{c + 2\alpha b},$$

$$x_2 = -\frac{d}{(1-\alpha)(c+2\alpha b)},$$

$$x_3 = \frac{d}{\alpha(c+2\alpha b)},$$

$$y_{1j} = \frac{-c \pm \sqrt{c^2 - 4b(a+d+f)}}{2b},$$

$$y_{2j} = y_{3j} = \frac{-d \pm \sqrt{d^2 - 4f(a+b+c)}}{2a}.$$

Appendix D

Box functions

The box diagram with exchange of two massive bosons

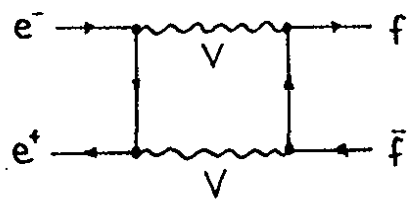

can be written with help of the notation

$$\gamma_\mu(a-b\gamma_5)\otimes\gamma^\mu(c-d\gamma_5) \equiv \bar{v}_e\gamma_\mu(a-b\gamma_5)u_e\cdot\bar{u}_f\gamma^\mu(c-d\gamma_5)v_f$$

in the following way for $V = Z$:

$$\begin{aligned} & i\frac{e^2}{s}\Big\{\gamma_\mu(v_e^2+a_e^2-2v_ea_e\gamma_5)\otimes\gamma^\mu(v_f^2+a_f^2-2v_fa_f\gamma_5)\cdot\frac{\alpha}{2\pi}I(s,t,M_Z) \qquad \text{(D.1)} \\ + \quad & \gamma_\mu\gamma_5(v_e^2+a_e^2-2v_ea_e\gamma_5)\otimes\gamma^\mu\gamma_5(v_f^2+a_f^2-2v_fa_f\gamma_5)\cdot\frac{\alpha}{2\pi}I_5(s,t,M_Z)\Big\}\ . \end{aligned}$$

For $V = W$ the corresponding expression is:

$$i\frac{e^2}{s}\frac{1}{(2s_W^4)}\gamma_\mu(1-\gamma_5)\otimes\gamma^\mu(1-\gamma_5)\cdot\frac{\alpha}{2\pi}\left[I(s,t,M_W)+I_5(s,t,M_W)\right]\ . \qquad \text{(D.2)}$$

For $f \neq b$, when the fermion masses can be neglected, the functions I and I_5 have a compact analytical form which has been calculated by Denner [104]:

$$\begin{aligned} I_5(s,t,M) \;=\; & \frac{s}{s+t}\left\{\frac{s+2t+2M^2}{2(s+t)}\left[\mathrm{Li}_2\left(1+\frac{t}{M^2}\right)-\frac{\pi^2}{6}-\log^2\left(-\frac{y_1}{y_2}\right)\right]\right. \qquad \text{(D.3)} \\ & +\frac{1}{2}\,\mathrm{Li}_2\left(-\frac{t}{M^2}\right)+\frac{y_2-y_1}{2s}\,\log\left(-\frac{y_1}{y_2}\right) \\ & \left.+\frac{s+2t-4M^2t/s+2M^2/t-2M^4/s}{2(s+t)(x_2-x_1)}\cdot J(s,t,M)\right\}, \end{aligned}$$

$$I(s,t,M) \;=\; I_5(s,t,M)\;+\;2\log^2\left(-\frac{y_1}{y_2}\right)\;+\;\frac{2}{x_1-x_2}\cdot J(s,t,M)\ ,$$

$$J(s,t,M) \;=\; \mathrm{Li}_2\frac{x_1}{x_1-x_2}+\mathrm{Li}_2\frac{x_1}{x_1-y_2}-\mathrm{Li}_2\frac{x_2}{x_2-y_1}-\mathrm{Li}_2\frac{x_2}{x_2-y_2}$$

with

$$x_{1,2} = \frac{1}{2}\left(1 \pm \sqrt{1 - \frac{4M^2}{s}\left(1 + \frac{M^2}{t}\right)}\right) ,$$

$$y_{1,2} = \frac{1}{2}\left(1 \pm \sqrt{1 - \frac{4M^2}{s}}\right) .$$

For $f = b$ the top mass dependence in the WW box

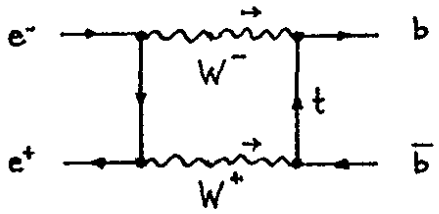

has to be taken into account. In this case we have to replace the expression $I + I_5$ in (D.2) by a more complicated term, which can be written in form of a parameter integral:

$$I(s,t,M) + I_5(s,t,M) = -\int_0^1 dx \int_0^1 dy \int_0^1 dz\, z(1-z)\left(\frac{s}{L} + \frac{(1 - z + z^2 y(1-y))st}{L^2}\right) \quad \text{(D.4)}$$

with

$$L = -(1-z)^2 x(1-x)s - z^2 y(1-y)t + (1-z)M^2 + z(1-y)m_t^2 .$$

For our concrete calculations this integral has been evaluated numerically. We do not give the complicated analytical expression in this place but refer to the systematic treatment of the heavy fermion case in our forthcoming article [88].

References

1. S.L. Glashow, Nucl. Phys. B 22 (1961) 579;
   S. Weinberg, Phys. Rev. Lett. 19 (1967) 19;
   A. Salam, in: "Elementary Particle Theory", p. 367, ed. N. Svartholm (Stockholm 1968)

2. S.L. Glashow, J. Illiopoulos, L. Maiani, Phys. Rev. D 2 (1970) 1285;
   M. Kobayashi, K. Maskawa, Progr. Theor. Phys. 49 (1973) 652

3. P. Langacker, Talk at the XXIV International Conference on High Energy Physics, München 1988

4. E.C.G. Stückelberg, Helv. Phys. Acta 14.32L (1941) 588;
   J. Schwinger, Phys. Rev. 74 (1948) 1439;
   F.J. Dyson, Phys. Rev. 75 (1949) 486, 1736;
   R.P. Feynman, Phys. Rev. 76 (1949) 749, 769

5. T. Kinoshita, "Recent Developments of QED", in: Proceedings of the 19th International Conference on High Energy Physics, Tokyo 1978, eds. S. Homma et al. (Tokyo 1979);
   J. Bailey et al., Nucl. Phys. B 150 (1979) 1

6. G. Arnison et al. (UA1 Collaboration) Phys. Lett. 126 B (1983) 398; Phys. Lett. 129 B (1983) 273;
   P. Bagnaia et al. (UA2 Collaboration) Phys. Lett. 129 B (1983) 130

7. G. 't Hooft, Nucl. Phys. B 33 (1971) 173; Nucl. Phys. B 35 (1971) 167

8. D. Haidt, H. Pietschmann, Landolt-Börnstein New Series I/10 (1988)

9. R.E. Behrends, R.J. Finkelnstein, A. Sirlin, Phys. Rev. 101 (1956) 866;
   T. Kinoshita, A. Sirlin, Phys. Rev. 113 (1959) 1652

10. J.M. Jauch, F. Rohrlich, "The Theory of Photons and Electrons", New York, Heidelberg, Berlin 1976

11. Yellow CERN Report: "Physics with LEP", eds. J. Ellis and R.D. Peccei, CERN 86-02 (1986)

12. Proceedings of the ECFA Workshop on LEP 200, Aachen 1986, eds. A. Böhm, W. Hoogland, CERN 87-08, ECFA 87/108 (1987)

13. G. Altarelli, in [14]

14. Yellow CERN Report: "Polarization at LEP", eds. G. Alexander et al., CERN 88-06 (1988)

15. G. Altarelli, in [11]

16. G.L. Fogli, D. Haidt, Z. Phys. C 40 (1988) 379

17. B.W. Lynn, M. Peskin, R.G. Stuart, in [11];
B.W. Lynn, in [14]

18. W. Hollik, in [14], and DESY 88-106 (1988)

19. M. Veltman, Phys. Lett. 91 B (1980) 95;
M. Green, M. Veltman, Nucl. Phys. B 169 (1980) 137; E: Nucl. Phys. B 175 (1980) 547

20. W.J. Marciano, Phys. Rev. D 20 (1979) 274

21. A. Sirlin, Phys. Rev. D 22 (1980) 971

22. W.J. Marciano, A. Sirlin, Phys. Rev. D 22 (1980) 2695

23. Proceedings of the International Workshop on Radiative Corrections in SU(2)×U(1), Trieste 1983, eds. B.W. Lynn and J.F. Wheater, Singapore 1984

24. A. Barroso et al., CERN-EP/87-70 (1987), and in [12]

25. F. Dydak, Talk at the ECFA Workshop on LEP 200, Aachen 1986

26. G. Passarino, M. Veltman, Nucl. Phys. B 160 (1979) 151

27. M. Greco, G. Pancheri, Y. Srivastava, Nucl. Phys. B 171 (1980) 118; E: Nucl. Phys. B 197 (1982) 543

28. F.A. Berends, R. Kleiss, S. Jadach, Nucl. Phys. B 202 (1982) 63

29. M. Böhm, W. Hollik, Nucl. Phys. B 204 (1982) 45; Z. Phys. C 23 (1984) 31

30. M. Böhm, W. Hollik, Phys. Lett. 139 B (1984) 213

31. R.W. Brown, R. Decker, E.A. Paschos, Phys. Rev. Lett. 52 (1984) 1192

32. W. Wetzel, Nucl. Phys. B 227 (1982) 1

33. B.W. Lynn, R.G. Stuart, Nucl. Phys. B 253 (1985) 216

34. W. Hollik, Phys. Lett. 152 B (1985) 121

35. E.A. Kuraev, V.S. Fadin, Sov. J. Nucl. Phys. 41 (1985) 446;
G. Altarelli, G. Martinelli, in [11]

36. F.A. Berends, G. Burgers, W.L. van Neerven, Phys. Lett. 185 B (1987) 395; Nucl. Phys. B 297 (1988) 429; E: Nucl. Phys. B 304 (1988) 921

37. O. Nicrosini, L. Trentadue, Phys. Lett. 196 B (1987) 551; Z. Phys. C 39 (1988) 479

38. S. Jadach, B.F.L. Ward, Tennessee University Preprints UTHEP-88-0101, UTHEP-88-0201 (1988)

39. A.A. Akhundov, D.Yu. Bardin, T. Riemann, Nucl. Phys. B 276 (1986) 1

40. W. Beenakker, W. Hollik, Z. Phys. C 40 (1988) 141

41. F.A. Berends, G. Burgers, W. Hollik, W.L. van Neerven, Phys. Lett. 203 B (1988) 177

42. G. Burgers, in [14], and CERN-TH 5119/88 (1988)

43. D.C. Kennedy, B.W. Lynn, SLAC-PUB 4039 (1986, revised 1988)

44. F.A. Berends, R. Kleiss, W. Hollik, Nucl. Phys. B 304 (1988) 712

45. M. Böhm, W. Hollik, H. Spiesberger, Fortschr. Phys. 34 (1986) 687

46. J. Fleischer, F. Jegerlehner, Phys. Rev. D 23 (1981) 2001

47. S. Sakakibara, Phys. Rev. D 24 (1981) 1149

48. K.I. Aoki, Z. Hioki, R. Kawabe, M. Konuma, T. Muta, Suppl. Progr. Theor. Phys. 73 (1982) 1

49. G. Burgers, W. Hollik, in [14], and CERN-TH 5131/88 (1988)

50. O.M. Fedorenko, T. Riemann, Acta Phys. Polon. B 18 (1987) 761;
D.Yu. Bardin, O.M. Fedorenko, T. Riemann, Dubna preprints JINR-E2-87-663, 664 (1987)

51. D.Yu. Bardin, M.S. Bilenkii, O.M. Fedorenko, T. Riemann, Dubna Preprint JINR-E2-88-324 (1988)

52. D.Yu. Bardin, A. Leike, T. Riemann, M.Sachwitz, Phys. Lett. 206 (1988) 539

53. S. Jadach, J.H. Kühn, R.G. Stuart, Z. Wąs, Z. Phys. C 38 (1988) 609;
J.H. Kühn, R.G. Stuart, Phys. Lett. 200 B (1988) 360

54. L.D. Faddeev, V.N. Popov, Phys. Lett. 25 B (1967) 29

55. A.A. Slavnov, Theor. Math. Phys. 10 (1972) 99;
J.C. Taylor, Nucl. Phys. B 33 (1971) 436

56. G. 't Hooft, Nucl. Phys. B 61 (1973) 455; Nucl. Phys. B 62 (1973) 444

57. D.A. Ross, J.C. Taylor, Nucl. Phys. B 51 (1973) 25

58. T. Kinoshita, J. Math. Phys. 3 (1962) 650;
T.D. Lee, M. Nauenberg, Phys. Rev. 133 (1964) 1549

59. Proceedings of the HERA Workshop, Hamburg 1987, ed. R.D. Peccei,
in particular the contributions by
W. Hollik, H. Spiesberger, J. Kripfganz and H. Perlt

60. D. Yu. Bardin, P.Ch. Christova, O.M. Fedorenko, Nucl. Phys. B 175 (1980) 435; Nucl. Phys. B 197 (1982) 1

61. J.C. Ward, Phys. Rev. 78 (1950) 1824

62. G. Gounaris, D. Schildknecht, CERN-TH 4940/87 (1987); CERN-TH 5078/88 (1988)

63. F. Jegerlehner, Z. Phys. C 32 (1986) 195

64. F.A. Berends, G.J. Komen, Phys. Lett. 63 B (1976) 432;
E.A. Paschos, Nucl. Phys. B 159 (1979) 285;
W. Wetzel, Z. Phys. C 11 (1981) 117

65. J. Cole, G. Penso, C. Verzegnassi, Trieste preprint 19/85/EP;
B.W. Lynn, G. Penso, C. Verzegnassi, SLAC-PUB-3742 (1985)

66. H. Burckhard, F. Jegerlehner, G. Penso, C. Verzegnassi, in [14]

67. U. Amaldi et al., Phys. Rev. D 36 (1987) 1385

68. G. Costa et al., Nucl. Phys. B 297 (1988) 244

69. A.A. Akhundov, D.Yu. Bardin, T. Riemann, Phys. Lett. 166 B (1986) 111

70. W. Hollik, H.J. Timme, Z. Phys. C 32 (1986) 125

71. F. Jegerlehner, Z. Phys. C 32 (1986) 425

72. A. Sirlin, Phys. Rev. D 29 (1984) 89

73. M. Veltman, Nucl. Phys. B 123 (1977) 89

74. J.J. van der Bij, F. Hoogeveen, Nucl. Phys. B 283 (1987) 477

75. M. Veltman, Acta Phys. Polon. B 8 (1977) 475

76. J.J. van der Bij, M. Veltman, Nucl. Phys. B 231 (1984) 205

77. M.Consoli, S. LoPresti, L. Maiani, Nucl. Phys. B 223 (1983) 474;
P. Antonelli, M. Consoli, C. Corbo, Phys. Lett. 99 B (1981) 475;
F. Jegerlehner, Z. Phys. C 32 (1986) 425

78. W. Wetzel, in [11]

79. W. Beenakker, W. Hollik, in [12]

80. J. Jersak, E. Laerman, P.M. Zerwas, Phys. Rev. D 25 (1980) 1218

81. T.H. Chang, K.J.F. Gaemers, W.L. van Neerven, Nucl. Phys. B 202 (1982) 407

82. K.G. Chetyrkin, A.L. Kataev, F.V. Tkachov, Phys. Lett. 85 B (1979) 277;
M. Dine, J. Sapirstein, Phys. Rev. Lett. 43 (1979) 668;
W. Celmaster, R. Gonsalves, Phys. Rev. Lett. 44 (1980) 560

83. S.G. Gorishny, A.L. Kataev, S.A. Larin, Preprint JINR Dubna and INR Moscow (1988)

84. W. de Boer, SLAC-PUB-4428 (1988);
S.L. Wu, Proceedings of the International Symposium on Lepton and Photon Interactions, Hamburg 1987, eds. W. Bartel and R. Rückl

85. W.J. Marciano, D. Wyler, Z. Phys. C 3 (1979) 81;
D. Albert, W.J. Marciano, D. Wyler, Nucl. Phys. B 166 (1980) 460

86. E. Franco, in [11]

87. F.A. Berends, R. Kleiss, Nucl. Phys. B 260 (1985) 32

88. W. Beenakker, W. Hollik, to appear

89. T. Riemann, M. Sachwitz, D. Yu. Bardin, XI Warsaw Symposium on Elementary Particle Physics, Kazimierz, Poland, 1988 (to appear in the Proceedings), and Berlin-Zeuthen PHE/88-11 (1988)

90. G. Burgers, W. Hollik, program GAMMAZ
G. Burgers, program ZAPPQ
G. Burgers, W. Hollik, program library EWCLIB

91. D.C. Kennedy, B.W.Lynn, C.J.C. Im, R.G. Stuart, SLAC-PUB-4128 (1988)

92. A. Djouadi, C. Verzegnassi, Phys. Lett. 195 B (1987) 265;
A. Djouadi, Nuovo Cim. 100 A (1988) 357

93. B.A. Kniehl, J.H. Kühn, R.G. Stuart, in [14];
B.A. Kniehl, M. Krawczyk, J.H. Kühn, R.G. Stuart, MPI-PAE/PTh 93/87 (1987);
B.A. Kniehl, J.H. Kühn, R.G. Stuart, MPI-PAE/PTh 36/88 (1988)

94. G. Passarino, Nucl. Phys. B 204 (1982) 237

95. M. Consoli, A. Sirlin, in [11]

96. D.R. Yennie, S.C. Frautschi, H. Suura, Annals of Phys. 13 (1961) 379

97. W. Hollik, in [23]

98. B.W. Lynn, C. Verzegnassi, Phys. Rev. D 35 (1987) 3326;
A. Djouadi, Z. Phys. C 39 (1988) 561

99. A. Blondel, B.W.Lynn, F.M. Renard, C. Verzegnassi, Nucl. Phys. B 304 (1988) 438

100. R. Kleiss, in [11]

101. M. Igarashi, N. Nakazawa, T. Shimada, Y. Shimizu, Nucl. Phys. B 263 (1986) 347

102. J. Drees, K. König, H. Staeck, S. Überschär, in [14]

103. G. 't Hooft, M. Veltman, Nucl. Phys. B 135 (1979) 365

104. A. Denner, Diplom Thesis, Würzburg University, 1984

105. M. Consoli, Nucl. Phys. B 160 (1979) 208;
M. Consoli, S. LoPresti, M. Greco, Phys. Lett. 113 B (1982) 415;
W. Hollik, Phys. Lett. 123 B (1983) 259;
M. Böhm, A. Denner, W. Hollik, R. Sommer, Phys. Lett. 144 B (1984) 414;
M. Greco, Phys. Lett. 177 B (1986) 97;
K. Tobimatsu, Y. Shimizu, Progr. Theor. Phys. 75 (1986) 905;
M. Böhm, A. Denner, W. Hollik, Nucl. Phys. B 304 (1988) 687;
F.A. Berends, R. Kleiss, W. Hollik, Nucl. Phys. B 304 (1988) 712

106. CHARM II proposal, CERN/SPSC/83-24 and 83-37